BLOCK COPOLYMERS CONTAINING A LOW-SURFACE-ENERGY BLOCK AND THEIR APPLICATIONS

by

Yu Wang

A thesis submitted to the Department of Chemistry

In conformity with the requirements for

the degree of Doctor of Philosophy

Queen's University

Kingston, Ontario, Canada

(July, 2016)

Abstract

This thesis reports the synthesis and/or applications of three types of block copolymers that each bear a low-surface-energy block.

First, poly(dimethylsiloxane)-*block*-poly(2-cinnamoyloxyethyl acrylate) (PDMS-*b*-PCEA) was synthesized and characterized. Cotton coating using a micellar solution of this block copolymer yielded superhydrophobic cotton fabrics. X-ray photoelectron spectroscopy (XPS) and surface property analyses indicated that the PDMS block topped the polymer coating. Photocuring the cotton swatches crosslinked the underlying PCEA layer and yielded permanent coatings. More interestingly, hydrophilically patterned superhydrophobic cotton fabrics were produced using photolithography that allowed the crosslinking of the coating around irradiated fibers but the removal, by solvent extraction, of the coating on fibers that were not irradiated. Since water-based ink only permeated the uncoated regions, such patterned fabric was further used to print ink patterns onto substrates such as fabrics, cardboard, paper, wood, and aluminum foil.

Then, another PDMS-based diblock copolymer poly(dimethylsiloxane)-*block*-poly(glycidyl methacrylate) (PDMS-*b*-PGMA) was prepared. Different from PCEA that photocrosslinked around cotton fibers, PGMA reacted with hydroxyl groups on cotton fiber surfaces to get covalently attached. Further, different PGMA chains crosslinked with each other. PDMS-*b*-PGMA-coated cotton fabrics have been used for oil-water separations. In addition, polymeric nanoparticles were grafted onto cotton fiber surface before PDMS-*b*-PGMA was used to cover the surfaces of the grafted spheres and the residual surfaces of the cotton fibers. These two types of fabrics, coated by the block copolymer alone or by the polymer nanospheres and then the copolymer, were characterized by scanning electron microscope (SEM), Fourier transform infrared spectroscopy (FT-IR), and water repellency analyses. A comprehensive comparative study was made of their performances in oil-water separation.

Finally, a fluorinated ABC triblock copolymer poly(acrylic acid)-*block*-poly(2-cinnamoyloxyethyl methacrylate)-*block*-poly(2-perfluorooctylethyl methacrylate) (PAA-*b*-PCEMA-*b*-PFOEMA) was used to

encapsulate air nanobubbles. The produced air nanobubbles were thermodynamically stable in water and were some 100 times more stable than commercially available perfluorocarbon-filled microbubbles under ultrasound. These nanobubbles, due to their small sizes and thus ability to permeate the capillary networks of organs and to reach tumors, may expand the applications of microbubbles in diagnostic ultrasonography and find new applications in ultrasound-regulated drug delivery.

Acknowledgements

First I would like to thank my supervisor, Prof. Guojun Liu, for giving me this great chance to study and conduct research at Queen's. In the past five years, I have learnt a lot of knowledge from him through his courses and the lab. He is a great hands-on supervisor and always happy to answer my questions. He taught me how to start a research project, how to design the experiments in details, how to present the results and how to write a good scientific paper. I greatly appreciate that he has spent a lot of time including countless evenings and weekends on my research. I would not be what I am today without his support, guidance and hard work. I am pretty sure that what I have learnt from him during the past five years will be my invaluable wealth and great weapon in my future work.

I am also thankful to the many distinguished researchers that I have been fortunate to work with during my years in the Liu group. Everyone has contributed with ideas and support. I am sincerely grateful to Dr. Xiaoyu Li for his patient supervision and TEM operation during my early research in the Liu group; Dr. Heng Hu for his great help including providing me with valuable advice and performing TEM/AFM operations in the past five years; Weijie Jiang for our friendship since my first day at Queen's; Jian Wang for her great help including the AFM operation and DLS instruction; and Dr. Ian Wyman for his proofreading of my papers and thesis. I am also grateful to many of my fellow including Dr. Dean Xiong, Dr. Muhammad Rabnawaz, Dr. Hongbo Wang, Dr. Guichao Kuang, Dr. John Dupont, Dr. Zengqian Shi, Dr. Ganwei Zhang, Dr. Claudia Grozea, Dr. Xu Wu, Dr. Kunzhi Shen, Danielle Macoretta, Bolu Peng, Prashant Agrawal, Zijie Wang, Shuaishuai Huang, Kaka Zhang, Zac Mah and Haili Zheng.

This work would not be what it is without the critical contributions of many other researchers outside of the Liu Group, including faculty, staff and students within the Chemistry Department and beyond. Therefore, I would like to thank my committee members Prof. Suning Wang and Prof. Richard Oleschuk for their assistance throughout this work. Furthermore, I am grateful to Prof. Amer Johri from the Department of Medicine and Terry Yantian Li from the Department of Biomedical and Molecular Science, Queen's University, for their help performing the ultrasound imaging tests. Terry's blood donation also

made the research work (in Chapter 4) much more meaningful. I am also grateful to Dr. Gabriele Schatte, Dr. Francoise Sauriol and Dr. Igor Kozin in Chemistry Department for their valuable instruction regarding XPS, NMR and FT-IR techniques, respectively. I also would like to thank Agatha Dobosz from the Department of Geological Science and Engineering for her help with the SEM operations.

I would like to thank my parents Jixiang Wang and Yanli Wang. Without their support, I could not grow up and get a chance to obtain a good education. Neither of them had a chance to go to university, however, they have always encouraged me to pursue the highest level of education and provided me every opportunity to achieve my dreams. I also would like to thank my parents-in-law Ke Li and Yanxi Zhai for their trust and support in the last several years.

Last but not least, I would like to thank my wife Yufei Li. In the past ten years, she has always accompanied me regardless of the location, including China, the USA and Canada. I would not be what I am today without her trust, encouragement and support.

Statement of Originality

I hereby certify that all of the work described within this thesis is the original work of the author under the supervision of Professor Guojun Liu. Any published (or unpublished) ideas and/or techniques from the work of others are fully acknowledged in accordance with the standard referencing practices.

(Yu Wang)

(July, 2016)

Table of Contents

List of Figures

List of Tables

List of Abbreviations

°	degree
°C	Celsius degree
γ_{lg}	interfacial energy of the liquid/gas
γ_{p}	surface tension of a polymer
γ_{sg}	interfacial energy of the solid/gas
γ_{sl}	interfacial energy of the solid/liquid
γ_{w}	surface tension of water
γ_{wp}	interfacial tension between water and a polymer
η_{r}	relative viscosity
θ	contact angle
µm	micrometer
µL	microliter
ρ	density
ΔG	Gibbs free energy change
A	surface area
Å	angstrom
ACF	PAA-*b*-PCMEA-*b*-PFOEMA
AFM	atomic force microscope
ATR	attenuated total reflection
ATRP	atom transfer radical polymerization
A_w	water absorption
BCF	PtBA-*b*-PCEMA-*b*-PFOEMA
C	concentration

CEHDA	coaxial electrohydrodynamic atomization
cm	centimeter
cm^{-1}	wavenumber
cmc	critical micelle concentration
C_o	oil absorption capacity
CRP	controlled radical polymerization
CTA	chain transfer agent
d_{AFM}	average diameter based on AFM measurements
d_h	hydrodynamic diameter
DLS	dynamic light scattering
DMAP	4-dimethylaminopyridine
DMF	*N*,*N*-dimethylformamide
DP	degree of polymerization
d_{TEM}	average diameter based on TEM measurements
DVB	divinylbenzene
EDC	1-ethyl-3-(3-dimethylaminopropyl)carbodiimide
EDTA	ethylenediaminetetraacetic acid
EIP	emulsion inversion point
eV	electronvolt
f	fraction of the solid/liquid interface
f_{HX}	hexane volume fraction
FSM	fluorinated silane molecules
FT-IR	Fourier transform infrared spectroscopy
g	gram
GCB	PGMA'-*b*-PCEMA-*b*-PtBA

h	hour
HEA-TMS	2-trimethylsiloxyethyl acrylate
IT	irradiation time
M	mole per liter
mg/mL	milligram per milliliter
min	minute
mL	milliliter
mm	millimeter
M_n	number-average molecular weight
mN/m	millinewtons per meter
MRI	magnetic resonance imaging
M_w	weight-average molecular weight
nm	nanometer
NMP	nitroxide mediated polymerization
NMR	nuclear magnetic resonance
Pa	pascal
PAA	poly(acrylic acid)
P_b	breakthrough pressure
PBA	poly(*n*-butyl acrylate)
PCEA	poly(2-cinnamoyloxyethyl acrylate)
PCEMA	poly(2-cinnamoyloxyethyl methacrylate)
PCL	poly(caprolactone)
P-cotton	PDMS-*b*-PGMA polymer coated cotton
PDI	polydispersity index
PDMAEMA	poly(dimethylaminoethyl methacrylate)

PDMS	poly(dimethylsiloxane)
PDMS-Br	bromide-terminated poly(dimethylsiloxane)
PDMS-OH	hydroxyl-terminated poly(dimethylsiloxane)
PEG	poly(ethylene glycol)
PEO-Pyrene	pyrene-terminated poly(ethylene oxide)
PFOEMA	poly(2-perfluorooctylethyl methacrylate)
PFPO	poly(perfluoropropylene oxide)
PGMA	poly(glycidyl methacrylate)
PGMA'	poly(glyceryl monomethacrylate)
PHEA	poly(2-hydroxyehtyl acrylate)
PHFA	poly(2,2,3,4,4,4-hexafluorobutyl acrylate)
PHFEMA	poly(heptadecafluorodecyl methacrylate)
PIBVE	poly(isobutyl vinyl ether)
PIPSMA	poly[3-(triisopropyloxysilyl)propyl methacrylate]
PIT	phase inversion temperature
P_L	Laplace pressure
PLD	pulsed laser deposition
PLGA	poly(L-lactide-*co*-glycolide)
PLLA	poly(L-lactide)
PMA	poly(methyl acrylate)
PMMA	poly(methyl methacrylate)
PP-cotton	particles + PDMS-*b*-PGMA polymer coated cotton
ppm	parts per million
PS	polystyrene
PSMA	poly(solketal methacrylate)

PtBA	poly(*tert*-butyl acrylate)
PTFE	polytetrafluoroethylene
PTFEMA	poly(trifluoroethyl methacrylate)
PVBA	poly(4-vinylbenzylazide)
PVD	physical vapor deposition
PVEC	poly[2-(vinyloxy) ethyl cinnamate]
R	radius
r	roughness factor
RAFT	reversible addition-fragmentation chain transfer
r_c	radius of capillary
R_C	weight residue of uncoated cotton
R_P	weight residue of polymer
R_{PC}	weight residue of polymer-coated cotton
rpm	revolutions per minute
s	second
SCB	PSMA-b-PCEMA-b-PtBA
SEC	size exclusion chromatography
SEM	scanning electron microscope
Teflon	polytetrafluoroethylene
TEM	transmission electron microscopy
TEOS	tetraethylorthosilicate
TFT	α,α,α-trifluorotoluene
TGA	thermogravimetric analysis
THF	tetrahydrofuran
UV	ultraviolet

V50	2,2’-azobis(2-methylpropionamidine) dihydrochloride
vol%	volume percent
WCA	water contact angle
WSA	water shedding angle
wt%	weight percent
x	grafting density
XPS	X-ray photoelectron spectroscopy

Chapter 1

Introduction

1.1 Block Copolymers

1.1.1 Definition of Block Copolymers

Macromolecules consisting of two or more chemically distinct polymer chains that are covalently linked together are called block copolymers. Each of the chemically distinct polymer chains in a block copolymer is called a block.[1] Depending on how many blocks are present within the copolymer chain, block copolymers can be described as diblock, triblock, tetrablock copolymers and so on. For example, PDMS-*b*-PCEA is an example of an AB diblock copolymer,[2] since it consists of two chemically distinct polymer chains that are connected together by a covalent bond. Analogically, polystyrene-*block*-polybutadiene-*block*-polystyrene (PS-*b*-PBD-*b*-PS) and PAA-*b*-PCEMA-*b*-PFOEMA are ABA and ABC triblock copolymers, respectively.[3, 4]

1.1.2 Synthesis of Block Copolymers

1.1.2.1 Anionic Polymerization

Block copolymers have attracted much attention since the discovery of living anionic polymerization by Michael Szwarc in 1956.[5] Anionic polymerization has been the dominant method to synthesize block copolymers for four decades, until the emergence of controlled/"living" radical polymerization techniques.[6] A general mechanism for a typical anionic polymerization in initiation and propagation steps is illustrated in Figure 1.1. Initiators can be compounds that will generate carbanions (such as butyl lithium) or oxyanions (such as potassium *tert*-butoxide), depending on the nature of the monomer. In order for a monomer to smoothly undergo anionic polymerization, it must be able to stabilize the negative charge of the growing polymer chain. This charge stabilization is achieved either through the inductive effect or via the conjugate effect.

According to the theory, anionic polymerizations are performed in a particular monomer sequence, which depends on the basicity of the growing polymeric anion.[7] For example, polystyrene-*block*-poly(methyl methacrylate) (PS-*b*-PMMA) is synthesized by initially polymerizing styrene and subsequently polymerizing methyl methacrylate (MMA). However, the reverse order, involving the polymerization of MMA prior to styrene polymerization, is not applicable because the styrenenyl anion is more basic than the MMA anion. In general, the following sequence exists for various classes of monomers in anionic polymerization: butadiene/styrene > methacrylate > oxiranes > siloxane.

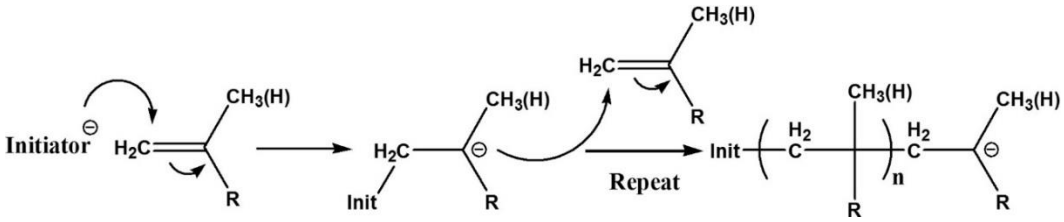

Figure 1.1 Reaction mechanism of an anionic polymerization.

The disadvantage of anionic polymerization that limits its large-scale practical application is the stringent synthetic conditions required for this reaction. However, the main advantage of anionic polymerization is that the length of each block of the resultant block copolymers can be precisely controlled. A typical polydispersity index (PDI) of a diblock or triblock copolymer that is synthesized via anionic polymerization can be smaller than 1.05. Therefore, this polymerization method is still the best choice for many researchers who focus on fundamental block copolymer-based research such as block copolymer self-assembly, where low PDI values are of key importance.

1.1.2.2 Controlled Radical Polymerization

The term controlled radical polymerization (CRP) refers to a radical polymerization that is performed in the presence of reagents that suppress the occurrence of irreversible chain

transfer/termination reactions.[6] In the past 20 years since its discovery, CRP has completely changed the synthetic landscape of polymer chemistry. The procedures involved with CRP are less tedious than those required for anionic polymerization, while this technique also provides a much higher degree of control over the polymerization process and thus the molecular weight of the resultant polymer than is available via conventional free radical polymerization. Among CRP methods, nitroxide mediated polymerization (NMP), reversible addition-fragmentation chain transfer (RAFT) polymerization and atom transfer radical polymerization (ATRP) have been widely studied and applied.[8, 9]

NMP is an important class of controlled radical polymerization reactions that was developed in the 1990s.[10] Polymers obtained via NMP often exhibit well-defined molecular weights and low PDIs that typically range between 1.1 and 1.2.[11] A general reaction mechanism for NMP is illustrated in Figure 1.2. First, homolysis of a C-O bond in an alkoxyamine occurs, thus generating two radicals. One radical species incorporates a transient carbon free radical that acts as an initiator, while the other species possesses a persistent secondary amine oxide radical. As shown in Figure 1.2, a transient radical can either react reversibly with the persistent radical to form a dormant species, or it can react with the monomer to initiate the polymerization.[12] On the other hand, persistent radicals are more stable than transient carbon radicals, due to the resonance of the single electron between the nitrogen and oxygen of the secondary amine oxide radical. Highly substituted amines or cyclic alkoxyamines are typically used in order to inhibit intermolecular coupling between the persistent radicals.

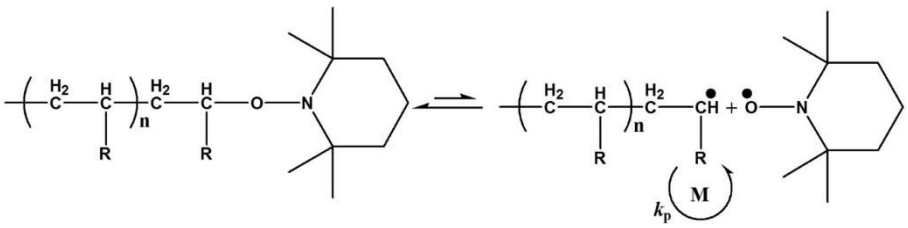

Figure 1.2 Reaction mechanism of NMP.

RAFT polymerization is another important class of controlled radical polymerization reactions. This technique was discovered in 1998 by John Chiefari *et al*.[13] The mechanism of a RAFT polymerization is shown in Figure 1.3. Briefly, a RAFT process consists of three basic components, which include an initiator, a monomer, and a RAFT agent. An initiating radical is generated by the decomposition of a latent initiator using heat or light to initiate the polymerization. A chain transfer agent (CTA), also called a RAFT agent, controls the generation process of the free radical. For example, thiocarbonylthio compounds that are substituted with various alkyl/aryl groups are typically used as CTAs. As depicted in Figure 1.3, the growing polymer chain ($P_n\bullet$) reacts with the CTA at the C=S bond, and undergoes rearrangement to generate another radical ($R\bullet$). The newly formed radical ($R\bullet$) then initiates a monomer to form a new polymer chain ($P_m\bullet$). The main equilibrium involved in the RAFT process is the reaction between the polymeric-CTA (dormant P_n) and the polymeric growing free radical ($P_m\bullet$), which in turn generates a dormant species and an active growing free radical. A faster equilibrium between a dormant species and an active species ensures the synthesis of well-defined polymers with narrow molecular weight distributions.[6] Additionally, RAFT polymerization has a unique advantage over the contemporary polymerization methods as it can be used to polymerize acidic monomers such as acrylic acid.[14, 15]

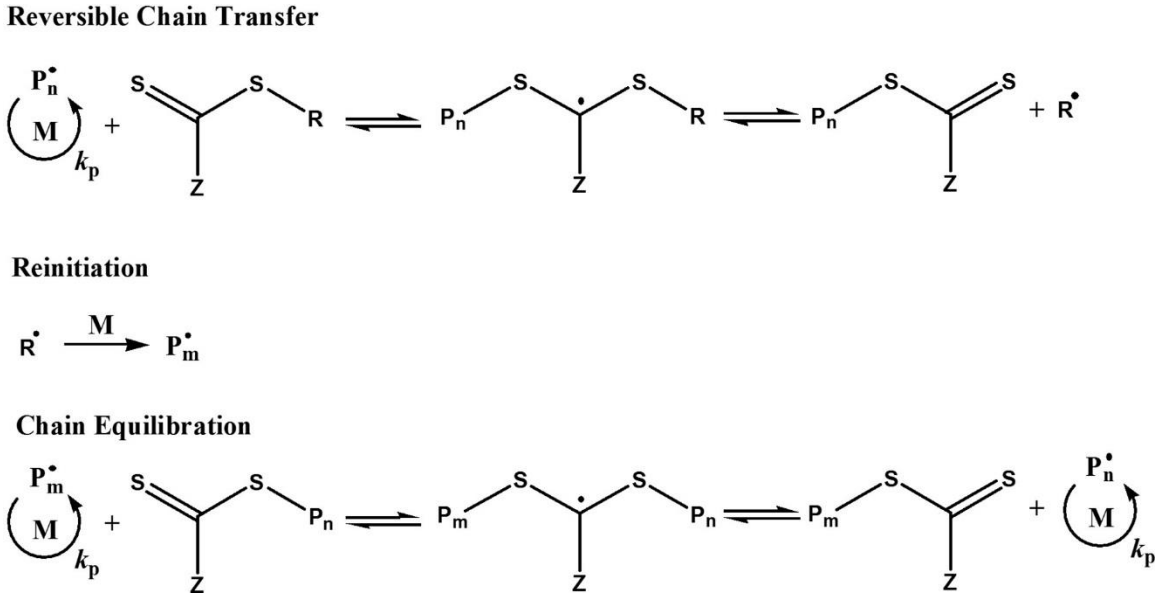

Figure 1.3 Reaction mechanism of RAFT polymerizaiton.

ATRP is another important class of controlled radical polymerization reactions, which will be emphasized in this section since two kinds of AB diblock copolymers described in Chapter 2 and Chapter 3, respectively, were synthesized via this polymerization technique. ATRP was discovered independently by Mitsuo Sawamoto *et al.*[16] as well as by Jinshan Wang and Krzysztof Matyjaszewski in 1995.[17] In a short period of time, it became a vital tool for the preparation of a diverse range of architectural block copolymers.

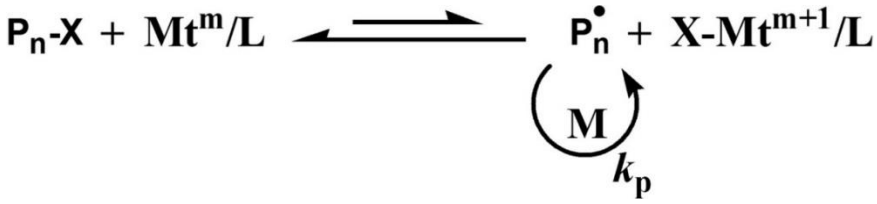

Figure 1.4 Reaction mechanism of ATRP.

A typical reaction mechanism of ATRP is illustrated in Figure 1.4. A polymeric halide P_n-X reversibly reacts with a transition metal-complex such as $Cu^{I}X/L$ to form a free radical $P_n\bullet$ and $Cu^{II}X_2/L$ (during the initiation step, P_n-X and $P_n\bullet$ can be replaced by Init-X and Init●, respectively).

The equilibrium favors the reverse direction in an ATRP reaction, and thus the active radical $P_n\bullet$ exists as a minor species, while the dormant polymer chain P_n-X is a major species. Therefore, polymers produced by ATRP have low PDIs, which are typically between 1.1 and 1.2, since each polymer chain grows at a similar rate. In addition, the number or concentration of radicals during the polymerization remains very low and hence the termination through radical combination is minimal.[18]

An ATRP system consists of various components, such as the initiator, monomer, catalyst and/or solvent. An ATRP initiator should contain a halo functional group that can reversibly exchange halogens with transition metal complexes. This exchange involves a single electron process, and the resultant alkyl radical generated through halogen exchange is capable of initiating the polymerization. Although the use of alkyl iodides as initiators has been reported,[18] only bromine and chlorine among the halogens are commonly used for ATRP reactions. An alkyl bromide initiator is more easily activated than an alkyl chloride initiator because of the weaker C-Br bond.

Various classes of monomers, such as styrenes, acrylates, methacrylates, acrylamides, methacrylamides, and acrylonitriles have been polymerized via ATRP.[18-21] However, acidic monomers cannot be polymerized by ATRP, as organic acids can poison a catalyst and consequently inhibit the ATRP reaction.[18]

Another very important component in an ATRP reaction is the catalyst. As shown in Figure 1.4, transition metals with two stable oxidation states that differ by a single electron can be used to catalyze ATRP reactions. Therefore, a wide range of transition metals including molybdenum,[22] chromium,[23] rhenium,[24] ruthenium,[16] copper[17] and iron[25] have been investigated as potential catalysts. Copper is the most commonly used transition metal for ATRP catalysis, because of its affinity for halogens as well as its relatively low cost. However, transition metals have to be used together with organic ligands in order to provide effective ATRP catalysts. Fundamentally, ligands

perform two equally important roles in an ATRP reaction. First, the organic ligands undergo complexation with inorganic transition metals, thus enhancing the solubility of the metal in organic solvents. Second, the rate of an ATRP reaction is highly dependent on the binding strength between the ligands and the metals. Stronger ligands yield a faster polymerization rate.

Finally, the solvent also plays a significant role in ATRP. For example, polymerization rates are higher in aprotic and polar solvents in comparison with those conducted in non-polar solvents. In addition, although bulk phase (solvent free) ATRP reactions have been used in polymer synthesis,[26, 27] the use of solvent dramatically decreases the viscosity of the reaction mixture, especially during the later stages of a reaction. Consequently, the use of a solvent can help the polymer chains to grow in a uniform manner. However, too much solvent will decrease the concentration of the monomer or initiator and thus decrease the reaction rate. This will affect an ATRP reaction significantly, especially in cases when a macroinitiator is used to synthesize a second block.

1.1.2.3 Cationic Polymerization

Living cationic polymerization was developed in the 1980s.[28] Generally, cationic polymerization is considered as a complimentary technique to anionic polymerization because monomers that cannot be polymerized via anionic polymerization, are often suitable for cationic polymerization.[29] Figure 1.5 describes the mechanism of a cationic polymerization. In contrast with anionic polymerization, this polymerization is initiated by a positively charged species, such as a carbenium ion or an oxonium ion. Monomers such as styrene, isobutene, vinyl ethers and tetrahydrofuran can undergo cationic polymerization. However, the main drawback of cationic polymerization is that it is more prone to side-reactions in comparison with anionic polymerization or ATRP. Therefore, it is not the best technique for the preparation of most common block copolymers.

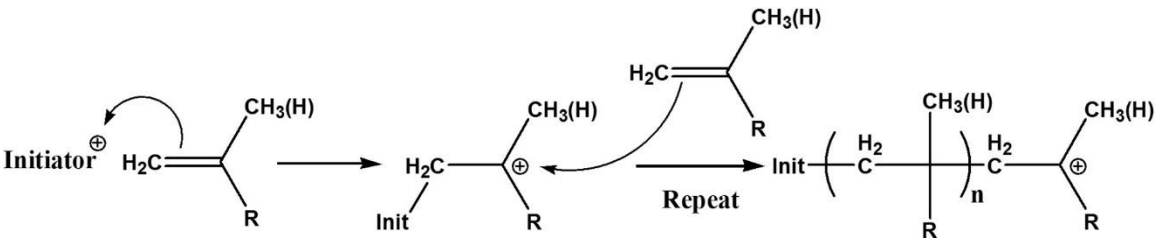

Figure 1.5 Reaction mechanism of cationic polymerization.

1.1.2.4 End-Coupling of Homopolymers

An end-coupling strategy involves a reaction between end-functionalized polymer chains to produce a block copolymer, as shown in Figure 1.6. This strategy initially involves the functionalization of terminals of the polymer chains with certain reactive functional groups. For example, the chains may incorporate different functionalized end-groups such as alkyne and azide groups to facilitate click chemistry.[30, 31] Alternatively, these end-groups may also be identical, with both chains incorporating C=C bonds to facilitate metathesis reactions.[32]

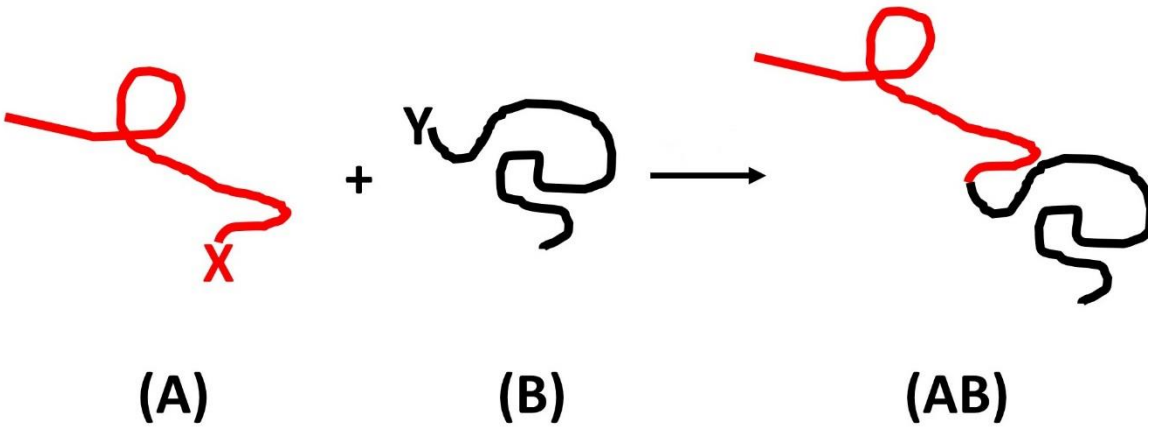

Figure 1.6 End-coupling of two pre-made polymer chains to form an AB diblock copolymer.

However, end-coupling strategies have certain disadvantages. These include the requirement of a suitable solvent as a reaction medium for the end-coupling reaction, the necessity of extensive post-reaction purification due to incomplete coupling, and the need for quantitative end-

functionalization of reactive functional groups on the polymer chains. For these reasons, the scope of end-coupling strategies in block copolymer synthesis is limited only to highly efficient and selective coupling reactions.

1.1.3 Applications of Block Copolymers

1.1.3.1 Surface Modifications Based on Block Copolymer Coatings

Block copolymers are very suitable for surface modification since they may form brush layers on various surfaces.[33-35] A suitable block copolymer for coating applications contains at least two different functional blocks, one of which serves to anchor the copolymer onto the substrate while the other block provides the desired surface properties such as a low surface tension (in the case of a fluorinated block) or other features. In comparison with small molecules or end-functionalized homopolymers, a block copolymer can provide more reactive sites to allow secure binding to a substrate via adjusting the length of its anchor block. In addition, the final coating thickness and properties can be tuned by adjusting the length of its exposed block.

Various surfaces have been modified by block copolymers. For example, flat surfaces such as glass have been coated by poly[3-(triisopropyloxysilyl)propyl methacrylate]-*block*-poly[2-(perfluorooctyl)ethyl methacrylate] (PIPSMA-*b*-PFOEMA) and poly(perfluoropropylene oxide)-*block*-poly-[3-(triisopropyloxysilyl)propyl methacrylate] (PFPO-*b*-PIPSMA), respectively (Figure 1.7). These diblock copolymers, which were synthesized via ATRP, were anchored onto glass surfaces through the sol-gel chemistry of the PIPSMA block. Their fluorinated blocks provided the initially hydrophilic glass surface with amphiphobic (both water- and oil-repellent) properties.[36]

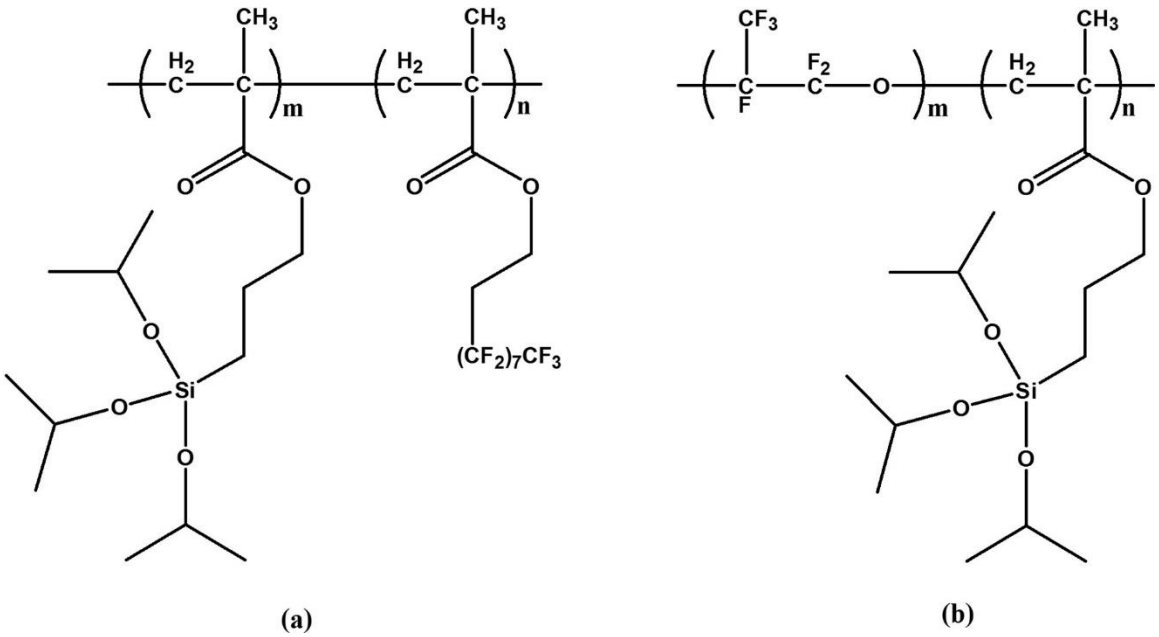

Figure 1.7 Chemical structures of PIPSMA-*b*-PFOEMA (a) and PFPO-*b*-PIPSMA (b).

Metal surfaces have also been coated by block copolymers, typically for anti-corrosion applications. For instance, the diblock copolymers poly(*n*-butyl acrylate)-*block*-poly(trifluoroethyl methacrylate) (PBA-*b*-PTFEMA) and poly(*n*-butyl acrylate)-*block*-poly(heptadecafluorodecyl methacrylate) (PBA-*b*-PHFEMA) were synthesized via NMP and used as monolayers to protect aluminium against corrosion (Figure 1.8).[37] The amorphous PBA block did not react with the metal surface, but provided elastomeric properties to the final coating.

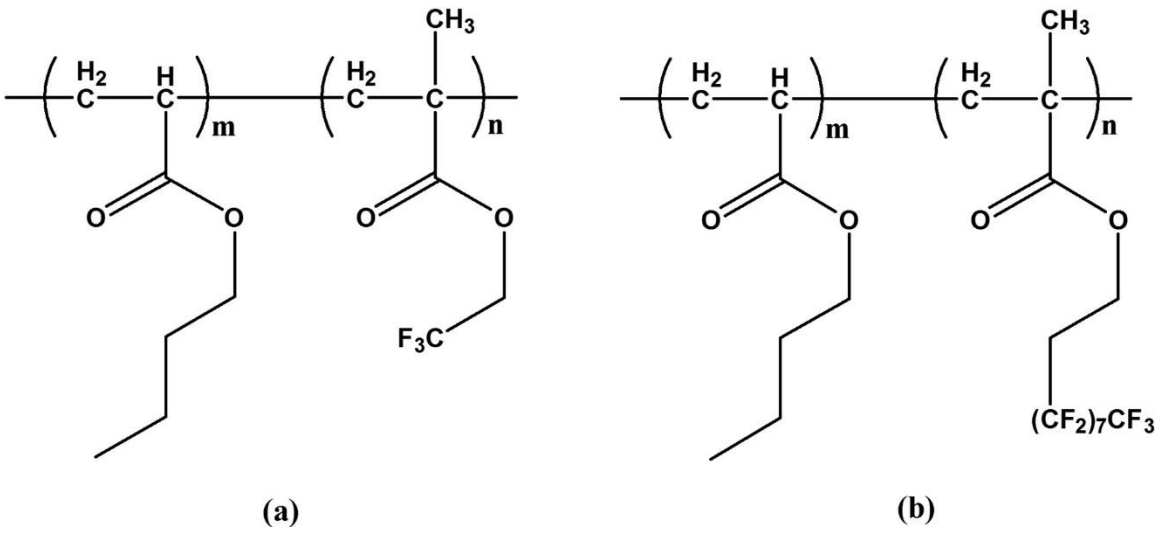

Figure 1.8 Chemical structures of PBA-*b*-PTFEMA (a) and PBA-*b*-PHFEMA (b).

Materials with non-flat surfaces such as glass capillary tubes also can be modified with block copolymers. A diblock copolymer poly(isobutyl vinyl ether)-*block*-poly[2-(vinyloxy) ethyl cinnamate] (PIBVE-*b*-PVEC), which was synthesized via cationic polymerization, was used to modify the inner walls of capillary tubes (Figure 1.9).[38] In a selective solvent, the insoluble PVEC block was absorbed onto the surface and the soluble PIBVE block stretched outwardly into the solution. The capillary action of the tubes was then changed due to their coating by these polymer brushes.

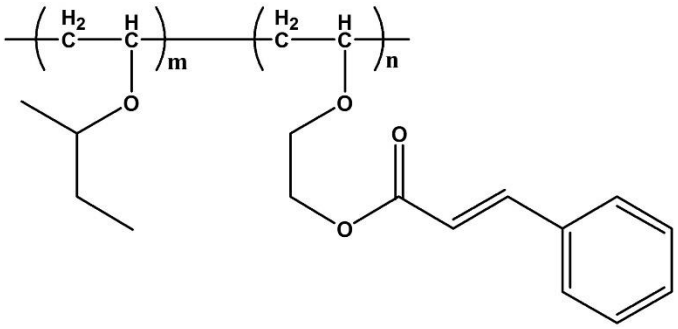

Figure 1.9 Chemical structure of PIBVE-*b*-PVEC.

The surfaces of nanomaterials have also been modified with various block copolymers. For example, the diblock copolymers poly[3-(triisopropyloxysilyl)propyl methacrylate]-*block*-poly(perfluorooctylethyl methacrylate) (PIPSMA-*b*-PFOEMA) and poly[3-(triisopropyloxysilyl)propyl methacrylate]-*block*-poly(*tert*-butyl acrylate) (PIPSMA-*b*-PtBA), were synthesized via anionic polymerization and simultaneously grafted onto silica nanoparticles (Figure 1.10).[39] Particulate coatings with tunable surface wetting properties were obtained by changing the proportion of these two grafted copolymers. In another example, the surfaces of carbon nanotubes were modified with a diblock copolymer poly(*tert*-butyl acrylate)-*block*-poly(4-vinylbenzylazide) (PtBA-*b*-PVBA), which was synthesized via RAFT polymerization.[40] After the PtBA had been converted to poly(acrylic acid) (PAA), the hydrophobic carbon nanotubes became hydrophilic (Figure 1.11).

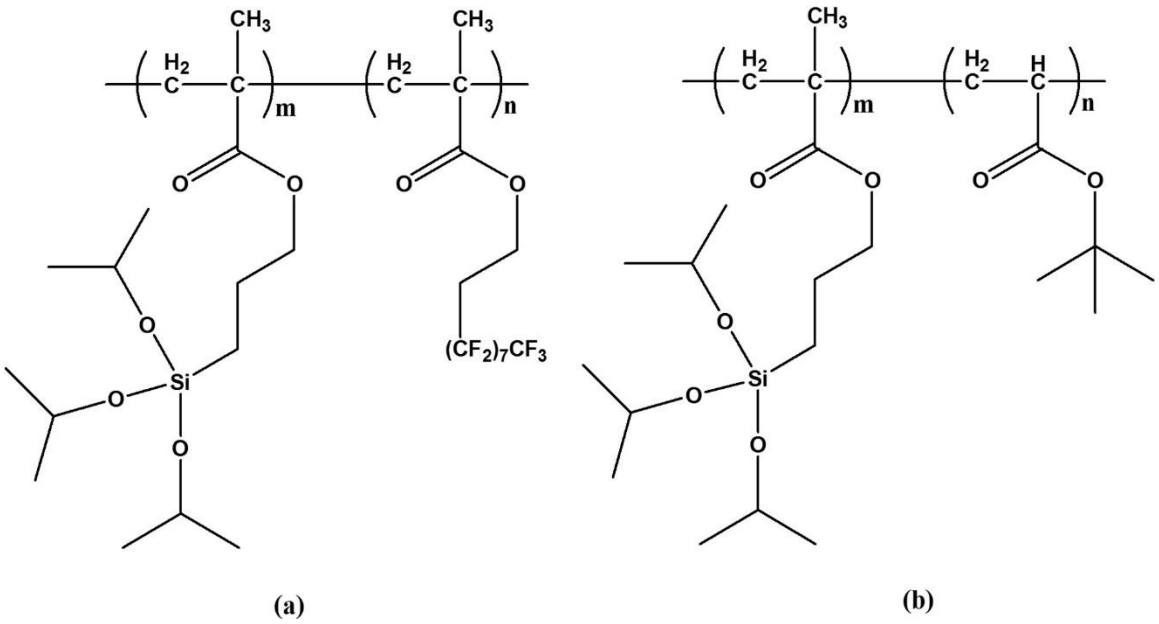

Figure 1.10 Chemical structures of PIPSMA-*b*-PFOEMA (a) and PIPSMA-*b*-PtBA (b).

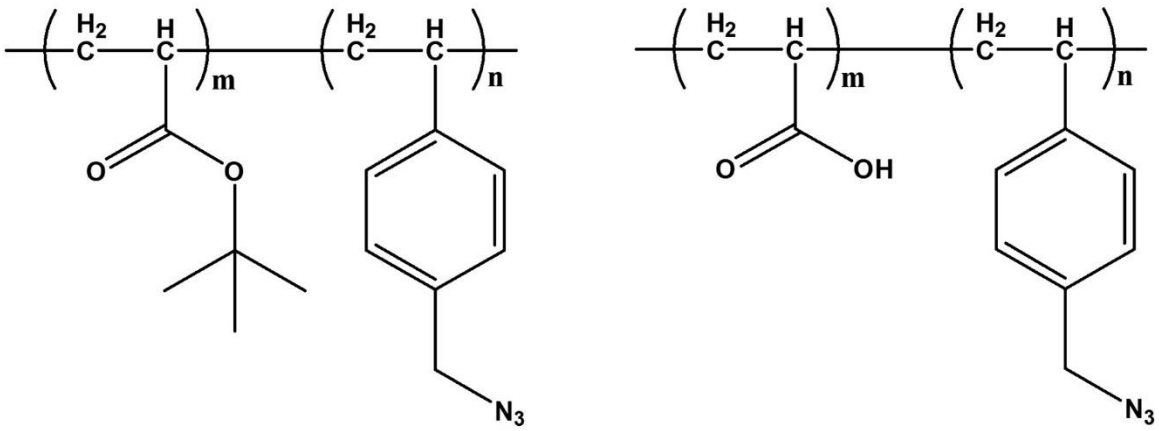

Figure 1.11 Chemical structures of PtBA-*b*-PVBA (a) and PAA-*b*-PVBA (b).

1.1.3.2 Nanomaterials Based on Block Copolymer Self-Assembly

Nanomaterials including nanospheres, nanofibers, nanocapsules, and nanotubes have various potential applications, such as drug delivery,[41-43] catalysis,[44] sensors,[45] and also in microelectronics and photovoltaic devices.[46]

As mentioned earlier, block copolymers consist of more than one chemically distinct polymer chain, and each of these chains may have a different solubility in a particular solvent. A block-selective solvent dissolves one or more of the block(s) selectively over the other(s). In block-selective solvents, block copolymers self-assemble to form nano-scaled aggregates with various shapes or morphologies. For example, if an AB diblock copolymer is initially dissolved in a good solvent, the addition of a selectively poor solvent for the B block will trigger the less soluble B block to collapse while the soluble A block remains stretched out into the solvent. The collapse of the B block occurs in order to minimize the unfavorable interactions between the B block and the solvent. If the concentration of the AB chains bearing collapsed B blocks is increased and reaches the critical micelle concentration (cmc), micelle formation occurs.[44] In general, micelles consist of an inner phase called a core domain that consists of insoluble blocks, and a soluble corona domain at the external layer that stretches outwardly into the solvent.

These morphologies are dependent on multiple factors that include the volume fractions of the individual blocks, nature of the solvent, pH, and various other parameters.[47-49] For example, Eisenberg *et al.* performed the very first systematic investigation of the self-assembled aggregates formed by polystyrene-*block*-poly(acrylic acid) (PS-*b*-PAA).[50] By changing the volume fractions of the two blocks, they were able to tune the morphologies of these aggregates from spheres (Figure 1.12A), to cylinders (Figure 1.12B), to vesicles (hollow spheres, Figure 1.12C), and to large compound micelles (Figure 1.12D).

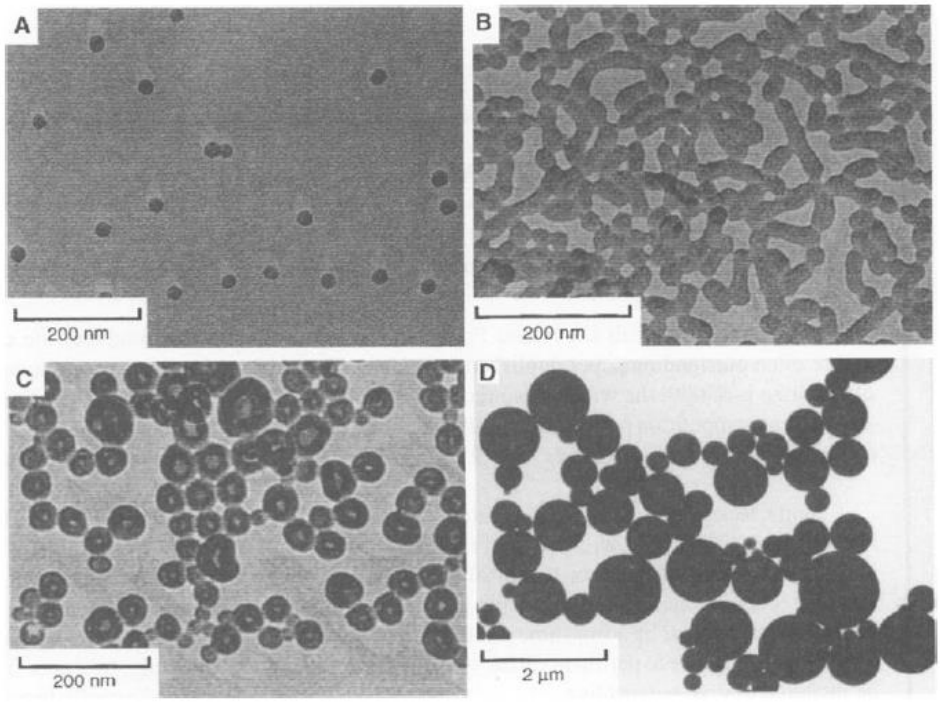

Figure 1.12 TEM images of common morphologies produced by an AB diblock copolymer, including spheres of PS_{500}-*b*-PAA_{58} (A), rod-like micelles of PS_{190}-*b*-PAA_{20} (B), vesicles of PS_{410}-*b*-PAA_{20} (C), and large compound micelles of PS_{200}-*b*-PAA_4 (D). Reprinted from Zhang, L.; Eisenberg, A. *Science*, 1995, **268**, 1728.

Some nanomaterials such as hollow nanospheres or nanotubes can be fabricated by another kind of self-assembly, in which two immiscible solvents are used instead of one selective solvent or miscible solvent mixture. This method is also known as emulsification. For instance, a block

copolymer that contains both hydrophobic and hydrophilic blocks can stabilize oil droplets in water or water droplets in oil as a macromolecular surfactant. Under particular conditions, nano-sized polymeric structures are formed when the droplets are small (Figure 1.13).[51] The shape and size of these nanostructures are dependent on many parameters such as the surfactant/dispersion phase ratio, the dispersion phase/continuous phase ratio, the temperature, and the stirring speed.[51-53]

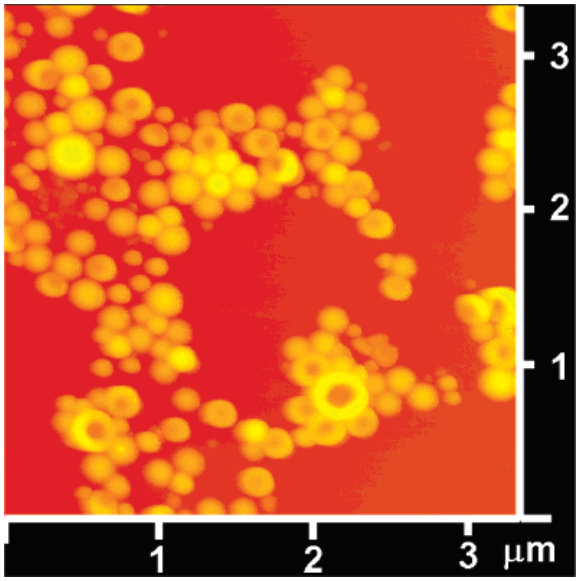

Figure 1.13 AFM image of ABC triblock copolymer nanocapsules fabricated via oil-in-water emulsification. Reprinted from Zheng, R.; Liu, G. *Macromolecules*, 2007, **40**, 5116.

1.2 Superhydrophobic Coatings

1.2.1 Basic Theories of Superhydrophobic Surfaces

1.2.1.1 Definition of Superhydrophobic Surfaces

A superhydrophobic surface is defined as a surface on which the water contact angle is larger than 150° and rolling off angle is smaller than 10°.[54, 55] Water contact angles are measured through careful analysis of the liquid droplet by observing where the liquid/gas interface meets the solid/liquid interface (Figure 1.14). The rolling off or sliding angle is defined as the minimal surface tilting angle required for a water droplet to roll off the corresponding surface.

Superhydrophobic surfaces have attracted broad interest in the field of materials science due to their various applications as self-cleaning surfaces, as corrosion resistant, anti-fogging, and anti-icing coatings, as well as for oil-water separation.[54-57] Two key factors play complementary roles in the fabrication of superhydrophobic surfaces: surface energy and surface roughness.

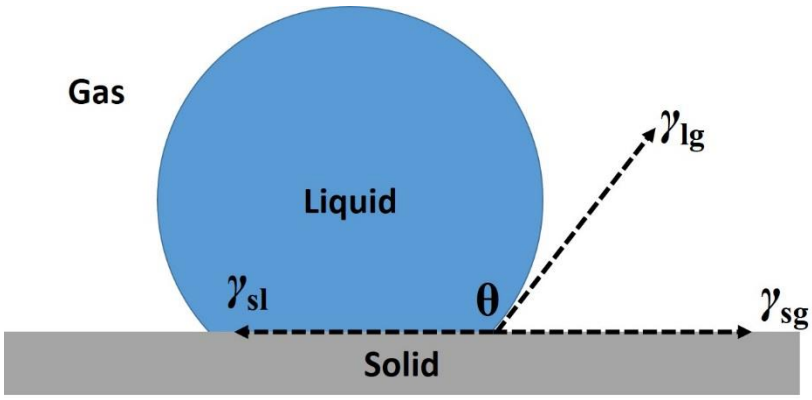

Figure 1.14 Schematic diagram of a liquid droplet showing the contact angle on a flat surface and terms described by Young's equation.[58]

1.2.1.2 Low Surface Energy

The chemical composition of a material's surface determines the surface energy, which has a significant influence on the contact angles of liquids placed on this surface. The contact angle θ on a flat surface is determined by Young's equation (equation 1.1):[58]

$$\cos\theta = (\gamma_{sg} - \gamma_{sl})/\gamma_{lg} \qquad (1.1)$$

where θ is the contact angle, γ_{sg}, γ_{sl} and γ_{lg} are the interfacial energies of the solid/gas, solid/liquid and liquid/gas interfaces, respectively. Young's equation shows the equilibrium state at which the total energy of the system has reached a minimum. Based on this theory, materials with low surface energies (γ_{sg}) can exhibit large water contact angles so that they repel water. Typically, many polymers such as poly(dimethylsiloxane) (PDMS) and fluorinated polymers have low surface energies. For example, the surface energy of PDMS is ~ 20 mN/m and surface energies of some

fluorinated polymers can be as low as ~7 mN/m.[59, 60] These materials are candidates for the fabrication of superhydrophobic surfaces.

1.2.1.3 High Surface Roughness

Besides introducing low surface energy materials to a substrate's surface, the hydrophobicity can also be enhanced by increasing the surface roughness.[61-64] Here, two basic theories have to be considered. If water can fill the gaps formed by rough surface beneath the droplet and come into full contact with the solid substrate, the system is in the "Wenzel state".[61] This scenario is described by Wenzel's equation (equation 1.2):

$$\cos\theta' = r\cos\theta \qquad (1.2)$$

where θ' is the apparent contact angle on a rough surface, θ is the intrinsic contact angle on a flat surface, and r is the roughness factor which equals the ratio between the actual surface area and the geometric surface area. A high degree of roughness can enhance the anti-wetting behavior of a substrate, so that it may become superhydrophobic ($\theta' > 150°$) if the ideal flat surface was already hydrophobic ($\theta > 90°$). However, the Wenzel theory has certain limitations. This theory only applies to homogeneous wetting situations, in which there is a full contact between the liquid and solid substrate.

In many cases, however, such full contact is not encountered. The droplet may sit on the top of the surface without penetrating its rough structure. This situation is described as the "Cassie-Baxter state".[62] Both the "Wenzel" and "Cassie-Baxter" states are illustrated in Figure 1.15. The modified Cassie's equation is shown in equation 1.3:

$$\cos\theta' = rf\cos\theta - (1 - f) \qquad (1.3)$$

where f is the fraction of the solid/liquid interface and $(1 - f)$ is that of the gas/liquid interface, which indicates that air may be trapped between a liquid droplet and a rough solid surface. In general, the contact angle increases as f decreases. The trapped air layer is able to contribute dramatically to

the superhydrophobicity of a surface. Therefore, the construction of rough structures such as microstructures, nanostructures or even hierarchical structures incorporating both micro- and nanoscaled structures is another important factor in the fabrication of superhydrophobic surfaces.

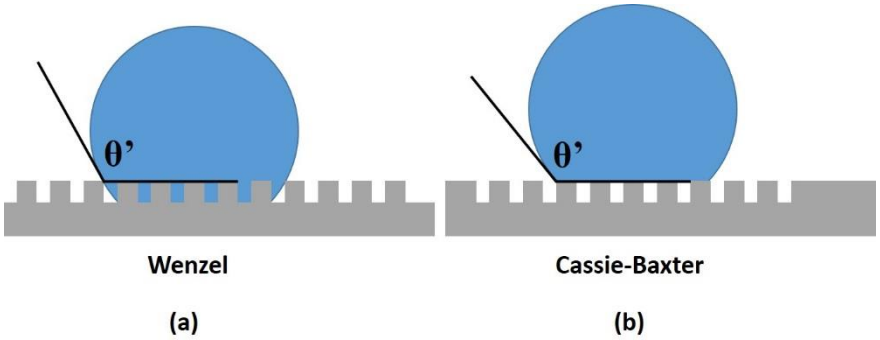

Figure 1.15 A water droplet on a rough surface that is in the "Wenzel state" (a) and the "Cassie-Baxter state" (b).

1.2.2 Superhydrophobic Cotton Coatings

1.2.2.1 Significance of Superhydrophobic Cotton Coatings

In the field of superhydrophobic surfaces, the fabrication of highly water-repellent cotton textiles has received significant attention due to the many potential applications of cotton fabrics with special wettability.[56, 65-68] Functionalized cotton can be used to prepare conventional waterproof or even self-cleaning products, such as jackets, shirts, ties and boots.[56, 65] In addition, superhydrophobic cotton fabrics can also be used to clean up oil-spills because they absorb oil but repel water.[66, 67] Partially water-repellent cotton fabrics with special hydrophilic patterns can even be used as flexible analytical devices.[68, 69] Recently, many methods have been developed to fabricate superhydrophobic cotton fabrics. A general strategy is to modify the cotton fibers with hydrophobic coatings. Further details of some of these approaches will be provided in the following sections.

1.2.2.2 Cotton Coatings Bearing Low Surface Energy Molecules

The surfaces of cotton fabrics are inherently rough, so coating these fabrics with small molecules that provide a low surface energy can yield highly water-repellent cotton textiles.[70-72] The most promising candidates are fluorinated small-molecule coupling agents that bear a fluorinated tail and a functional head-group. Their fluorinated tail is used to provide a low surface energy, while the head-group is used to react with the cotton substrate in order to provide the covalent attachment. Fluorinated silanes have been used in this manner. For instance, Fan and coworkers developed hydrophobic cellulose materials (cotton and paper) by coating the substrate with fluorinated silane molecules (FSM, Figure 1.16) using an electro-spraying technique.[70] In another case, a small molecule bearing a fluorinated tail and a photo-reactive diazirine head-group was covalently attached onto cellulose fibers to fabricate hydrophobic cotton fabric.[71]

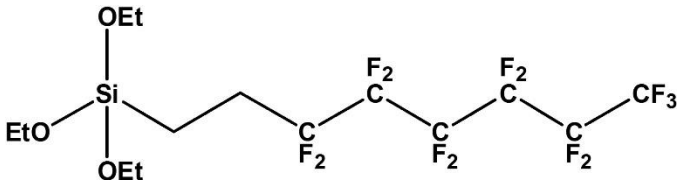

Figure 1.16 Chemical structure of a typical fluorinated coupling agent.

Due to their flexibility, good processability and low surface energies, polymers have become one of the most promising materials for the construction of superhydrophobic surfaces.[73] Therefore, cotton fabrics have been coated with polymers through both physical deposition and chemical grafting techniques. These coating strategies will be briefly described below.

Physical deposition is a relatively facile method for coating a substrate. The commercially-available polymer polytetrafluoroethylene (Teflon) has been deposited onto cotton fabrics by both the sputtering[74] and pulsed laser deposition (PLD) techniques.[75] Hydrophobic or even superhydrophobic cotton textiles were fabricated through these approaches without the use of solvents or other additives. Nevertheless, a drawback of the physical vapor deposition (PVD)

method is the poor durability of the resultant coatings, which limits the practical application of this technique.

To overcome the shortcomings of physical deposition, the chemical grafting of polymers onto cotton surfaces provides an efficient method. Li and coworkers reported a superhydrophobic cotton fabric that was prepared by radiation-induced graft polymerization of a commercially-available fluorinated acrylate monomer, 1H,1H,2H,2H-nonafluorohexyl-1-acrylate (F4, Figure 1.17), onto the cotton substrate.[76] With a high degree of polymer grafting (27.3 wt%), the treated cotton fabric still retained its superhydrophobicity after it was subjected to a laundering test, which indicated that the chemical grafting improved the stability of the coating.

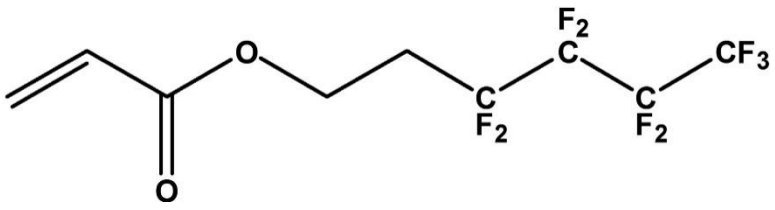

Figure 1.17 Chemical structure of the 1H,1H,2H,2H-nonafluorohexyl-1-acrylate monomer.

1.2.2.3 Cotton Coating with Nanomaterials and Low Surface Energy Molecules

As mentioned previously, increasing the surface roughness can enhance the hydrophobicity of a surface according to both Wenzel's and Cassie's theories. Therefore, various modified inorganic/organic hybrid nanomaterials such as nanoparticles,[66, 67, 77-81] nanorods[82, 83] and nanotubes[84, 85] have been used to prepare superhydrophobic cotton fabrics.

Coating silica nanoparticles onto cotton fibers is a typical strategy for fabricating superhydrophobic cotton textiles. Silica nanoparticles can be easily produced via hydrolysis and condensation reactions involving a silane precursor under acidic or basic conditions. For example, Lin and coworkers reported a technique that utilized a silica nanoparticle-based coating solution that was prepared by the co-hydrolysis and condensation of tetraethylorthosilicate (TEOS) and a

fluorinated alkyl silane under alkaline conditions.[78] This solution could be easily coated onto various substrates, including cotton fabrics, to form a superhydrophobic surface by dip-coating and spray-coating approaches. The coated cotton fabrics exhibited extremely large water contact angles of 173.7 ± 3.2° due to the high roughness and low surface energies of the fluorinated silica nanoparticles (Figure 1.18).

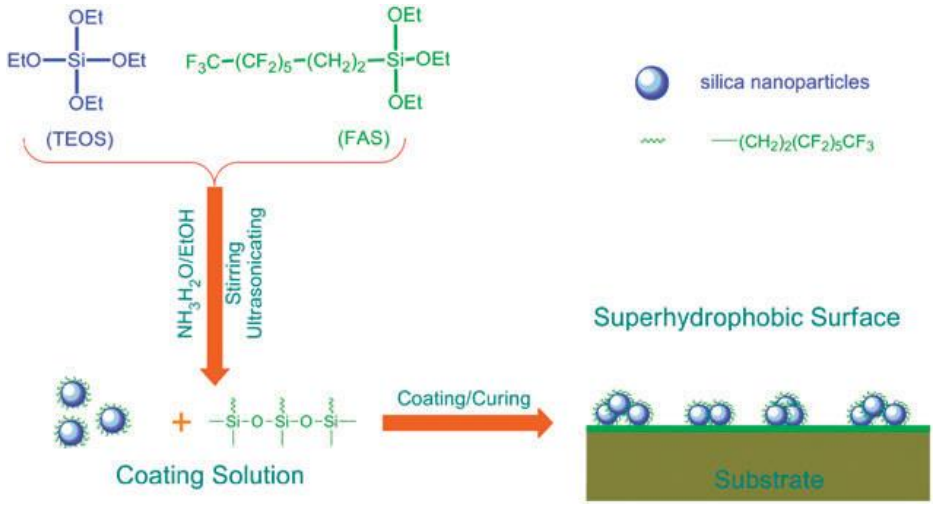

Figure 1.18 Schematic depiction of the preparation and coating of fluorinated silica nanoparticles. The structure of the resultant surface is also shown. Reprinted from Wang, H.; Fang, J.; Cheng, T.; Ding, J.; Qu, L.; Dai, L.; Wang, X.; Lin, T. *Chem. Commun*. **2008**, 877-879.

Besides silica nanoparticles, metal and metal oxide nanoparticles are also used to coat fiber substrates and to fabricate superhydrophobic cotton textiles. Guo and coworkers have reported that a series of metal/metal oxide nanoparticles could be coated onto cotton textiles to fabricate superhydrophobic surfaces after a simple modification involving alkyl thiols (Figure 1.19).[66] They pointed out that the interactions between the metals and the oxygens of the textiles improved the stability of the coating, while similar interactions between the metals and sulfur atoms of the thiol groups also allowed the facile preparation of stable coatings.

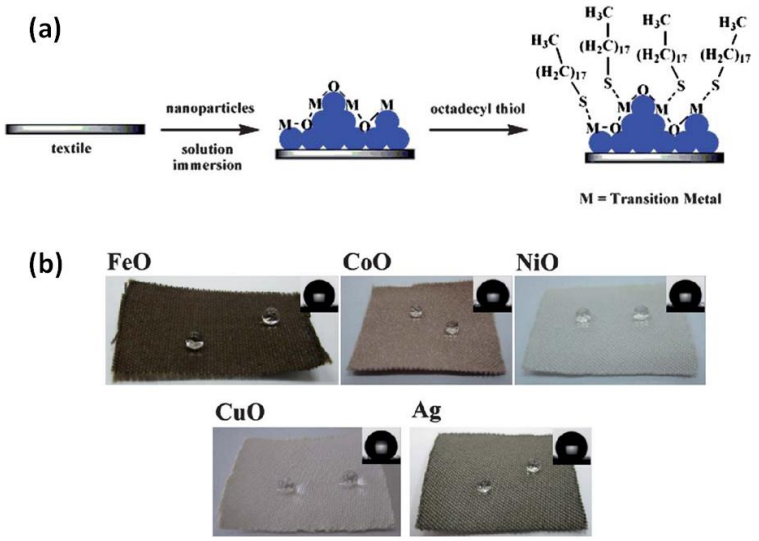

Figure 1.19 Preparation of nanoparticle-based coatings and their subsequent modification with octadecyl thiol groups (a). Images of water droplets placed on the surfaces of cotton textiles that had been coated with various metal/metal oxide nanoparticles (b). Reprinted from Li, J.; Shi, L.; Chen, Y.; Zhang, Y.; Guo, Z.; Su, B.; Liu, W. *J. Mater. Chem.* **2012**, *22*, 9774-9781.

Other nanostructures such as nanorods and nanotubes can also be used to fabricate superhydrophobic cotton textiles. A typical example is the work reported by Bai and coworkers that described the fabrication of superhydrophobic cotton textiles by dip-coating fabrics with carbon nanotube-azide polymer composites and subsequently exposing these textiles to UV irradiation (Figure 1.20).[85] The carbon nanotubes and the polymer provided a high degree of roughness and a low surface energy, respectively, to improve the hydrophobicity. The authors also pointed out that the azide groups underwent photo-reactions to generate nitrene, which could covalently bind to the cotton fabrics and thus improve the coating's stability.

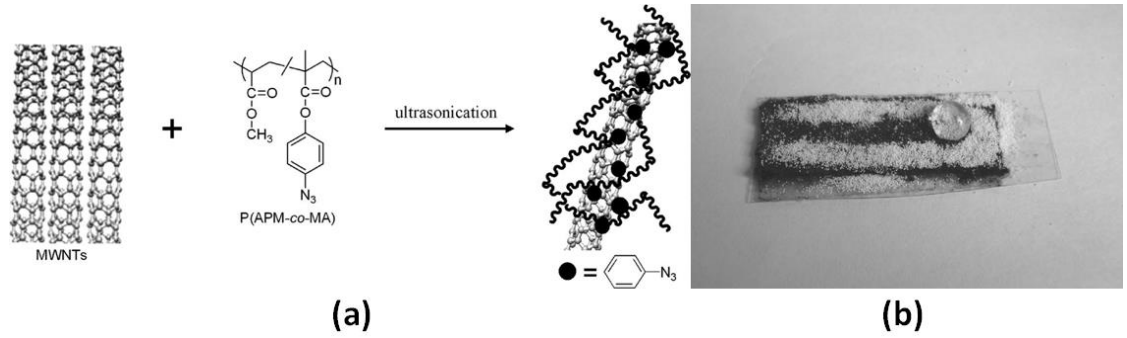

Figure 1.20 Structures of copolymer and carbon nanotube-azide polymer composites (a). Self-cleaning behavior of a cotton fabric that was coated with these materials (b). Reprinted from Li, G.; Wang, H.; Zheng, H.; Bai, R. *Langmuir* **2010**, *26*, 7529-7534.

Although introducing modified nanostructures onto a cotton surface can provide it with both a high degree of roughness and a low surface energy, there are significant barriers that must be addressed before this method can provide practical applications. In many cases, the interactions between premade nanostructures and cotton fabrics are weak, which limits the durability of the coating. On the other hand, although the stability can be enhanced by the use of metals or modified ligands that have stronger interactions with cotton fibers, coating a cotton substrate with too many heavy particles or too much of a complex composite will change the intrinsic properties of the fabric.

1.2.3 Superhydrophobic Cotton Coatings with Block Copolymers Bearing a Low Surface Energy Block

Grafting premade polymers bearing functional groups which can undergo covalent binding with cotton substrates has the potential to improve the performance of polymer-based superhydrophobic cotton coatings.[86-88] In this regard, block copolymers provide ideal candidates due to their structural diversity and their versatility. With a suitable design, the appropriate block copolymer can provide both an anchoring block and an exposed block. The anchoring block would bear functional groups that can react with or undergo crosslinking around cotton fibers to yield a covalently grafted layer. Meanwhile, an exposed block with a low surface energy could impart

superhydrophobicity. Furthermore, the grafting of such premade polymers onto a substrate can be accomplished through a solution coating method that is simple and can also produce a uniform coating.

An example of a suitable premade polymer is an azide-bearing triblock copolymer incorporating a poly(2,2,3,4,4,4-hexafluorobutyl acrylate) block, which was used to fabricate superhydrophobic cotton fabric by a solution coating approach.[87] The structure of this copolymer is shown in Figure 1.21a. Evidently, the copolymers were covalently attached onto the surface of the cotton fabric by the reaction of the azide groups with the cotton fibers upon UV irradiation, while the fluorinated polymer chains transformed the cotton fabric from a hydrophilic to a superhydrophobic fabric. This coating procedure was significantly easier than those that require a polymerization to be performed on the cotton substrate. In addition, this solution coating strategy could be successfully performed using only a very small amount of coating materials. As shown in Figure 1.21b, the concentration of the polymer coating solution did not exceed 1 wt%, and a concentration of only 0.2 wt% was sufficient to achieve stable superhydrophobicity.

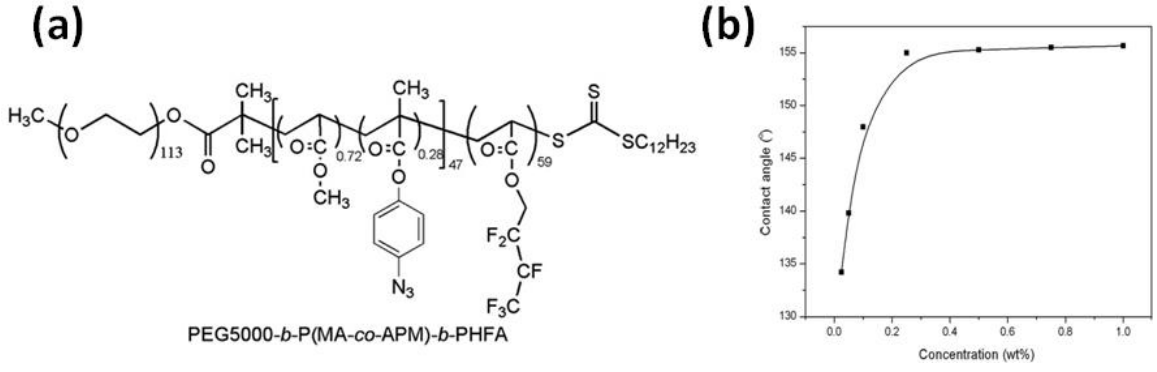

Figure 1.21 Chemical structure of the triblock copolymer PEG-*b*-P(MA-*co*-APM)-*b*-PHFA (a). The variation of the water contact angle with the concentration of the copolymer in the coating solution (b). Reprinted from Li, G.; Zheng, H.; Wang, Y.; Wang, H.; Dong, Q.; Bai, R. *Polymer* **2010**, *51*, 1940-1946.

Our group has reported that a diblock copolymer consisting of a sol-gel-forming block and a fluorinated block could be used to coat cotton fabrics, thus yielding superamphiphobic (both superhydrophobic and superoleophobic) cotton textiles.[88] The molecular structure of this copolymer is shown in Figure 1.22a. The silane-bearing anchoring block can hydrolyze and then undergo condensation with the hydroxyl groups on the surface of the cotton and with one another, thus forming a cross-linked covalently grafted layer that surrounds the cotton fibers. Superamphiphobicity was achieved due to the exposure of the fluorinated block, which has an extremely low surface energy.[60] In this study, the grafting degree of the polymer on the final cotton fabrics was also investigated. In comparison with the method of performing the polymerization directly on the cotton surface, which required a grafting degree of 10 wt%,[76] a grafting degree of only 1.0 wt% was sufficient to achieve stable superhydrophobicity via this block copolymer solution coating method. The effectiveness of such a low loading amount can be attributed to the uniform and thin grafted polymer layer.

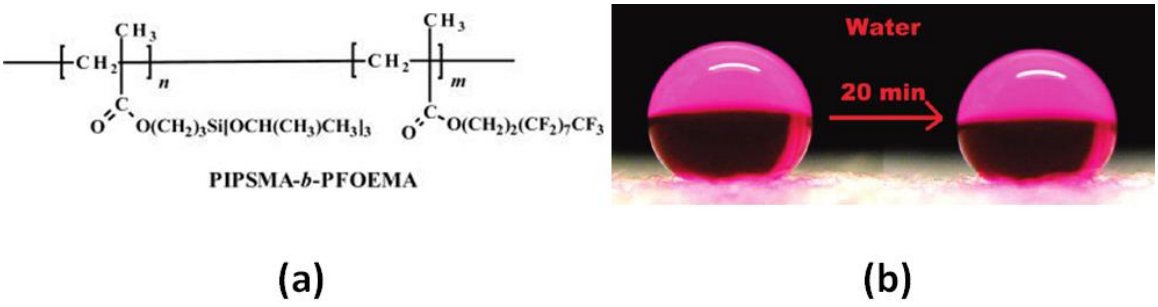

Figure 1.22 Chemical structure of the diblock copolymer PIPSMA-*b*-PFOEMA (a). Demonstration of the stable superhydrophobicity of a cotton fabric that was coated with this copolymer (b). Reprinted from Xiong, D.; Liu, G.; Duncan, E. *Langmuir* **2012**, *28*, 6911-6918.

Recently, another type of diblock copolymer poly(dimethylsiloxane)-*block*-poly[3-(triisopropyloxysilyl)propyl methacrylate] (PDMS-*b*-PIPSMA, Figure 1.23)[89] has been synthesized in our lab and used to coat cotton fabrics. The anchoring block PIPSMA is identical to that in the last example. However, in contrast with the PFOEMA block which is amphiphobic,

the exposed PDMS block is hydrophobic and oleophilic. Therefore, the coated cotton fabrics were investigated as candidates for oil-water separation applications.

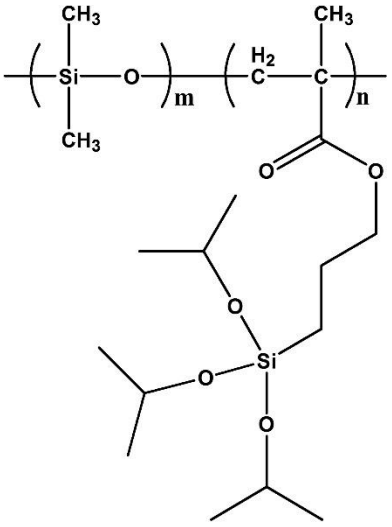

Figure 1.23 Chemical structure of PDMS-*b*-PIPSMA.

1.3 Micro/nanobubbles

1.3.1 Significance of Micro/nanobubbles

For many types of medical diagnosis, ultrasound represents the safest, fastest and least expensive method of scanning among existing diagnostic techniques.[90] However, the image quality of ultrasonography is often inferior in comparison with some other techniques such as magnetic resonance imaging (MRI).[91] Therefore, methods for improving image contrast are highly desirable. Gas micro/nanobubbles have become well established over the past three decades as the most effective type of contrast agent available for ultrasound radiography.[92] Due to their strong discontinuity in acoustic impedance as well as their high compressibility, they act as strong reflectors so that they are able to scatter ultrasound far more efficiently than red blood cells.[93] Therefore, they can allow one to observe the flow of blood under an ultrasonic field. Moreover, at moderate excitation pressures they exhibit a non-linear response which enables their scattered

signal to be clearly distinguished from that due to the tissue.[93, 94] They can thus enhance the contrast between blood and tissues that provide an excellent means of imaging tissue perfusion, particularly for cardiovascular applications and cancer diagnosis.[93, 95, 96] In addition, micro/nanobubbles have also shown great promise in therapeutic applications including targeted drug delivery, gene therapy, and focused ultrasound surgery.[97-99]

1.3.2 Development of Micro/nanobubbles

The development of micro/nanobubble ultrasound contrast agents came about as the result of an accidental discovery by Dr. Claude Joyner in the late 1960's when he injected the dye indocyanine green into a patient's left ventricle.[100] After each injection of the dye, a temporary enhancement of the ultrasound signal from the ventricle was observed. Initially it was thought that this contrast enhancement was due to the nature of the dye. It was subsequently discovered, however, that the same effect could be observed with a range of other fluids, including saline solution. Gramiak and Shah suggested that this effect was, in fact, due to the formation of air microbubbles at the catheter tip.[101]

1.3.2.1 First Generation Micro/nanobubbles

Since the discovery of ultrasound signal enhancement based on air bubbles, the first generation of microbubbles have been used as contrast agents in diagnostics, especially those focused on cardiology.[102-105] These bubbles are simply free air bubbles that are forced out of solution either by agitation or by cavitation during the solution injections. A variety of fluids such as saline solution and compounds such as indocyanine green and renografin were studied during the early stages of this research.[106, 107] It was found that the intensity of the resultant echoes varied with the type of solution used. The more viscous the solution, the more microbubbles were trapped in a bolus for a sufficient length of time to become visible in the image.

However, such free air bubbles dissolve very rapidly due to the high surface tension at the gas-air interface. As a result, the contrast enhancement is both short-lived and difficult to reproduce in

a consistent manner. Moreover, these free air bubbles (Figure 1.24) are typically very large (on the scale of several micrometers to tens of micrometers), and thus their applications are limited. For example, they are too large to cross the pulmonary capillary bed and could not be used to image the left side of the heart or to observe arterial circulation.[93, 108]

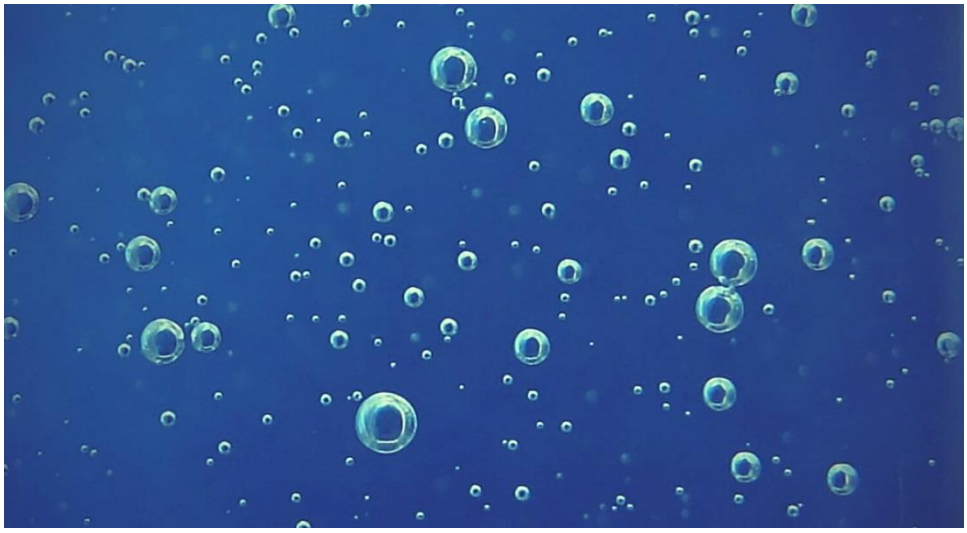

Figure 1.24 Free air bubbles in water.

1.3.2.2 Second Generation Micro/nanobubbles

To overcome the instability of the free gas bubbles, attempts were made to encapsulate gas within a shell so as to create bubbles with better stability. For example, Carroll and coworkers encapsulated nitrogen bubbles in gelatin and used them as ultrasound contrast agents.[109] However, these bubbles were still too large (~ 80 μm). The challenge to produce stable encapsulated microbubbles that could survive passage through the heart and the pulmonary capillary network was first met by Feinstein and his coworkers in 1984.[110] They mixed a suspension of microbubbles with a small amount of the patient's blood. The stability of the resultant microbubbles was found to be due to the formation of a coating of serum albumin on the surfaces of the bubbles, which counteracted the effects of surface tension. This discovery led to the development of one of the

first commercial contrast agents, Albunex® (Molecular Biosystems now part of Mallinckrodt Inc. Hazelwood, MO, USA). Subsequently, various other commercial air microbubbles were fabricated by using different encapsulating materials such as lipids (Levovist®, Schering Inc.), spray-dried albumin (Quantison™, Quadrant Inc.), galactose matrix (Ecovist®, Schering Inc.) and sonicated dextrose albumin (PESDA®, Porter Inc.).[93]

1.3.2.3 Third Generation Micro/nanobubbles

The shells of the microbubbles described in the previous section are typically extremely thin so that they can allow a gas such as air to diffuse outwardly and return into the bloodstream. Despite their improvements, the second generation of microbubbles are not sufficiently stable for widespread applications. Therefore, a newer version of micro/nanobubbles has been developed. Instead of air, some types of perfluorocarbons have been used as the core of these bubbles. Their ultra-low water solubility decreases the dissolution rate, thus increasing the longevity of the contrast agent in the blood.

Various perfluorocarbon compounds have been encapsulated to fabricate more stable micro/nanobubbles. Some of them have been commercialized including albumin-encapsulated perfluoropropane (Optison®, Mallinickrodt Inc.), surfactant-coated dodecafluoropentane (Echogen®, Sonus Inc.) and phospholipid shell-protected sulphur hexafluorane (SonoVue™, Bracco Inc.).[93] One of the most popular commercially available microbubbles is Definity® (Figure 1.25), which consists of a perfluoropropane-filled core that is encapsulated by a particularly flexible bilipid shell. This microbubble has also been used as a control sample in Chapter 4. In fact, many of these examples, especially the commercial "nanobubbles", possessed perfluorocarbon liquid droplets instead of gas bubbles as their cores. They are still called "nanobubbles" because these nanoemulsion droplets of highly volatile fluorinated liquids gasify under ultrasonication and become transient bubbles.[111, 112]

Figure 1.25 Image of the commercially available third generation microbubble Definity®. Reprinted from http://www.definityimaging.com/how-administration.html.

1.3.3 Preparation of Micro/nanobubbles

Various techniques have been developed for the preparation of micro/nanobubbles. They include conventional methods such as emulsification, as well as some new techniques that take advantage of micro/nanoscale devices.[108] In this section, some of the most useful protocols are briefly discussed.

1.3.3.1 Emulsification via Sonication

The most commonly used method for micro/nanobubble preparation is sonication, which involves dispersing a gas or liquid into a suspension of a suitable coating material using high intensity ultrasound waves.[113-115] There are thought to be two mechanisms underlying this process.[116] Firstly, the liquid is emulsified to form a suspension of micro/nanodroplets and a coating (such as a protein or a surfactant) becomes adsorbed onto their surfaces via interfacial self-assembly. Secondly, the high temperatures and pressures generated as a result of the inertial cavitation in the suspension modifies the structure of the surface layer and enhances its stability. In the case of protein coatings, this is due to the crosslinking that is promoted by the presence of superoxide from the sonolysis of water.[117] It has also been shown that the structure of the surfactant is significantly altered[118] but the processes involved are not well understood. The size and size

distribution of the resultant droplets/bubbles depends upon the frequency and power of the ultrasound. However, there is no simple theoretical relationship between these variables and thus the fabrication protocols are developed empirically.[119] The size distribution of the micro/nanobubbles obtained via sonication is inevitably relatively broad (Figure 1.26) and for microbubbles that are to be injected intravenously, it is normally necessary to fractionate and/or filter the suspension to remove any large bubbles in order to avoid the risk of an embolism.[120]

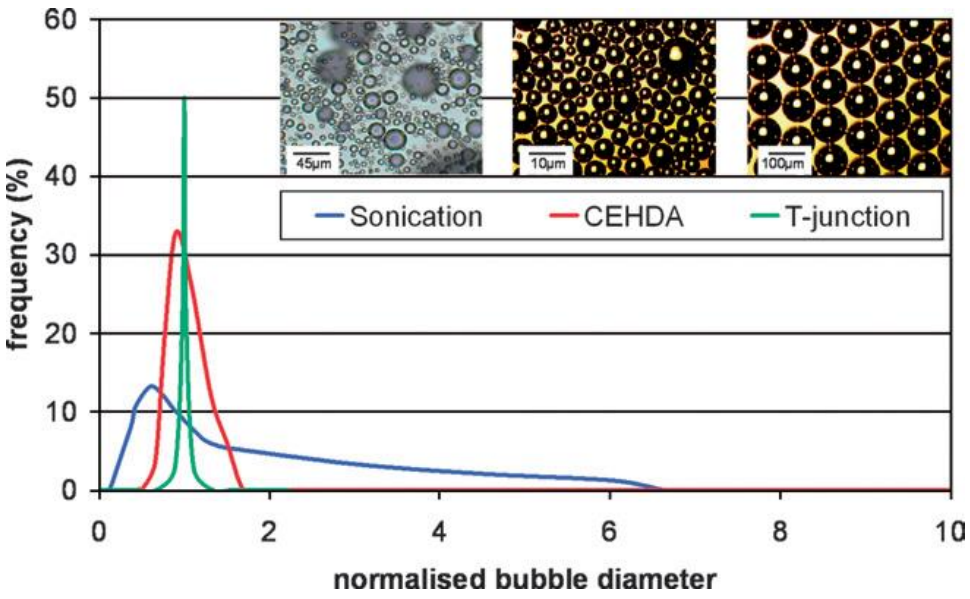

Figure 1.26 Typical size distributions of microbubbles prepared from a phospholipid suspension via sonication, using CEHDA and a microfluidic T-junction device. Reprinted from Stride, E.; Edirisinghe, M. *Soft Matter* 2008, **4**, 2350-2359.

1.3.3.2 Emulsification via High Shear Force

Another method that is commonly used, particularly for preparing polymer coated microbubbles, is to produce an oil-in-water emulsion using a polymeric surfactant (which was initially dissolved in a suitable solvent) by high shear stirring.[121, 122] The produced microspheres are washed to remove excess solvent/additive and then freeze-dried to produce gas-filled shells. In some cases, the liquid filling may only be partially removed if the microspheres are to be used for

therapeutic applications. The microbubble size distribution depends on that of the droplets in the initial emulsion and upon any fragmentation or coalescence of the microspheres during subsequent processing. Thus, for applications where the microbubble size is critical, additional filtration or fractionation may also be required.

Recently, some new strategies such as the phase inversion temperature (PIT) method and the emulsion inversion point (EIP) method have been developed for the preparation of emulsion, especially nanoemulsion, droplets with relatively narrow size distributions.[123] These approaches are suitable for the fabrication of nanocapsules (liquid-filled) and even nanobubbles (gas-filled). In the EIP method, for example, the polymeric surfactant is typically dissolved/dispersed in an oil phase first. As shown in Figure 1.27, during the addition of the water phase, a water-in-oil emulsion forms when the volume fraction of the water phase is small. During this stage, the size distribution of the water droplets is as large as that in a conventional emulsification. When more water is added into the system, the polymeric surfactant is no longer able to stabilize all of the water droplets, and thus bicontinuous or lamellar structures may form. When the amount of water reaches a critical point, phase inversion occurs spontaneously between the dispersed water phase and the continuous oil phase. An oil-in-water emulsion with a narrow size distribution finally forms.[123, 124] The nanocapsules, which were subsequently converted to nanobubbles, described in Chapter 4 were prepared by this method.

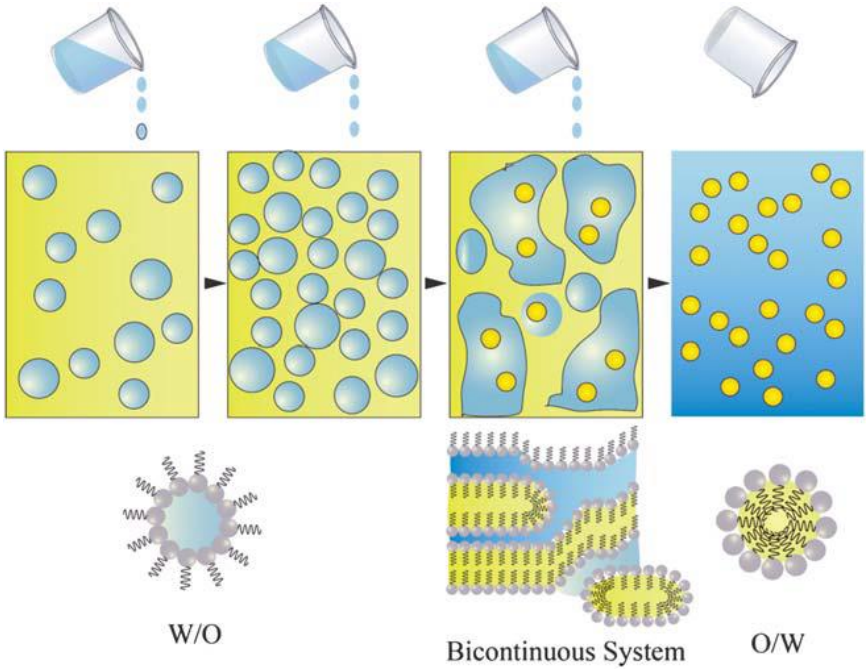

Figure 1.27 Schematic representation of the proposed mechanism for emulsification by the EIP method. Reprinted from McClements, D. *Soft Matter*, 2011, **7**, 2297–2316.

1.3.3.3 Coaxial Electrohydrodynamic Atomisation (CEHDA)

A relatively new technique that has recently been applied to microbubble preparation is coaxial electrohydrodynamic atomization (CEHDA).[125, 126] In CEHDA, a coaxial jet of two fluids is formed and then atomized to form uniform droplets. Provided that the fluids are immiscible, it is possible to encapsulate one fluid within the other. As shown in Figure 1.28, two needles are coaxially arranged and supplied with fluid from a pair of precision syringe pumps. For microbubble formation, the inner needle is supplied with gas, whilst the outer needle is supplied with a solution of the desired coating material. An electrical potential difference of several kilovolts is applied between the needles and an earthed ring electrode, which is positioned a short distance below their tips. A continuous stream of microbubbles can be produced only with certain combinations of the gas flow rate, the liquid flow rate and the applied voltage. The size of the bubbles and their size distribution can be controlled by adjusting these parameters within this range.

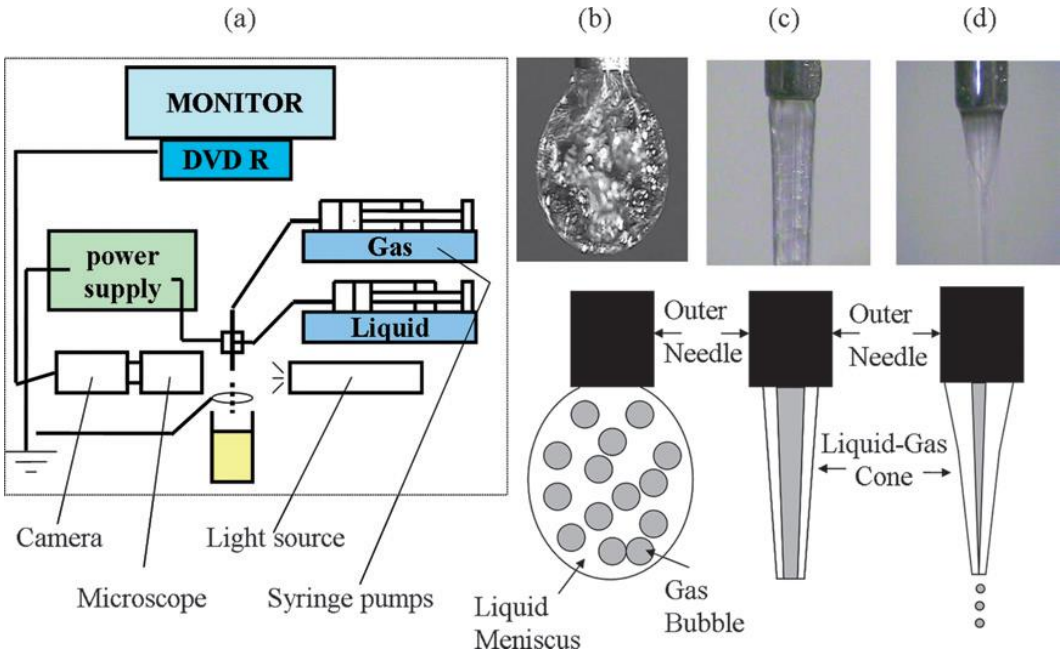

Figure 1.28 Microbubble preparation by coaxial electrohydrodynamic atomization (CEHDA): schematic depiction of a CEHDA apparatus (a); CEHDA mode 1: bubble dripping (b); CEHDA mode 2: coning (c); and CEHDA mode 3: continuous microbubbling (d). Reprinted from Stride, E.; Edirisinghe, M. *Soft Matter* 2008, **4**, 2350-2359.

The advantage of CEHDA in comparison with emulsification techniques is that the produced bubbles have a uniform size. Furthermore, a significant additional advantage is that gas bubbles can be formed in a single step without the need for further processing. Moreover, for therapeutic applications, CEHDA offers the potential for preparing microbubbles with multi-layered coatings, again in a single step, by increasing the number of liquid streams from which the coaxial jet is formed. The drawback of CEHDA in comparison with emulsification is also obvious. The apparatus required for this method is relatively complex and the rate of micro/nanobubble fabrication is relatively slow.

1.3.3.4 Microfluidic Devices

Microbubbles can also be prepared with a high degree of control over their size and polydispersity using microfluidic devices.[127] However, unlike a CEHDA apparatus, microfluidic devices only offer operational control under very limited pressure and flow rate conditions. This

method is well established for the preparation of monodisperse liquid droplets[128-130] and more recently it has been used to prepare microbubble suspensions.[131-133] To date there are two classes of microfluidic devices that have been used for bubble preparation. These include flow focusing units that are produced using soft lithography techniques[131, 133] and mechanically assembled units consisting of capillaries housed in a polymeric block arranged to form a T-junction.[132] In both cases, the essential feature of the device is an orifice at which a column of gas impinges upon a liquid flow and is focused into a jet. Subsequently, at a certain distance from the orifice, the gas–liquid interface becomes unstable and bubbles are formed by a ‘‘pinch-off’’ process (Figure 1.29).[134]

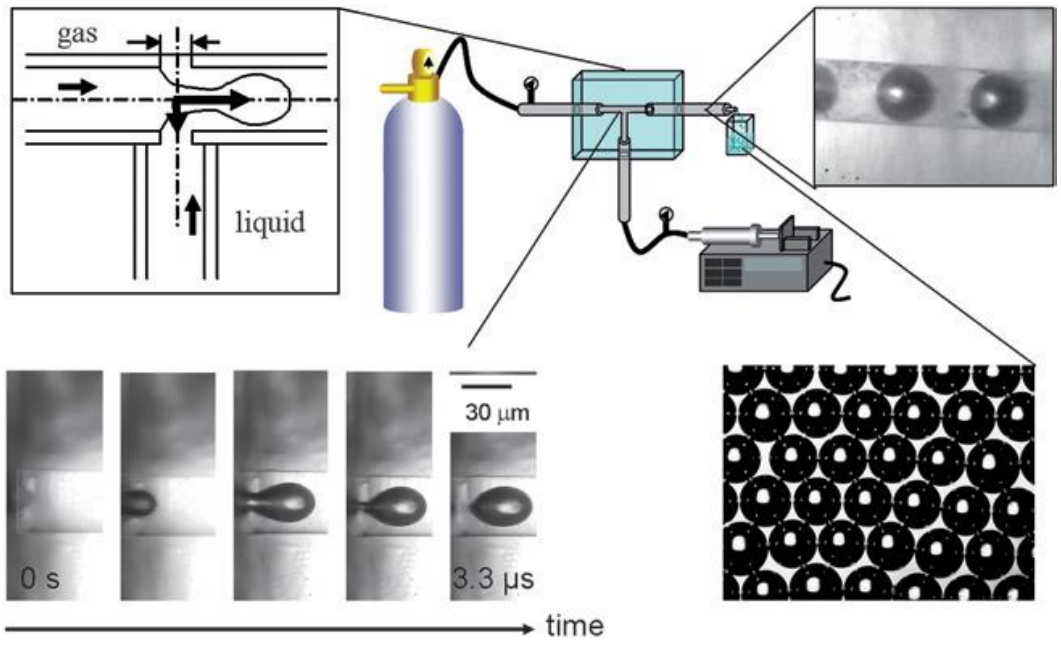

Figure 1.29 Microbubble preparation by a microfluidic T-junction device. Reprinted from Stride, E.; Edirisinghe, M. *Soft Matter* 2008, **4**, 2350-2359.

Microbubbles with diameters in the range of 1~100 μm have been prepared using microfluidic devices.[131, 132, 135] As with CEHDA, microfluidic devices enable bubbles to be produced in a single step and also have the potential to be used for the fabrication of multi-layered coatings.

1.3.4 Micro/nanobubbles Encapsulated by Block Copolymers

In order to increase the thickness of the encapsulating shell surrounding the micro/nanobubbles and thus enhance their stability, block copolymers, which serve as much longer surfactants, have also been used as droplet coatings. In addition, micro/nanobubbles composed of a copolymer shell are stable due to their excellent mechanical strength. The elasticity of the shell can also be controlled by adjusting the chemical composition and the molecular weight of the copolymer. As described in Section 1.1.2, there are numerous synthetic methods available to control and adjust the chemical compositions and chain lengths of block copolymers. The long polymer chains can also act as drug carriers or as ligands for targeted imaging or targeted drug delivery.[136, 137]

With outstanding biocompatibility and biodegradability,[138, 139] poly(L-lactide-*co*-glycolide) (PLGA, Figure 1.30) has been one of the most popular synthetic "block copolymers" for the encapsulation of micro/nanobubbles.[140, 141] It is often misnamed as a "block copolymer" in many papers. In fact, it is a common statistical copolymer although it can be used as a surfactant, like many block copolymers, to lower the interfacial tension during emulsification. This commercially available copolymer slowly degrades *in vivo* into lactic and glycolic acid. In addition, these products can further degrade into carbon dioxide and water via the tricarboxylic acid cycle.

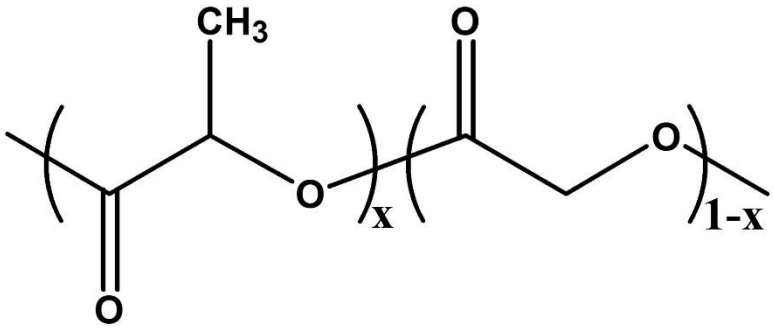

Figure 1.30 Chemical structure of PLGA.

A few types of true block copolymers have been used as micro/nanobubble coatings.[142-144] For example, Rapoport and coworkers have employed the amphiphilic block copolymers poly(ethylene glycol)-*block*-poly(L-lactide) (PEG-*b*-PLLA) and poly(ethylene glycol)-*block*-poly(caprolactone) (PEG-*b*-PCL, Figure 1.31) to form polymeric micelles as well as perfluorocarbon-filled micro/nanoemulsions for theranostic applications combining ultrasonic tumor imaging and targeted chemotherapy.[143] These block copolymers are also typical biodegradable polymers.

However, the stability enhancement achieved using the above mentioned copolymer-based coatings is still very limited in comparison with those of natural materials such as phospholipids or serum albumin. Therefore, exploiting more kinds of block copolymers with new functions that can significantly increase the stability of micro/nanobubbles is important. That is the motivation of the research described in Chapter 4.

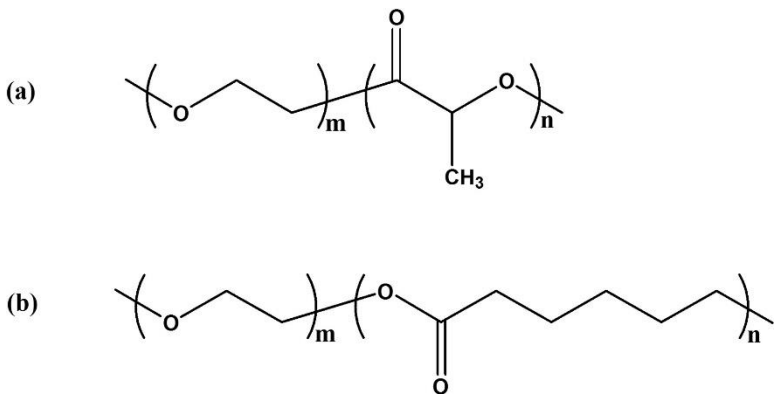

Figure 1.31 Chemical structures of PEG-*b*-PLLA (a) and PEG-*b*-PCL (b).

The research described in this thesis focuses on the synthesis and/or the applications of block copolymers bearing a low surface energy block. As first described in Chapter 2, a new diblock copolymer poly(dimethylsiloxane)-*block*-poly(2-cinnamoyloxyethyl acrylate) (PDMS-*b*-PCEA, Figure 1.32) was synthesized via atom transfer radical polymerization (ATRP) and chemical derivatization. This diblock copolymer was used as a building block for general and hydrophilically-patterned superhydrophobic cotton coatings. A new application, using this

patterned superhydrophobic cotton fabric as a cotton-based stamp, was subsequently developed. As described in Chapter 3, another diblock copolymer poly(dimethylsiloxane)-*block*-poly(glycidyl methacrylate) (PDMS-*b*-PGMA, Figure 1.32) was also synthesized via ATRP. This diblock copolymer was used as a coating to prepare a novel superhydrophobic cotton fabric, which was subsequently used to perform oil-water separations. In addition, one more type of coated cotton was fabricated. In this latter case, crosslinked polymeric nanoparticles composed of poly(styrene-*co*-glycidyl methacrylate) were chemically attached to the surfaces of cotton fibers before they were subsequently coated with PDMS-*b*-PGMA. The oil-water separation capabilities of these two types of cotton fabrics, which were coated either with a diblock copolymer alone or alternatively with both nanoparticles and a diblock copolymer, were comprehensively investigated and compared. Based on our group's research experience with these hydrophobic and even amphiphobic surface coatings, a fluorinated triblock terpolymer poly(acrylic acid)-*block*-poly(2-cinnamoyloxyethyl methacrylate)-*block*-poly(2-perfluorooctylethyl methacrylate) (PAA-*b*-PCEMA-*b*-PFOEMA, Figure 1.32) was synthesized via anionic polymerization and chemical derivatization as described in Chapter 4. This triblock terpolymer was used to prepare unprecedented stable water-dispersible air nanobubbles which had great potential in ultrasound-based diagnostics and therapies. Using this unconventional thinking, this work had not only exploited a novel application for our block copolymer bearing an ultra-low surface energy block, but also significantly enhanced the stability of air nanobubbles, which has been a primary challenge hindering the development of existing micro/nanobubbles.

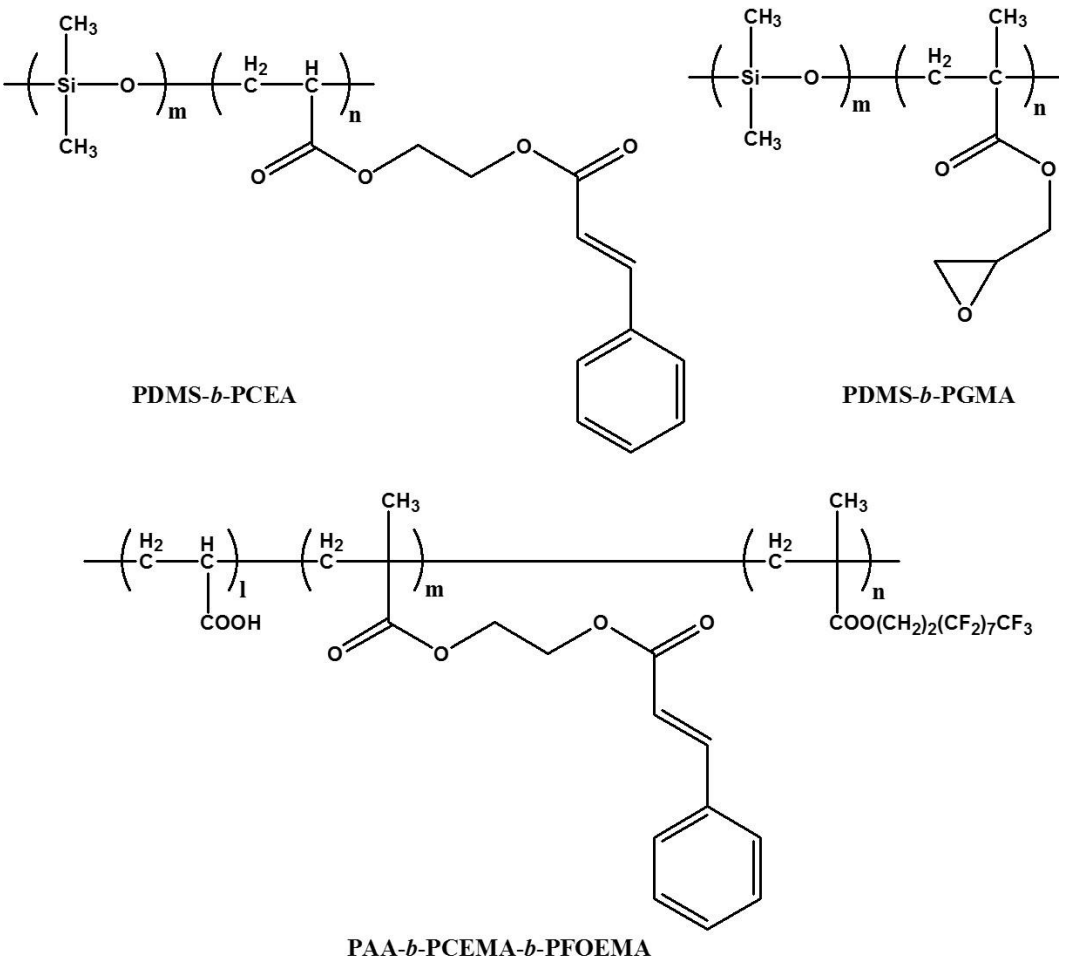

Figure 1.32 Chemical structures of the key block copolymers reported in this thesis.

References

1. A. D. Jenkins, P. Kratochvil, R. F. T. Stepto and U. W. Suter, *Pure Appl. Chem.*, 1996, **68**, 2287-2311.

2. K. Yu and A. Eisenberg, *Macromolecules*, 1996, **29**, 6359-6361.

3. A. Knoll, R. Magerle and G. Krausch, *J. Chem. Phys.*, 2004, **120**, 1105-1116.

4. W. B. Zha, C. D. Han, H. C. Moon, S. H. Han, D. H. Lee and J. K. Kim, *Polymer*, 2010, **51**, 936-952.

5. M. Szwarc, M. Levy and R. Milkovich, *J. Am. Chem. Soc.*, 1956, **78**, 2656-2657.

6. W. A. Braunecker and K. Matyjaszewski, *Prog. Polym. Sci.*, 2007, **32**, 93-146.

7. H. L. Q. Hsieh, R.P., *Anionic Polymerization: Principles and Practical Applications*, Marcel Dekker, New York, 1996.

8. K. Matyjaszewski, *Controlled Radical Polymerization*, ACS symposium Series 685, Washington, DC, 1998.

9. F. Schue, *Controlled/Living Radical Polymerization. Progress in ATRP, NMP, and RAFT*, ACS Symposium Series 768, Washington, DC, 2000.

10. V. Sciannamea, R. Jerome and C. Detrembleur, *Chem. Rev.*, 2008, **108**, 1104-1126.

11. H. Fischer, *Chem. Rev.*, 2001, **101**, 3581-3610.

12. L. Tebben and A. Studer, *Angew. Chem. Int. Ed.*, 2011, **50**, 5034-5068.

13. J. Chiefari, Y. K. Chong, F. Ercole, J. Krstina, J. Jeffery, T. P. T. Le, R. T. A. Mayadunne, G. F. Meijs, C. L. Moad, G. Moad, E. Rizzardo and S. H. Thang, *Macromolecules*, 1998, **31**, 5559-5562.

14. D. Taton, A. Z. Wilczewska and M. Destarac, *Macromol. Rapid Commun.*, 2001, **22**, 1497-1503.

15. C. L. McCormack and A. B. Lowe, *Acc. Chem. Res.*, 2004, **37**, 312-325.

16. M. Kato, M. Kamigaito, M. Sawamoto and T. Higashimura, *Macromolecules*, 1995, **28**, 1721-1723.

17. J. S. Wang and K. Matyjaszewski, *Macromolecules*, 1995, **28**, 7901-7910.

18. K. Matyjaszewski and J. H. Xia, *Chem. Rev.*, 2001, **101**, 2921-2990.

19. T. E. Patten and K. Matyjaszewski, *Adv. Mater.*, 1998, **10**, 901-908.

20. M. Teodorescu and K. Matyjaszewski, *Macromolecules*, 1999, **32**, 4826-4831.

21. K. Matyjaszewski, *Chem. Eur. J.*, 1999, **5**, 3095-3102.

22. F. Stoffelbach, J. Claverie and R. Poli, *Comptes Rendus Chimie*, 2002, **5**, 37-42.

23. M. A. Stump, D. M. Haddleton, A. McCamley, D. Duncalf, J. A. Segal and D. J. Irvine, *Polym. Prepr.*, 1997, **213**, 346-347.

24. Y. Kotani, M. Kamigaito and M. Sawamoto, *Macromolecules*, 1999, **32**, 2420-2424.

25. T. Ando, M. Kamigaito and M. Sawamoto, *Macromolecules*, 1997, **30**, 4507-4510.

26. Y. Wang, X. W. Teng, J. S. Wang and H. Yang, *Nano Lett.*, 2003, **3**, 789-793.

27. Q. L. Fan, K. G. Neoh, E. T. Kang, B. Shuter and S. C. Wang, *Biomaterials*, 2007, **28**, 5426-5436.

28. M. Miyamoto, M. Sawamoto and T. Higashimura, *Macromolecules*, 1984, **17**, 265-268.

29. M. Sawamoto, *Prog. Polym. Sci.*, 1991, **16**, 111-172.

30. W. D. Zhang, W. Zhang, Z. B. Zhang, J. Zhu, Q. M. Pan and X. L. Zhu, *Polym. Bull.*, 2009, **63**, 467-483.

31. V. Ladmiral, G. Mantovani, G. J. Clarkson, S. Cauet, J. L. Irwin and D. M. Haddleton, *J. Am. Chem. Soc.*, 2006, **128**, 4823-4830.

32. L. A. Ding, M. R. Xie, D. Yang and C. M. Song, *Macromolecules*, 2010, **43**, 10336-10342.

33. S. T. Milner, T. A. Witten and M. E. Cates, *Macromolecules*, 1988, **21**, 2610-2619.

34. S. T. Milner, *Science*, 1991, **251**, 905-914.

35. W. J. Brittain and S. Minko, *J. Polym. Sci. A Polym. Chem.*, 2007, **45**, 3505-3512.

36. D. Macoretta, M. Rabnawaz, C. M. Grozea, G. J. Liu, Y. Wang, A. Crumblehulme and M. Wyer, *ACS Appl. Mater. Inter.*, 2014, **6**, 21435-21445.

37. V. Roche, F. Vacandio, D. Bertin, D. GigrneS and M. Eyraud, *Comptes Rendus Chimie*, 2008, **11**, 1055-1062.

38. G. J. Liu, X. Q. Xu, K. Skupinska, N. X. Hu and H. Yao, *J. Appl. Polym. Sci.*, 1994, **53**, 1699-1707.

39. D. A. Xiong, G. J. Liu and E. J. S. Duncan, *ACS Appl. Mater. Inter.*, 2012, **4**, 2445-2454.

40. Z. L. Li, M. Tang, J. W. Dai, T. S. Wang and R. K. Bai, *Polymer*, 2016, **85**, 67-76.

41. A. Car, P. Baumann, J. T. Duskey, M. Cham, N. Bruns and W. Meier, *Biomacromolecules*, 2014, **15**, 3235-3245.

42. M. L. Adams, A. Lavasanifar and G. S. Kwon, *J. Pharm. Sci.*, 2003, **92**, 1343-1355.

43. K. Kataoka, A. Harada and Y. Nagasaki, *Adv. Drug Delivery Rev.*, 2001, **47**, 113-131.

44. G. Riess, *Prog. Polym. Sci.*, 2003, **28**, 1107-1170.

45. Z. Y. Li, H. N. Zhang, W. Zheng, W. Wang, H. M. Huang, C. Wang, A. G. MacDiarmid and Y. Wei, *J. Am. Chem. Soc.*, 2008, **130**, 5036.

46. G. Krausch and R. Magerle, *Adv. Mater.*, 2002, **14**, 1579.

47. E. A. Lysenko, T. K. Bronich, E. V. Slonkina, A. Eisenberg, V. A. Kabanov and A. V. Kabanov, *Macromolecules*, 2002, **35**, 6351-6361.

48. E. A. Lysenko, T. K. Bronich, E. V. Slonkina, A. Eisenberg, V. A. Kabanov and A. V. Kabanov, *Macromolecules*, 2002, **35**, 6344-6350.

49. L. F. Zhang and A. Eisenberg, *Polym. Adv. Technol.*, 1998, **9**, 677-699.

50. L. F. Zhang and A. Eisenberg, *Science*, 1995, **268**, 1728-1731.

51. R. H. Zheng and G. J. Liu, *Macromolecules*, 2007, **40**, 5116-5121.

52. G. D. Fu, G. L. Li, K. G. Neoh and E. T. Kang, *Prog. Polym. Sci.*, 2011, **36**, 127-167.

53. I. Wyman, G. Njikang and G. J. Liu, *Prog. Polym. Sci.*, 2011, **36**, 1152-1183.

54. S. Wang and L. Jiang, *Adv. Mater.*, 2007, **19**, 3423-3424.

55. B. Bhushan and Y. C. Jung, *Prog. Mater. Sci.*, 2011, **56**, 1-108.

56. X. Yao, Y. L. Song and L. Jiang, *Adv. Mater.*, 2011, **23**, 719-734.

57. S. Nishimoto and B. Bhushan, *RSC Adv.*, 2013, **3**, 671-690.

58. T. Young, *Philos. Trans. R. Soc. Lond.* , 1805, **95**, 65-87.

59. J. E. Mark, *Polymer Data Handbook. Oxford University Press*, 1999.

60. A. Hirao, K. Sugiyama and H. Yokoyama, *Prog. Polym. Sci.*, 2007, **32**, 1393-1438.

61. R. N. Wenzel, *Ind. Eng. Chem.*, 1936, **28**, 988-994.

62. A. B. D. Cassie and S. Baxter, *Trans. Faraday Soc.*, 1944, **40**, 0546-0550.

63. X. J. Feng and L. Jiang, *Adv. Mater.*, 2006, **18**, 3063-3078.

64. A. Tuteja, W. Choi, M. Ma, J. M. Mabry, S. A. Mazzella, G. C. Rutledge, G. H. McKinley and R. E. Cohen, *Science*, 2007, **318**, 1618-1622.

65. Editorial, *Nat. Mater.*, 2005, **4**, 355-355.

66. J. Li, L. Shi, Y. Chen, Y. B. Zhang, Z. G. Guo, B. L. Su and W. M. Liu, *J. Mater. Chem.*, 2012, **22**, 9774-9781.

67. B. Wang, J. Li, G. Wang, W. Liang, Y. Zhang, L. Shi, Z. Guo and W. Liu, *ACS Appl. Mater. Inter.*, 2013, **5**, 1827-1839.

68. A. Nilghaz, D. H. B. Wicaksono, D. Gustiono, F. A. A. Majid, E. Supriyanto and M. R. A. Kadir, *Lab Chip*, 2012, **12**, 209-218.

69. S. Y. Xing, J. Jiang and T. R. Pan, *Lab Chip*, 2013, **13**, 1937-1947.

70. M. K. Sarkar, F. A. He and J. T. Fan, *Thin Solid Films*, 2010, **518**, 5033-5039.

71. S. Ghiassian, H. Ismaili, B. D. W. Lubbock, J. W. Dube, P. J. Ragogna and M. S. Workentin, *Langmuir*, 2012, **28**, 12326-12333.

72. B. Tomsic, B. Simoncic, B. Orel, L. Cerne, P. F. Tavcer, M. Zorko, I. Jerman, A. Vilcnik and J. Kovac, *J. Sol-Gel Sci. Techn.*, 2008, **47**, 44-57.

73. Z. Xue, M. Liu and L. Jiang, *J. Polym. Sci. Polym. Phys.*, 2012, **50**, 1209-1224.

74. D. Y. Wi, I. W. Kim and J. Kim, *Fiber Polym.*, 2009, **10**, 98-101.

75. W. A. Daoud, J. H. Xin, Y. H. Zhang and C. L. Mak, *Thin Solid Films*, 2006, **515**, 835-837.

76. B. Deng, R. Cai, Y. Yu, H. Q. Jiang, C. L. Wang, J. A. Li, L. F. Li, M. Yu, J. Y. Li, L. D. Xie, Q. Huang and C. H. Fan, *Adv. Mater.*, 2010, **22**, 5473-5477.

77. M. Yu, G. Gu, W. Meng and F. Qing, *Appl. Surf. Sci.*, 2007, **253**, 3669-3673.

78. H. Wang, J. Fang, T. Cheng, J. Ding, L. Qu, L. Dai, X. Wang and T. Lin, *Chem. Commun.*, 2008, 877-879.

79. M. Lee, G. Kwak and K. Yong, *ACS Appl. Mater. Inter.*, 2011, **3**, 3350-3356.

80. H. F. Hoefnagels, D. Wu, G. de With and W. Ming, *Langmuir*, 2007, **23**, 13158-13163.

81. B. Leng, Z. Shao, G. de With and W. Ming, *Langmuir*, 2009, **25**, 2456-2460.

82. B. Xu and Z. S. Cai, *Appl. Surf. Sci.*, 2008, **254**, 5899-5904.

83. B. Xu, Z. S. Cai, W. M. Wang and F. Y. Ge, *Surf. Coat. Tech.*, 2010, **204**, 1556-1561.

84. Y. Y. Liu, R. H. Wang, H. F. Lu, L. Li, Y. Y. Kong, K. H. Qi and J. H. Xin, *J. Mater. Chem.*, 2007, **17**, 1071-1078.

85. G. A. Li, H. Wang, W. T. Zheng and R. K. Bai, *Langmuir*, 2010, **26**, 7529-7534.

86. J. Vince, B. Orel, A. Vilcnik, M. Fir, A. S. Vuk, V. Jovanovski and B. Simoncic, *Langmuir*, 2006, **22**, 6489-6497.

87. G. Li, H. T. Zheng, Y. X. Wang, H. Wang, Q. B. Dong and R. K. Bai, *Polymer*, 2010, **51**, 1940-1946.

88. D. A. Xiong, G. J. Liu and E. J. S. Duncan, *Langmuir*, 2012, **28**, 6911-6918.

89. M. Rabnawaz, Z. J. Wang, Y. Wang, I. Wyman, H. Hu and G. J. Liu, *RSC Adv.*, 2015, **5**, 39505-39511.

90. C. J. Harvey, J. M. Pilcher, R. J. Eckersley, M. J. K. Blomley and D. O. Cosgrove, *Clin. Radiol.*, 2002, **57**, 157-177.

91. T. D. Karamitsos, J. M. Francis, S. Myerson, J. B. Selvanayagam and S. Neubauer, *J. Am. Coll. Cardiol.*, 2009, **54**, 1407-1424.

92. D. Cosgrove, *Eur. J. Radiol.*, 2006, **60**, 324-330.

93. H. Becher and P. Burns, *Handbook of Contrast Echocardiography* Springer, Frankfurt and New York, 2000.

94. E. Stride and N. Saffari, *Proc. Inst. Mech. Eng. H J. Eng. Med.*, 2003, **217**, 429-447.

95. J. R. Lindner, *Nat. Rev. Drug Discov.*, 2004, **3**, 527-532.

96. F. Frauscher, A. Klauser, E. J. Halpern, W. Horninger and G. Bartsch, *Lancet*, 2001, **357**, 1849-1850.

97. J. L. Bull, *Expert Opin. Drug Deliv.*, 2007, **4**, 475-493.

98. S. P. Bao, B. D. Thrall and D. L. Miller, *Ultrasound Med. Biol.*, 1997, **23**, 953-959.

99. G. T. Clement, *Ultrasonics*, 2004, **42**, 1087-1093.

100. Feigenba.H, J. M. Stone, D. A. Lee, W. K. Nasser and S. Chang, *Circulation*, 1970, **41**, 615-&.

101. R. Gramiak and P. Shah, *Invest. Radiol.*, 1968, **3**, 356-366.

102. R. E. Kerber, J. M. Kioschos and R. M. Lauer, *Am. J. Cardiol.*, 1974, **34**, 722-727.

103. C. L. Reid, D. T. Kawanishi, C. R. McKay, U. Elkayam, S. H. Rahimtoola and P. A. N. Chandraratna, *Am. J. Cardiol.*, 1983, **52**, 519-524.

104. L. M. Valdescruz and D. J. Sahn, *J. Am. Coll. Cardiol.*, 1984, **3**, 978-985.

105. J. Roelandt, *Ultrasound Med. Biol.*, 1982, **8**, 471.

106. M. C. Ziskin, Bonakdar.A, Weinstei.Dp and P. R. Lynch, *Invest. Radiol.*, 1972, **7**, 500-505.

107. F. W. Kremkau, R. Gramiak, Carstens.El, P. M. Shah and D. H. Kramer, *J. Acoust. Soc. Am.*, 1969, **45**, 340.

108. E. Stride and M. Edirisinghe, *Soft Matter*, 2008, **4**, 2350-2359.

109. B. A. Carroll, R. J. Turner, E. G. Tickner, D. B. Boyle and S. W. Young, *Invest. Radiol.*, 1980, **15**, 260-266.

110. S. B. Feinstein, F. J. Tencate, W. Zwehl, K. Ong, G. Maurer, C. Tei, P. M. Shah, S. Meerbaum and E. Corday, *J. Am. Coll. Cardiol.*, 1984, **3**, 14-20.

111. R. Cavalli, A. Bisazza and D. Lembo, *Int. J. Pharm.*, 2013, **456**, 437-445.

112. N. Rapoport, K. H. Nam, R. Gupta, Z. G. Gao, P. Mohan, A. Payne, N. Todd, X. Liu, T. Kim, J. Shea, C. Scaife, D. L. Parker, E. K. Jeong and A. M. Kennedy, *J. Controlled Release*, 2011, **153**, 4-15.

113. E. C. Unger, T. P. McCreery, R. H. Sweitzer, V. E. Caldwell and Y. Q. Wu, *Invest. Radiol.*, 1998, **33**, 886-892.

114. Y. Z. Zhao, H. D. Liang, X. G. Mei and M. Halliwell, *Ultrasound Med. Biol.*, 2005, **31**, 1237-1243.

115. C. Christiansen, H. Kryvi, P. C. Sontum and T. Skotland, *Biotechnol. Appl. Biochem.*, 1994, **19**, 307-320.

116. K. S. Suslick, Y. Didenko, M. M. Fang, T. Hyeon, K. J. Kolbeck, W. B. McNamara, M. M. Mdleleni and M. Wong, *Philos. T R Soc. A*, 1999, **357**, 335-353.

117. K. S. Suslick and M. W. Grinstaff, *J. Am. Chem. Soc.*, 1990, **112**, 7807-7809.

118. W. H. Wang, C. C. Moser and M. A. Wheatley, *J. Phys. Chem.*, 1996, **100**, 13815-13821.

119. M. W. Grinstaff and K. S. Suslick, *Proc. Natl. Acad. Sci. USA*, 1991, **88**, 7708-7710.

120. W. L. Nyborg, *Ultrasound Med. Biol.*, 2001, **27**, 301-333.

121. K. Bjerknes, K. Dyrstad, G. Smistad and I. Agerkvist, *Drug Dev. Ind. Pharm.*, 2000, **26**, 847-856.

122. B. B. Jiang, C. Y. Gao and J. C. Shen, *Colloid Polym. Sci.*, 2006, **284**, 513-519.

123. N. Anton, J.-P. Benoit and P. Saulnier, *J. Controlled Release*, 2008, **128**, 185-199.

124. D. J. McClements, *Soft Matter*, 2011, **7**, 2297-2316.

125. U. Farook, E. Stride, M. J. Edirisinghe and R. Moaleji, *Med. Biol. Eng. Comput.*, 2007, **45**, 781-789.

126. U. Farook, H. B. Zhang, M. J. Edirisinghe, E. Stride and N. Saffari, *Med. Eng. & Phys.*, 2007, **29**, 749-754.

127. G. M. Whitesides, *Nature*, 2006, **442**, 368-373.

128. S. L. Anna, N. Bontoux and H. A. Stone, *Appl. Phys. Lett.*, 2003, **82**, 364-366.

129. Q. Y. Xu and M. Nakajima, *Appl. Phys. Lett.*, 2004, **85**, 3726-3728.

130. P. Garstecki, I. Gitlin, W. DiLuzio, G. M. Whitesides, E. Kumacheva and H. A. Stone, *Appl. Phys. Lett.*, 2004, **85**, 2649-2651.

131. K. Hettiarachchi, E. Talu, M. L. Longo, P. A. Dayton and A. P. Lee, *Lab Chip*, 2007, **7**, 463-468.

132. K. P. Pancholi, U. Farook, R. Moaleji, E. Stride and M. J. Edirisinghe, *Eur. Biophys. J. Biophy.*, 2008, **37**, 515-520.

133. B. Dollet, W. van Hoeve, J. P. Raven, P. Marmottant and M. Versluis, *Phys. Rev. Lett.*, 2008, **100**.

134. K. Pancholi, E. Stride and M. Edirisinghe, *Langmuir*, 2008, **24**, 4388-4393.

135. E. Talu, K. Hettiarachchi, R. L. Powell, A. P. Lee, P. A. Dayton and M. L. Longo, *Langmuir*, 2008, **24**, 1745-1749.

136. K. E. Uhrich, S. M. Cannizzaro, R. S. Langer and K. M. Shakesheff, *Chem. Rev.*, 1999, **99**, 3181-3198.

137. S. Hernot and A. L. Klibanov, *Adv. Drug Delivery Rev.*, 2008, **60**, 1153-1166.

138. R. A. Jain, *Biomaterials*, 2000, **21**, 2475-2490.

139. R. C. Mundargi, V. R. Babu, V. Rangaswamy, P. Patel and T. M. Aminabhavi, *J. Controlled Release*, 2008, **125**, 193-209.

140. F. Forsberg, J. D. Lathia, D. A. Merton, J. B. Liu, N. T. Le, B. B. Goldberg and M. A. Wheatley, *Ultrasound Med. Biol.*, 2004, **30**, 1281-1287.

141. W. J. Cui, J. Z. Bei, S. G. Wang, G. Zhi, Y. Y. Zhao, X. S. Zhou, H. W. Zhang and Y. Xu, *J. Biomed. Mater. Res. B Appl. Biomater.*, 2005, **73B**, 171-178.

142. Z. Gao, A. M. Kennedy, D. A. Christensen and N. Y. Rapoport, *Ultrasonics*, 2008, **48**, 260-270.

143. N. Rapoport, Z. G. Gao and A. Kennedy, *J. Natl. Cancer Inst.*, 2007, **99**, 1095-1106.

144. N. Y. Rapoport, A. M. Kennedy, J. E. Shea, C. L. Scaife and K. H. Nam, *J. Controlled Release*, 2009, **138**, 268-276.

Chapter 2

Hydrophilically Patterned Superhydrophobic Cotton Fabrics Coated with Poly(dimethylsiloxane)-based Diblock Copolymer Bearing Photo-Crosslinkable Block

2.1 Introduction

Coating a hydrophilic cotton fabric with hydrophobic moieties may turn the fabric superhydrophobic.[1-9] Superhydrophobic cotton fabrics strongly repel water because they possess water contact and shedding angles exceeding 150° and below 10°, respectively.[10-12] Superhydrophobic fabrics have a wide range of applications.[13, 14] For example, they can be used for waterproof tents, canvas, or umbrellas. If the fabrics still possesses good hand (feel) and breathability, they can be used for waterproof outerwear.

The simplest method to coat cotton is to polymerize a hydrophobic monomer and crosslink the resultant polymer around the cotton fibers.[1, 7, 15-18] An alternative method is to graft an alkyl compound onto cotton fibers.[19-21] The coating obtained from the latter process may be a thin monolayer, with a thickness less than 1 nm. To increase the monolayer thickness to the scale of nanometers or tens of nanometers, block copolymers can be used to coat cotton fabrics. A suitable block copolymer for such a coating would bear an anchoring block that becomes covalently linked to or crosslinked around the cotton fibers and another block that renders the desired water-repellency (and sometimes also oil-repellency) to the textile.[4, 22-24]

A coating provides water and sometimes also oil repellency because it reduces the surface tension of the cotton substrate. While alkyl compounds can reduce surface tensions down to 25 - 30 mN/m, a fluorinated compound reduces the surface tension down to ~6.7 mN/m.[25, 26] These

values are substantially smaller than the surface tension of water, which is 72.8 mN/m at room temperature.[27] High water contact angles and low shedding angles are possible on coated fabrics also because of their intrinsic roughness.[28-31] Fabrics are woven from threads that are composed of bundles of fibers and void spaces thus exist between the different threads and the different fibers. A water droplet that is in the Wenzel state[30] (droplet bottom in full contact with the substrate) does not spread as much on a rough but inherently hydrophobic surface as on a flat surface because the same degree of spreading on the former surface creates a larger water/substrate contact area and costs more energy. Analogously, a water droplet that is in the Cassie state[31] (hanging over protrusions and trapping air in the cavities) does not readily spread so that it can minimize the free energy.

Unimolecular block copolymer coatings have so far been applied onto cotton fabrics by grafting one block of a copolymer onto cotton fibers or crosslinking the block around them or by using the grafting and crosslinking mechanisms simultaneously.[4, 22-24] The trigger for these coating reactions has included catalysts or heat. In principle, light can also be used to trigger these reactions. This chapter describes the synthesis of a diblock copolymer poly(dimethylsiloxane)-*block*-poly(2-cinnamoyloxyethyl acrylate) (PDMS-*b*-PCEA, Figure 2.1), and the subsequent use of this copolymer to coat cotton fabrics. The PCEA block wraps around cotton fibers during cotton coatings and crosslinks during UV photolysis via the dimerization of the pendant CEA double bonds of different PCEA chains.[32-34] In addition, the PDMS block has a low surface tension of ~20 mN/m at room temperature[26] and thus provides the water-repellency.

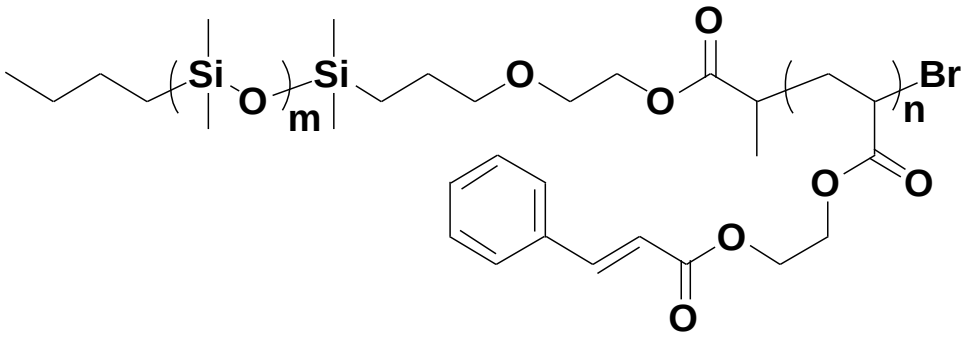

Figure 2.1 Chemical structure of PDMS-*b*-PCEA.

The photo-crosslinking of PCEA also offers the possibility for creating patterned coatings. After the cotton textile fibers are wrapped by PCEA after coating by the diblock copolymer, one can protect certain regions of the fabric with a mask and subsequently irradiate the fabric. While the polymer in the exposed regions becomes crosslinked and cannot be removed by solvent extraction, the coating can be readily removed from the non-irradiated regions to re-generate the hydrophilic fibers. Thus, this chapter also describes the use of the above method to create a superhydrophobic cotton fabric that bears a hydrophilic pattern.

Patterns possessing different wettability have so far been prepared on substrates of inorganic materials,[35, 36] polymer films,[37, 38] paper,[19, 39-41] electrospun fibers,[42] and woven silk.[43] These surfaces with patterned wettability can be used to regulate liquid transport,[39, 44-46] liquid evaporation and condensation,[47, 48] guide self-assembly of molecules or nanoparticles,[37, 42] as well as encode chemical information.[49] Even nature has this kind of patterned surfaces as well. For example, the wings of the Stenocara beetles of the Namib Desert consist of hydrophilic bumps surrounded by a hydrophobic matrix. These hydrophilic bumps collect water droplets from the morning fog. Once the condensed droplets become large enough so that their gravitational force overcomes the van der Waals force between the droplets and the hydrophilic bumps, the droplets roll down the hydrophobic regions into the beetle's mouth.[48]

Hydrophilically-patterned cotton fabrics have also been prepared and have even been used as inexpensive microfluidic devices for facile medical diagnostic tests or biofluidic transport.[50, 51] To

prepare hydrophobic patterns on cotton fabrics, the traditional batik painting technique can be used.[50] In batik painting, molten wax is first infused into regions to create hydrophobic patterns that do not need to be dyed. The hydrophilic regions are then dyed to produce a colored pattern. Hydrophilic patterns have also been prepared by stitching hydrophilic cotton yarn into a hydrophobic fabric substrate.[51] However, the use of block copolymers in the fabrication of hydrophilically-patterned superhydrophobic cotton fabrics has not been reported. In addition, this chapter also describes the use of hydrophilically-patterned superhydrophobic cotton fabrics as a stamp for ink printing.

2.2 Experimental

2.2.1 Materials

Plain-weave cotton fabric used was purchased from a local store. Based on our previous characterization (optical, scanning electron and atomic force microscopy), the fabrics had warp and weft thread diameters of 270 ± 10 and 620 ± 10 μm, respectively.[4] In addition, the fibers were imperfect cylinders with rough surfaces. Before use, a 20 cm x 20 cm swatch of the fabric was stirred at 300 rpm in 500 mL of an aqueous 5.0 wt% Fisher Sparkleen detergent at room temperature for 15 min before it was transferred into 500 mL of distilled water and was stirred at 300 rpm for 15 min. This rinsing process was repeated thrice before the swatch was dried at 120 °C for 20 min. The sample was subsequently cut into small pieces with various sizes to be used for various experiments. The substrates used for ink printing included cotton fabrics, semi-synthetic fabric (65% polyester/35% cotton), cardboard, printing paper, wood and aluminum foil. All of these substrates were purchased from local stores and used as received.

Tetrahydrofuran (THF, Fisher) was distilled over sodium and a trace amount of benzophenone. Pyridine (Fisher) was refluxed and distilled over CaH_2. 2-Trimethylsiloxyethyl acrylate (HEA-TMS) was synthesized according to a literature method[52] and distilled over CaH_2 before use. CuBr

(Aldrich, 99.999%) was stirred with glacial acetic acid and washed with pure ethanol. Chloroform (Fisher, 99.9%) was passed through a membrane filter (Durapore, 0.45μm) before it was used as a SEC eluent. 2-Bromopropionyl bromide (Aldrich, 97%), cinnamoyl chloride (Acros, 98%), triethylamine (Alfa Aesar, 99%), $CuBr_2$ (Aldrich, 99.999%), 2,2'-dipyridyl (Acros, 99+%), hydrochloride acid (Fisher, 37%), acetonitrile (Fisher, 99.96%), hexanes (Caledon, 98.5%), methanol (Caledon, 99.8%), ethanol (Commercial Alcohols), dichloromethane (ACP, 99.5%), poly(ethylene oxide) (PEO, Polysciences Inc., M_w = 100,000 g/mol), and blue ink (Parker Quink) were used as received. In addition, chloroform-*d* (Aldrich, 99.8%) was purchased for NMR analysis and was used as received.

The fluorescent polymer PEO-Pyrene was synthesized previously by reacting poly(ethylene glycol) methyl ether (M_w = 2000 g/mol) with 1-pyrenebutyric acid, in the presence of 1-ethyl-3-(3-dimethylaminopropyl)carbodiimide (EDC) and 4-dimethylaminopyridine (DMAP), in CH_2Cl_2 at room temperature.[53]

2.2.2 Fractionation of PDMS-OH

The crude PDMS-OH sample was purchased from Sigma-Aldrich. Based on ^{1}H NMR analysis by comparing protons from the end group (those close to hydroxyl group) and protons from methyl groups on Si, the crude polymer had 60 repeat units, which was consistent with the calculated value obtained based on the provided molecular weight (M_n = ~4670 g/mol). Size exclusion chromatography (SEC) analysis indicated that the polymer had a PDI of 1.21 in terms of polystyrene standards.

To fractionate the polymer, 9.70 g of the crude polymer was dissolved in 98.5 mL of THF (10.0 wt%) before enough methanol (155 mL) was slowly added to just turn the solution cloudy. The resultant solution was left idle overnight at ~4 °C to yield two phases. The top layer was collected and the solvent was removed via rotary evaporation to yield an oil. This oil was dried under vacuum for 24 h to yield 7.52 g of the polymer (yield ≈ 78%).

2.2.3 Synthesis of Macroinitiator PDMS-Br

A modified literature method was followed to prepare PDMS-Br.[54-56] Fractionated PDMS-OH (7.52 g, 1.65 mmol), triethylamine (0.83 g, 8.24 mmol) and 2-bromopropionyl bromide (1.78 g, 8.24 mmol) were dissolved in 10.3 mL of THF. This mixture was stirred for 72 h at room temperature and then for 1 h at 60 °C. The final mixture was centrifuged at 3600 rpm to remove the insoluble salt and the solvent was subsequently removed via rotary evaporation. The resulting oil was washed three times with 30.0 mL of ethanol, centrifuged, and subsequently collected. The light yellow crude product was dissolved in 20.0 mL of hexanes and filtered through a silica gel column. Finally, most of the solvent was removed via rotary evaporation and the oil was dried under vacuum for 48 h to yield 5.20 g of PDMS-Br (yield ≈ 70%).

2.2.4 Synthesis of Diblock Copolymer PDMS-*b*-PCEA

The precursor of the copolymer, PDMS-*b*-PHEA, was first prepared according to a modified literature procedure,[57] in which PDMS-Br (0.51 g, 0.12 mmol) and HEA-TMS (0.61 mL, 3.00 mmol) were initially mixed together in a two-necked round-bottom flask. Subsequently, THF (1.10 mL), 2,2'-dipyridyl (56.2 mg, 0.36 mmol) and $CuBr_2$ (4.1 mg, 0.018 mmol) were added to the mixture. The flask was then purged with N_2 before CuBr (25.8 mg, 0.18 mmol) was added and the contents of the flask were degassed by three freeze-pump-thaw cycles. The final N_2-filled flask was immersed in a preheated oil bath that was kept at 60 °C. The reaction was stopped after 19 h by quenching with liquid nitrogen and subsequently introducing air. The crude mixture was warmed to room temperature, diluted with THF (8.0 mL) and filtered through a neutral alumina column using THF as the eluent. Subsequently, a 1.0 M of HCl solution (a 13.0 M aqueous HCl solution that had been diluted with THF) was slowly added into the collected polymer solution under vigorous stirring to hydrolyze the TMS group. After this HCl solution had been added to the polymer solution, the final HCl concentration was 0.025 M. After 10 min, the polymer solution was concentrated to 1.0 mL and poured into 30.0 mL of acetonitrile. The precipitated polymer was

collected after it had been centrifuged and was subsequently re-dissolved into 1.0 mL THF. This dissolution-precipitation-centrifugation purification treatment was repeated twice before the product PDMS-*b*-PHEA was air dried in a fume hood for 48 h. Finally, 0.78 g of the product was obtained (yield ≈ 90%).

To synthesize the final diblock copolymer PDMS-*b*-PCEA, 0.78 g of PDMS-*b*-PHEA and 0.52 g of cinnamoyl chloride were added into 15.0 mL of dry pyridine. After the mixture had been stirred in the dark at room temperature for 13 h, it was subsequently added dropwise into 100 mL of ethanol to precipitate the final polymer PDMS-*b*-PCEA. The polymer was collected after centrifugation and re-dissolved in 5.0 mL THF. Subsequently, 45.0 mL of ethanol was added slowly under stirring to precipitate the polymer again. This dissolution-precipitation-centrifugation purification treatment was repeated three times and the final product was dried under vacuum in the dark for 24 h to obtain 0.72 g of PDMS-*b*-PCEA (yield ≈ 70%).

2.2.5 Polymer Characterizations

Size exclusion chromatography (SEC) was performed at 25 °C using a Wyatt Optilab rEX refractive index detector. The three columns were packed by MZ-Analysentechnik with 5 μ AM 500, 10,000 and 100,000 Å gels. The system was calibrated with monodisperse polystyrene (PS) standards. Chloroform was used as the eluent with a flow rate of 1.0 mL/min. The solution samples were filtered by syringe filters (Dikma, PTFE, 0.22 μm) before they were injected into the SEC system. ^{1}H NMR characterization was performed using a Bruker Avance-500 instrument at 25 °C using chloroform-*d* ($CDCl_3$) as the solvent.

2.2.6 Cotton Coatings with PDMS-*b*-PCEA

The general protocol for coating the cotton samples involved the following steps. First, the copolymer was dissolved in THF. Second, hexane was added to a particular hexane volume fraction, denoted as f_{HX}. Third, 1.0 cm x 1.0 cm cotton swatches were immersed in the coating solution for 3.0 min. Fourth, the cotton swatches, which had become saturated with the polymer

solution, were withdrawn from the solution and dried in the air for 2 h. Fifth, the dried cotton samples were subsequently annealed at 120 °C for 15 min. Sixth, the coated swatches were irradiated for a particular length of time on each side with a focused UV beam that was generated by a 500 W Hg lamp that was housed in an Oriel 6140 lamp case. The UV beam was passed through a 270-nm cut-off filter before it reached the cotton samples. Seventh, the polymers that had not become grafted around the fibers were subsequently removed via solvent extraction treatment. This extraction treatment involved immersing the coated cotton samples in 5.0 mL of CH_2Cl_2 at 35 °C for 2 h and subsequently rinsing them three times with 5.0 mL of CH_2Cl_2 at room temperature for 15 min. Lastly, the coated cotton samples were completely dried at 120 °C for 15 min before they were evaluated.

To investigate the effect of changing the polymer concentration (C) on the wetting properties of the coated cotton, f_{HX} was set at 40% and the irradiation time was set at 30 min for each side of the cotton samples. The copolymer concentrations were varied between 1.0 and 50.0 mg/mL, with concentrations of 1.0, 2.0, 3.0, 4.0, 5.0, 10.0, 20.0, 30.0, and 50.0 mg/mL being employed. In addition, uncoated cotton samples were also investigated for comparison.

To examine the effect of varying the irradiation time (*IT*) on the stability of the coating layer, f_{HX} was set at 80% and the copolymer concentration was set at 20.0 mg/mL. The irradiation times on the side of the cotton whose wetting properties would be evaluated were varied between 0 and 240 min. In particular, these irradiation times included 0, 5, 15, 30, 60, 120, and 240 min.

The effect of varying f_{HX} was examined by fixing the copolymer concentration to 5.0 mg/mL and the irradiation time to 30 min on each side. The f_{HX} values investigated included 20%, 40%, 60% and 80%. For the controlled experiment in which the PCEMA homopolymer was applied as a coating on the cotton sample, the coating procedure was identical to that applied for the diblock copolymer-based cotton coating. The conditions used for this PCEMA-based coating were C = 5.0 mg/mL, IT = 30 min and f_{HX} = 0% (pure THF) respectively.

2.2.7 Water Repellency Measurements

Images of 5.0 μL water (Milli-Q) droplets were captured at room temperature (21 °C) with a Canon PowerShot A700 camera and processed with the ImageJ software package to yield the water contact angles (WCAs). The contact angle reported for each sample represented the average of five measurements together with the calculated standard deviations.

Water shedding angles (WSAs) were measured at room temperature (21 °C) according to a literature method.[11] First, a coated cotton swatch was attached to a glass plate with double-sided adhesive tape. This glass plate was then placed on a custom-built tilting stage, and a syringe containing water was mounted 1.0 cm above the testing spot (Figure 2.2). To determine the WSA, measurements were started at a tilting angle of 70°. Water droplets (10 μL in volume) were dispensed onto five different spots on the coated cotton samples. If all of the water droplets bounced or rolled off the sample, the tilting angle was reduced by ~1° via reducing the height of the adjustable end of the tilting stage. This procedure was repeated until one or more of the water droplets would not completely roll off the surface. The lowest tilting angle at which all of the drops completely bounced or rolled off the sample surface was noted as the WSA. The WSA reported for each sample represented the average of five measurements together with the calculated standard deviations.

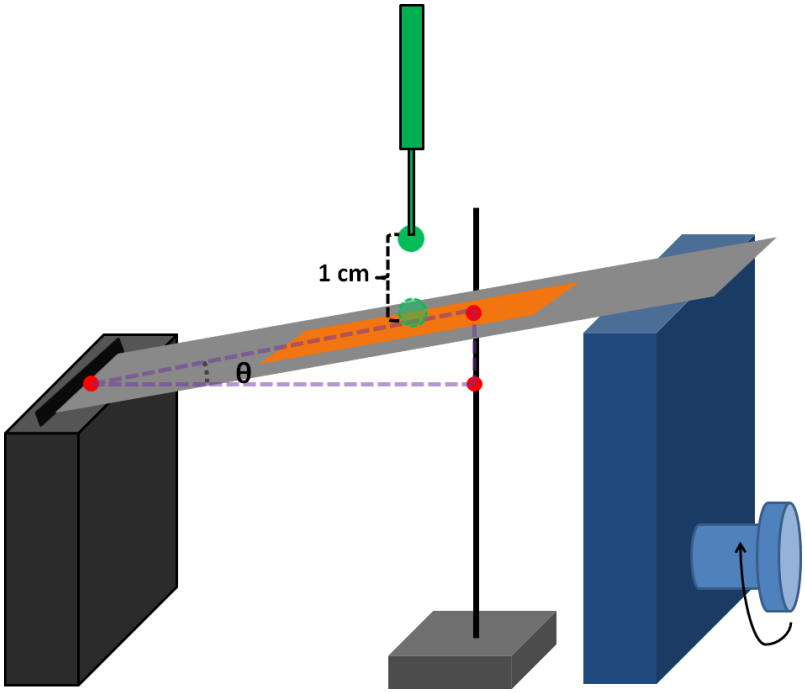

Figure 2.2 Setup used for the water shedding angle measurements.

2.2.8 Gravimetric Analysis

To determine the polymer grafting density x on the cotton fabrics, four cotton samples with weights ranging between 4.0 and 20 mg were prepared for gravimetric analysis. First, the weights of all of the uncoated cotton samples were recorded using a microbalance (± 0.002 mg) after they had been dried under vacuum at 100 °C until their weights reached constant values. These weights were denoted as W_0. Subsequently, all of these samples were immersed into 2.0 mL of a 20 mg/mL micellar copolymer solution (THF/hexane at f_{HX} = 80%) for 3 min. These samples were withdrawn from the coating solution and dried in air for 2 h followed by thermal annealing at 120 °C for 15 min. Subsequently, all of the samples were irradiated for 1 h on each side, extracted with CH_2Cl_2 and dried under vacuum at 100 °C until the weights reached constant values. These final weights observed after the solvent extraction treatment were also recorded using the microbalance and they were denoted as W_1. The polymer grafting density x was determined as the weight increases exhibited by the samples, as determined by equation (2.1):

$$x = (W_1 - W_0)/W_0 \text{ x } 100\% \qquad (2.1)$$

The reported x value represented the average values for all four samples together with the calculated standard deviations.

2.2.9 SEM Characterization

Five 1.0 cm x 1.0 cm cotton samples denoted as S1-S5, respectively, were prepared for SEM characterization. S1 was an uncoated cotton sample, while S2-S5 were coated with the copolymer. To coat samples S2-S5, they were immersed into 3.0 mL of a 20 mg/mL micellar copolymer solution (THF/hexane at f_{HX} = 80%) for 3 min. After the samples had been withdrawn from the coating solution and air-dried for 5 min, S2 was irradiated for 1 h on one of its sides to photo-crosslink the copolymer before it was characterized via SEM. Meanwhile, samples S3-S5 were dried in the air for 2 h after they were removed from the coating solution. Subsequently, S3 was irradiated for 1 h on one side to crosslink the polymer. Meanwhile, after S4-S5 had been air-dried, they were annealed at 120 °C for 15 min. After these samples had been annealed, both S4 and S5 were irradiated for 1 h on one side. Finally, S5 was subjected to extraction treatment under similar conditions as described in the cotton coating section. SEM images of the cotton samples were recorded using a FEI-MLA Quanta 650 FEG-ESEM instrument that was operated at 10 kV. In the case of samples S2-S5, the irradiated side was recorded via SEM. The samples were not coated with Au prior to SEM observation.

2.2.10 AFM Study of Coatings on Silicon Wafers

PDMS-*b*-PCEA micelles were deposited on four ~0.5 × 0.5 cm^2 Si wafers and treated differently to yield samples S2-S5 for AFM analysis. S1 was an uncoated Si wafer. To coat samples S2-S5, they were immersed into 2.0 mL of a 20 mg/mL micellar copolymer solution (THF/hexane at f_{HX} = 80%) for 3 min. After the samples had been withdrawn from the coating solution and air-dried for 5 min, one sample was irradiated for 1 h to photo-crosslink PCEA to yield S2. Meanwhile, samples S3-S5 were dried in the air for 2 h after they were removed from the

coating solution. Irradiating a sample at this stage for 1 h yielded S3. The left two samples were annealed at 120 °C for 15 min. The sample not treated further was denoted as S4. S5 was obtained after the annealed and irradiated sample was extracted with CH_2Cl_2. The samples were analyzed by a Veeco Multimode instrument that was equipped with a Nanoscope IIIa controller and operated in the Tapping Mode.

2.2.11 Other Techniques

X-ray photoelectron spectroscopy (XPS) measurements were performed using a Thermo Instruments Microlab 310F surface analysis system (Hastings, U.K.). Thermogravimetric analysis (TGA) was performed using a TA Q500 instrument under nitrogen. A typical TGA measurement involved heating the samples from room temperature to 150 °C at 10 °C/min, holding the temperature at 150 °C for 15 min, and increasing the temperature further to 800 °C at 10 °C/min. Each residual weight reported was normalized relative to that determined at 150 °C and represented the average of three measurements.

2.2.12 Hydrophilically-Patterned Cotton Fabric and Assembly of Cotton Stamp

To prepare a hydrophilically-patterned cotton fabric, a circular cotton swatch with a diameter of 5.0 cm was immersed into 5.0 mL of a 20.0 mg/mL micellar copolymer solution (THF/hexane at f_{HX} = 80%) for 3 min. After the cotton swatch had been removed from the coating solution and air-dried for 2 h, it was annealed at 120 °C for 15 min. Subsequently, one side of the swatch was irradiated for 1 h while it was covered with a photo-mask to allow selective photo-crosslinking of the unmasked regions. To remove the polymers that had not become crosslinked, the swatch was subsequently washed with 20.0 mL of CH_2Cl_2 at 35 °C for 2 h and then rinsed three times with 20.0 mL of CH_2Cl_2 at room temperature for 15 min. Finally, the patterned cotton sample was completely dried at 120 °C for 15 min before it was used as the face of the stamp.

To assemble the cotton stamp, a hydrophilically-patterned superhydrophobic cotton fabric that served as the stamp face was attached to the support base of a commercially available sinter glass

filter funnel. This funnel served as both the stamp handle and also as the ink reservoir, and the edges of the fabric were affixed to the support base of this funnel with tape. Thus, the support base of the funnel was inverted, with the cotton fabric-covered head of the base (the face of the stamp) facing downward and the stem of the base facing upward. In addition, a sealed-in coarse porosity fritted disc was placed inside the base (between the cotton-covered head and the stem) to serve as a sieve. Various aqueous ink solutions (with volumes ranging between 1.0 and 3.0 mL) were loaded into the reservoir of cotton-based stamp through the stem of the funnel support base using a plastic syringe. Subsequently, the ink-filled stamp was pressed onto various substrates for ~2 s to imprint patterns from the cotton template onto these substrates.

2.2.13 Pattern Printing on Different Substrates Using Cotton Stamp

Different aqueous ink solutions were prepared first. A diluted ink solution was prepared by adding distilled water into the commercial ink, so that the volume ratio between the ink and the distilled water was 1:20 (ink:water). A viscous ink solution, PEO-containing ink, was prepared by adding PEO (M_w = 100,000 g/mol) into the commercial ink at a concentration of 10.0 mg/mL. A fluorescent polymer dye solution was prepared by dissolving PEO-Pyrene into distilled water at a concentration of 10.0 mg/mL. The relative viscosities (η_r) of various aqueous ink solutions used for the pattern printing experiments were measured with an Ostwald viscometer at 25 °C using water as a reference.

2.3 Results and Discussion

2.3.1 Fractionation of PDMS-OH

The polydispersity index (PDI) of commercially available PDMS-OH was firstly characterized with SEC and the result showed that the PDI was as large as 1.21. A shoulder peak was observed in shorter retention time region of its SEC trace (Figure 2.3, black). This indicated that small amount of larger molecular weight polymer chains existed in this homopolymer. Therefore, this

homopolymer was fractionated to remove these large molecular weight chains that to narrow down the polydispersity. Theoretically, during the addition of poor solvent into a homopolymer solution, polymer chains with larger molecular weight will precipitate first. Using this method, PDMS-OH was dissolved in THF (10.0 wt%), then poor solvent methanol was added dropwise until the solution just turned light cloudy. After standing for overnight, the bottom layer oil due to the precipitation was removed. The major product, in the top layer, was collected by evaporating all the solvent. After optimization, when the methanol volume fraction was 61% in the final solution, the larger molecular weight polymer chains corresponding to the shoulder region were totally removed (Figure 2.3, red). The final PDI of PDMS-OH was 1.10.

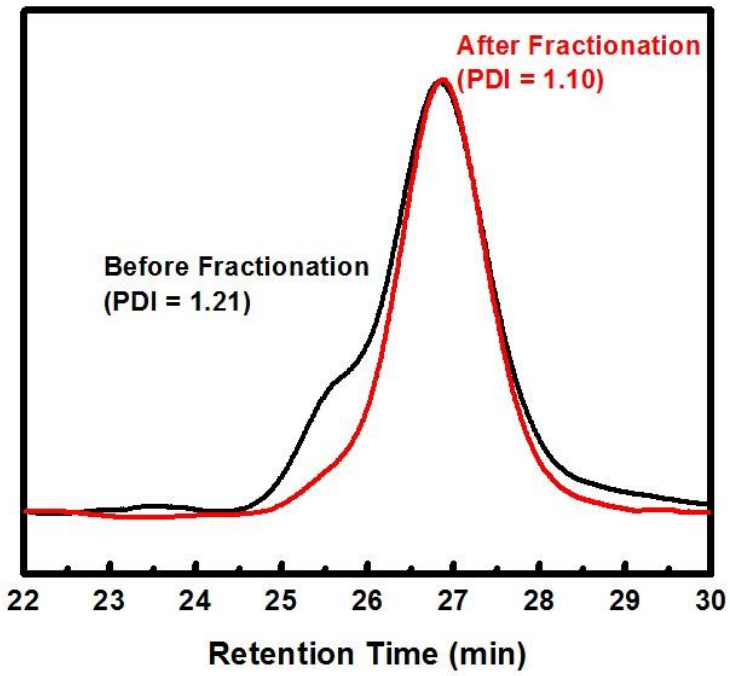

Figure 2.3 SEC traces of PDMS-OH before (black) and after (red) fractionation.

2.3.2 Synthesis of the Macroinitiator PDMS-Br

The macroinitiator PDMS-Br was obtained by reacting hydroxyl-terminated PDMS (PDMS-OH with 2-bromopropionyl bromide (Figure 2.4, first step).[54-56] The synthesized PDMS-Br

macroinitiator and its PDMS-OH precursor were both characterized by ^{1}H NMR using $CDCl_3$ as the solvent. Figure 2.5a compares the spectra of the two samples in the region where the end group protons displayed signals. By comparing the signal integrations of the end groups with the integration of the signal at 0.08 ppm corresponding to the dimethylsiloxane polymer backbone (not shown here), we obtained for these polymers the repeat units numbers of 58. The key observation in the spectral region ranging from 3.0 to 4.8 ppm was that the signals corresponding to the *b* and *c* protons of the original PDMS-OH polymer were completely replaced by the new peaks denoted as *b*' and *c*' after the polymer had been reacted with 2-bromopropionyl bromide. In addition, a new peak denoted as *d*' corresponding to the methyne group of the attached 2-bromopropionyl group appeared. The integration ratio between *b*', *c*', and *d*' was 1.99:1.93:1.00, which was consistent with the theoretical values of 2:2:1. These results suggest that PDMS-OH had been quantitatively end-capped by the 2-bromopropionyl group.

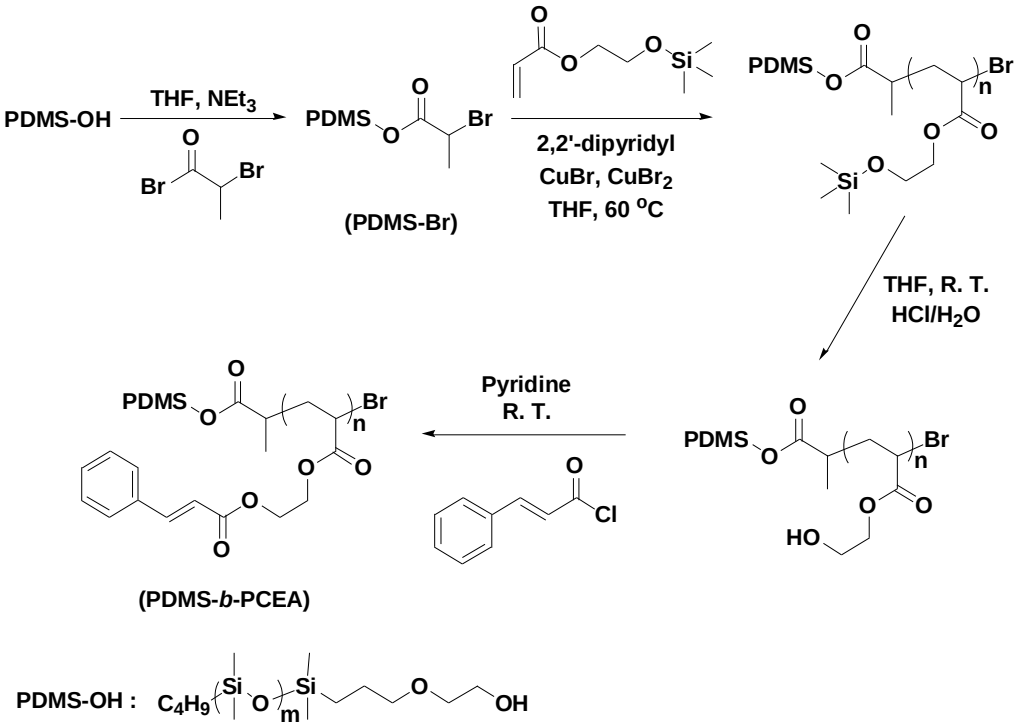

Figure 2.4 Syntheses of the macroinitiator PDMS-Br and diblock copolymer PDMS-*b*-PCEA.

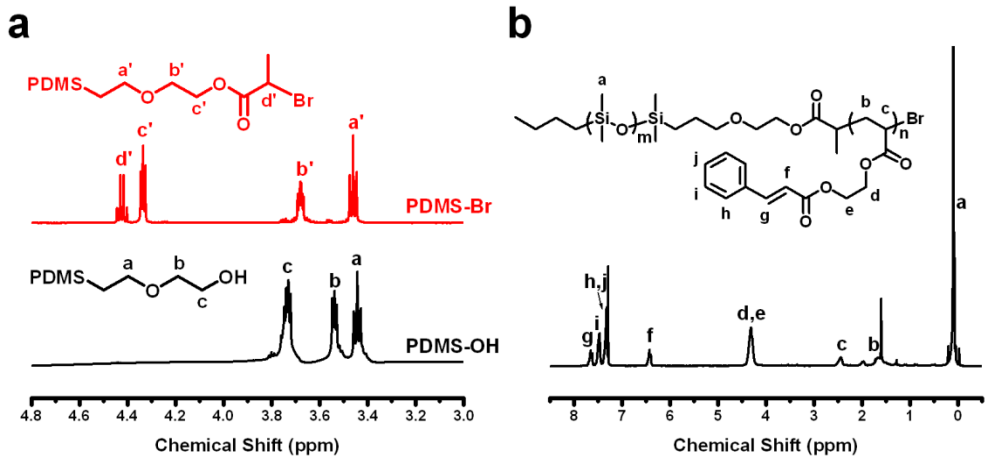

Figure 2.5 ^{1}H NMR spectra of PDMS-Br (a-top) and PDMS-OH (a-bottom) in the 3.0-4.8 ppm region and the diblock copolymer PDMS-*b*-PCEA (b).

2.3.3 Synthesis of Diblock Copolymer PDMS-*b*-PCEA

PDMS-Br was then used as a macroinitiator to polymerize 2-trimethylsiloxyethyl acrylate (HEA-TMS). This was followed by the removal of the trimethylsilyl protecting groups under acidic conditions and the cinnamation of the resultant poly(2-hydroxyethyl acrylate) block by cinnamoyl chloride to yield PDMS-*b*-PCEA (Figure 2.4). The final product PDMS-*b*-PCEA was analyzed by ^{1}H NMR using $CDCl_3$ as the solvent, as shown in Figure 2.5b. The integration ratio between the signal denoted as *a* corresponding to the PDMS backbone and the signals corresponding to the PCEA block (labeled as *f*, *g*, *i* etc.) suggested that the repeat unit ratio between PDMS and PCEA was 3.6:1.0. Thus, the PCEA block was 16 units long based on a PDMS repeat unit number of 58. The copolymer was also analyzed by SEC using $CHCl_3$ as the eluent. The SEC trace recorded for the diblock copolymer shifted to the higher-molecular weight side relative to its PDMS-Br precursor. Additionally, there was little overlap between the copolymer and the PDMS-Br peak (Figure 2.6). Thus, the initiation efficiency of PDMS-Br was high. In terms of polystyrene standards the diblock copolymer had a polydispersity index of 1.19, which was reasonable for a polymer that had been synthesized via ATRP.[58]

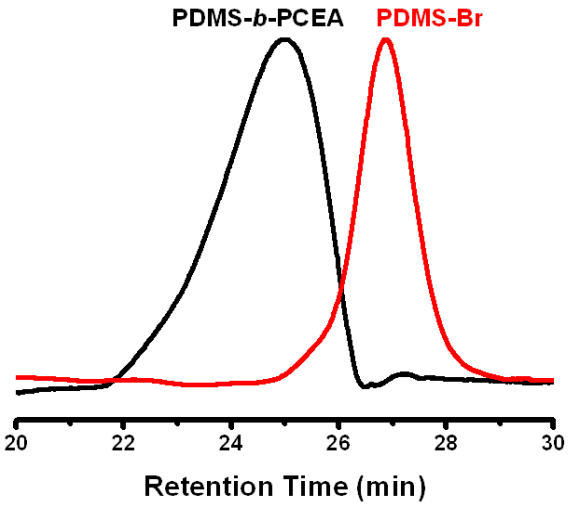

Figure 2.6 Comparison of SEC traces of PDMS-b-PCEA and the macroinitiator PDMS-Br.

2.3.4 Cotton Coatings with PDMS-*b*-PCEA

To coat cotton, a micellar solution was first prepared by dissolving the copolymer in THF and then adding hexanes to a volume fraction f_{HX} (A→B, Figure 2.7). Since only PDMS was soluble in such mixtures, the micelles would have a PCEA core and PDMS corona. Subsequently, a cotton swatch was immersed in the micellar solution for 3 min. We hoped that the polymer micellar solution would have infiltrated the cotton matrix by this stage and some micelles would have deformed and adsorbed on the cotton fiber surfaces via their insoluble PCEA core (B→C). The cotton swatch was next withdrawn, dried in the air to remove most of the solvent (C→D). We anticipated that more polymer would have deposited during this process, yielding clustered or aggregated micelles on the fiber surfaces. In a further step, the dried cotton was annealed at 120 °C for 15 min to facilitate coating smoothening due to the increased polymer chain mobility at 120 °C (D→E). We further anticipated that the rubbery PDMS block would migrate to the polymer/air

interface to reduce the surface tension of the coating and the PCEA block would wrap around the fiber to form an underlying layer (D→E).[59, 60] Evidently, the deposited polymer amount on the fiber would increase with the concentration of coating polymer solution. At low polymer concentrations, the deposited polymer would form a sub-saturated diblock copolymer unimolecular layer. Above a critical concentration, a saturated unimolecular layer together with excess surface micelles would form on the fiber surfaces (E). After this, we photolyzed the cotton with a focused UV beam that was from a 500-W Hg lamp and passed a 270 nm cut-off filter to crosslink the PCEA anchoring layer via a [2 + 2] cycloaddition among CEA units[32] of different chains to yield an encasing stable PCEA network around cotton fibers (E→F). In the last step, the swatch was rinsed with CH_2Cl_2, a good solvent for both PDMS and uncrosslinked PCEA, to remove the crosslinked micelles that were expelled from the crosslinked unimolecular layer (F→G).

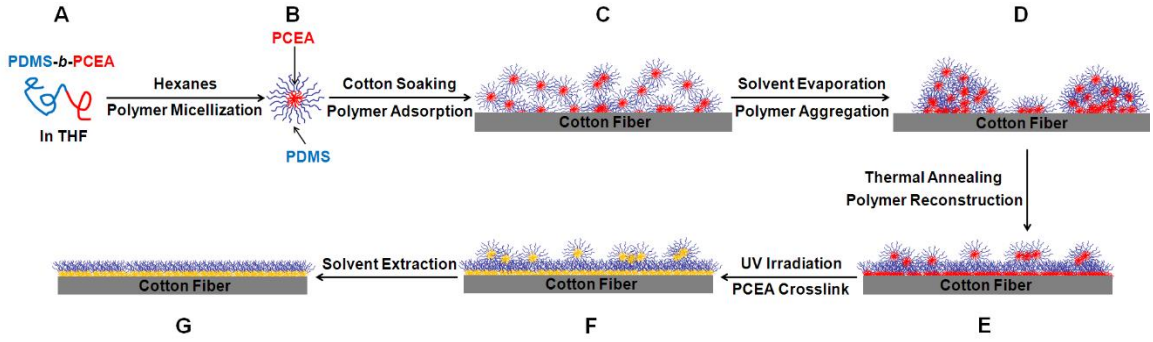

Figure 2.7 Illustration of steps involved in the preparation of cotton coatings from micellar PDMS-*b*-PCEA solutions.

2.3.5 SEM Characterization

To gain evidence supporting this hypothesized coating mechanism, cotton samples were taken at different stages during coating and were then analyzed via scanning electron microscopy (SEM). Figure 2.8 shows SEM images of these specimens. The cotton fibers that had been soaked in a coating solution for 3 min and subsequently dried in the air for 5 min (Figure 2.8b) or for 2 h (Figure

2.8c) exhibited new semi-spherical or spherical structures. These new structures indicated that the polymers had been successfully adsorbed onto the cotton fibers. By comparing the diameters of these (semi)spherical structures (300-400 nm) with the calculated length of 18 nm for the fully stretched polymer chain of 74 repeat units, we conclude that these (semi)spherical structures were not individual micelles, but instead were aggregates of micelles. These micellar aggregates were formed probably during solvent evaporation as we hypothesized in Figure 2.7 from step C to D. However, after thermal annealing was performed at 120 °C for 15 min, the large aggregates disappeared (Figure 2.8d). This result supported the possibility of surface smoothening and reconstruction at 120 °C. Finally, after UV irradiation and extraction with dichloromethane the surfaces of the cotton fibers exhibited no further changes (Figure 2.8e) because our SEM could not resolve the small spherical micelles. Therefore, our SEM results supported our hypothesized coating formation mechanism.

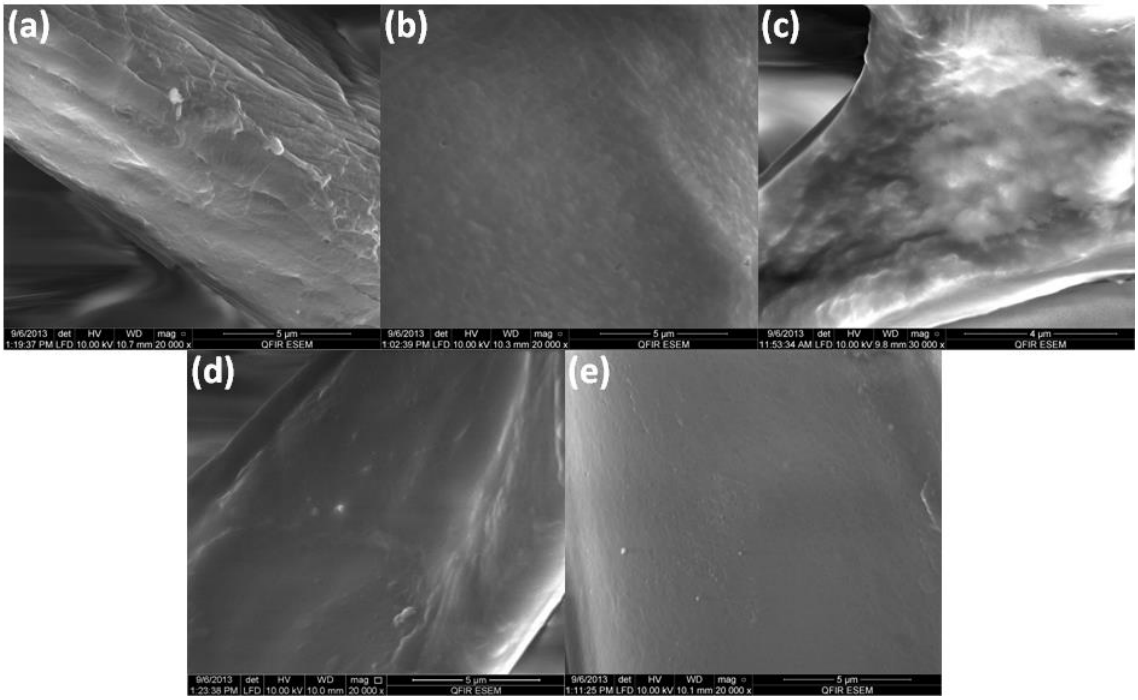

Figure 2.8 SEM images recorded for specimens prepared from cotton samples taken at different stages during the coating procedure. Image (a) shows an uncoated cotton fiber. Meanwhile, samples (b)-(e) had been soaked in the coating solution for 3 min and subsequently removed and dried for 5 min (b) or 2 h (c-e) in the air. In addition, sample (d) was annealed at 120 °C for 15 min and samples (b)-(d) were all irradiated with UV light to lock in their structures prior to SEM analysis. Sample (e) was not only irradiated but also extracted by dichloromethane.

2.3.6 Optimization of Coating Condition

According to the hypothesized coating mechanism, the concentration of the polymer coating solution (C), the UV irradiation time (IT), and the hexane volume fraction (f_{HX}) in the coating solution should affect final performance of the coating. Thus, we investigated the effect of varying these parameters on the water contact angles (WCAs) and water shedding angles (WSAs) on the coated cotton fabrics.

When other factors were fixed (IT = 30 min on each side and f_{HX} = 40%), increasing the concentration of the coating solution increased the WCAs and decreased the WSAs on the coated cotton (Figure 2.9a) after the cotton had undergone the standard treatments including coating, air drying, thermal annealing, and solvent extraction. While an uncoated cotton sample absorbed water

immediately, cotton swatches that were coated at C = 10.0 mg/mL had WCA = 151 ± 5° and WSA = 22 ± 2°. A low WSA of 9 ± 1° was obtained when C = 30.0 mg/mL or at this point the coated cotton were superhydrophobic. In addition, the trend of an enhanced water-repellency with increases in C diminished when C was increased beyond ~30.0 mg/mL. This trend agreed our hypothesized coating mechanism. As we discussed above, increasing the concentration of the polymer coating solution would increase the amount of copolymer deposited on the cotton fibers. The increased polymer amount would have helped build an increasingly dense unimolecular layer around the fibers until the layer got saturated. After saturation, the excess deposited polymer might not incorporate into the crosslinked first layer but exist as crosslinked spherical micellar particles. These particles would get extracted by CH_2Cl_2 and would not help improve water repellency. A leveling-off behavior in water repellency with coating solution concentration has been observed by others as well.[4, 22, 23]

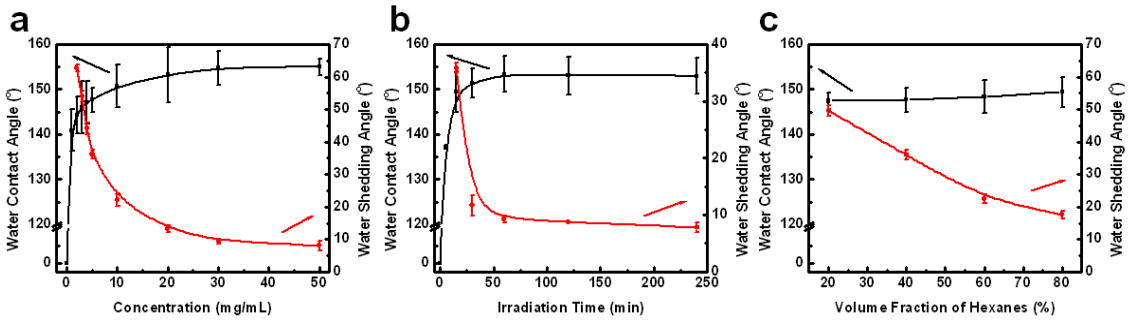

Figure 2.9 Variation of the WCAs and WSAs of cotton surfaces with changes in the copolymer concentration of the coating solution (a), UV irradiation time (b) and f_{HX} (c).

When other factors were fixed (C = 20.0 mg/mL and f_{HX} = 80%), prolonging the irradiation time yielded higher WCAs and lower WSAs (Figure 2.9b) on coated and CH_2Cl_2-extracted cotton. Irradiating the sample for 30 min provided both a high WCA (151 ± 3°) and a low WSA (12 ± 2°). Increasing the irradiation time on each side of the cotton swatches to 1 h improved the water-repellency further, providing the fabric with superhydrophobic properties (WCA = 153 ± 4° and

WSA = 9 ± 1°). This influence of the irradiation time on the water repellency can be explained upon consideration that the photo-crosslinkable PCEA block needs a particular length of time to become crosslinked enough to resist extraction by CH_2Cl_2. We also tested a sample that was not irradiated (*IT* = 0 min). In this case, the resultant fibers were hydrophilic after CH_2Cl_2 extraction. Instead of beading up, an applied water droplet was immediately absorbed by this cotton sample, giving an apparent WCA of 0°. Thus, polymer chains deposited around the cotton fibers but were not irradiated could be removed from the cotton, regenerating the original hydrophilic cotton. On the other hand, coated cotton samples that were irradiated for more than 60 min and extracted by CH_2Cl_2 were superhydrophobic.

When the other factors were fixed (*C* = 5.0 mg/mL and *IT* = 30 min), varying the volume fraction of hexanes (f_{HX}) from 20% to 80% did not affect the WCAs significantly but decreased the WSAs (Figure 2.9c). Increasing f_{HX} would decrease solubility of PCEA. This might have helped increase the interaction between the insoluble PCEA and the cotton fibers during the cotton soaking and solvent evaporation stages and helped push more PDMS chains to the surface. An increasing density of PDMS chains on the surface would provide the cotton fibers with a lower surface tension (~20 mN/m)[26] than that provided by PCEA (~35 mN/m)[61]. The difference in surface energy between these two chains may not be large enough to significantly influence the WCAs but only the WSAs.

A cotton fabric sample was also coated with a homopolymer of poly(2-cinnamoyloxyethyl methacrylate) (PCEMA, DP = 75, M_w/M_n = 1.06), which had similar properties as those of PCEA, under similar conditions (*C* = 5 mg/mL in THF and *IT* = 30 min on each side). This coated cotton sample exhibited a high WCA (145 ± 3°). However, the water droplet could not roll off the cotton surface, even as the tilting angle was set to 70° in the standard WSA measurement.[11] Therefore, exposed PCEMA homopolymer could provide a high WCA but not a low WSA. To achieve a

relatively low WSA, more of the PDMS chains from this particularly diblock copolymer-based coating need to be exposed on the surface.

Based on results of the above systematic study we have chosen the following standard coating conditions: a copolymer concentration of 20.0 mg/mL, 1 h of irradiation time on each side of a coated cotton swatch, and an f_{HX} of 80%. Figure 2.10 shows a comparison of the water-repellency exhibited by a cotton sample that had been coated under these conditions and by an uncoated cotton sample. The coated cotton sample exhibited a WCA of 153 ± 4° (Figure 2.10a) and a WSA of 9 ± 1°, while the uncoated cotton swatch absorbed the water droplet immediately (Figure 2.10b). The coated cotton swatch did not wet even when it was pushed into water. In particular, when the coated sample was submerged into water a layer of air (a plastron layer) became trapped between the water and the coated cotton swatch, giving rise to a reflective sheen (Figure 2.10c). In contrast, no such reflective plastron layer was observed when the uncoated cotton sample was submerged underwater (Figure 2.10d).

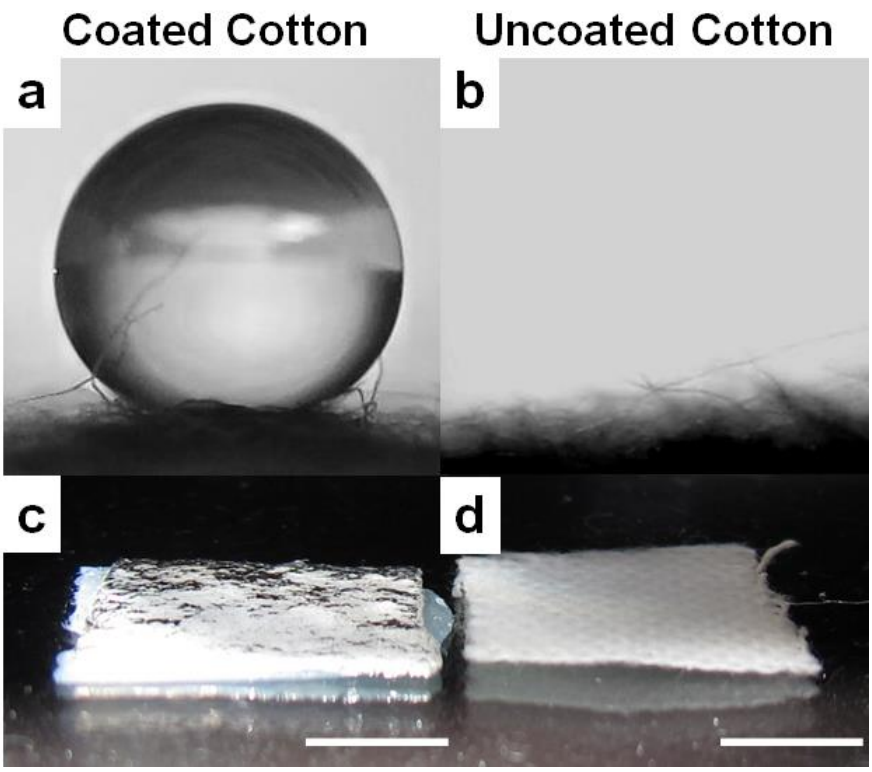

Figure 2.10 Photographs of water droplet dispensed on (a) coated and (b) uncoated cotton as well as of (c) coated and (d) uncoated cotton swatch submersed under water. The dispensed water was immediately absorbed by the uncoated cotton and the double-sided tape was used to glue the cotton swatches upon the glass substrates. The scale bars represent 5.0 mm.

2.3.7 Coating Characterization by XPS

X-ray photoelectron spectroscopy (XPS) was used to characterize the diblock copolymer coating prepared under the standard conditions. After UV irradiation and extraction by dichloromethane, the coated cotton surface exhibited Si_{2s} and Si_{2p} peaks at 154.0 and 102.0 eV, respectively (Figure 2.11a_3). These signals were not observed from the uncoated cotton (Figure 2.11a_1). They were absent also from the XPS spectrum of the coated cotton that was not irradiated by UV but was extracted by CH_2Cl_2 (Figure 2.11a_2).

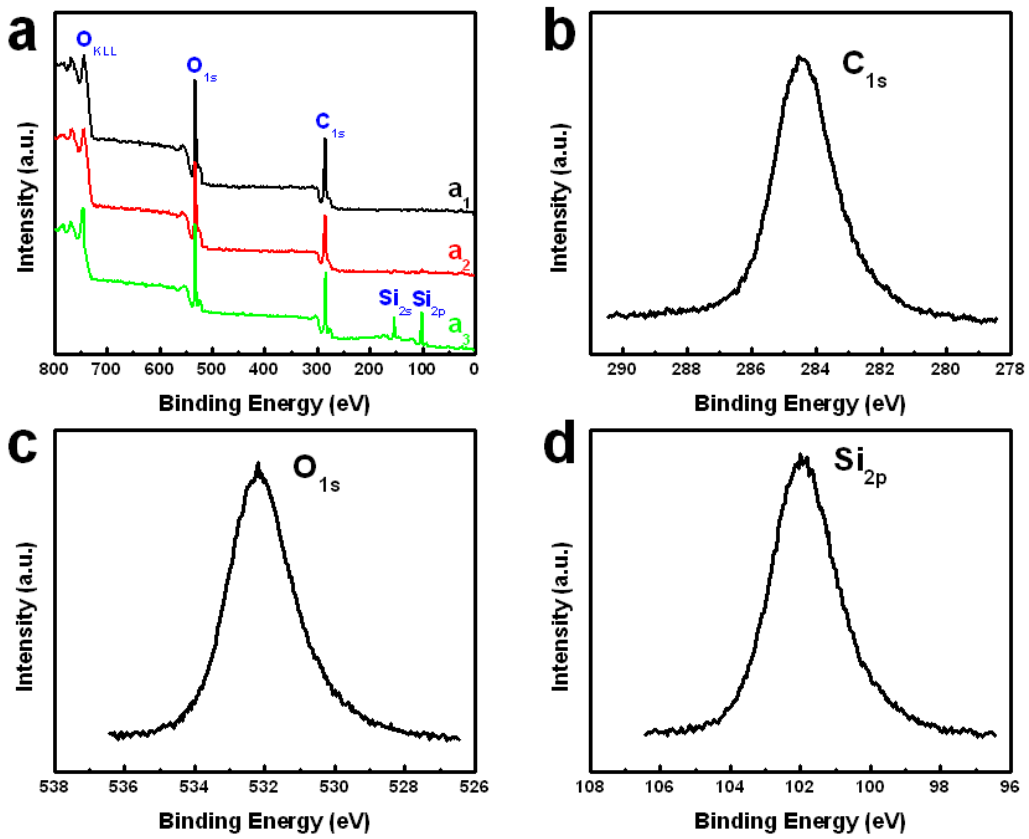

Figure 2.11 XPS spectra of (a_1) uncoated cotton, (a_2) coated cotton that were not irradiated but extracted by CH_2Cl_2, and (a_3) coated cotton that were irradiated and extracted by CH_2Cl_2. High-resolution (b) C_{1s}, (c) O_{1s} and (d) Si_{2p} XPS spectra of coated and extracted cotton.

The PDMS Si peaks (Figure 2.11a_3) demonstrated the stability of the photolyzed coating. The absence of these Si peaks in Figure 2.11a_2 confirmed that the non-crosslinked polymers were rinsed away by CH_2Cl_2. The XPS results again confirmed the possibility for fabricating hydrophilically-patterned superhydrophobic cotton fabrics by photolithography and CH_2Cl_2 extraction.

In addition, high resolution C_{1s}, O_{1s} and Si_{2p} XPS spectra were obtained. All the C_{1s}, O_{1s} and Si_{2p} peaks were single and symmetric (Figure 2.11b, 2.11c and 2.11d respectively), suggesting the presence of a single C, O, or Si species on the cotton fiber surface. These three peaks at 284.5, 532.2 and 102.0 eV were attributed to C^*-Si-O, C-Si-O^*, and C-Si^*-O, respectively. Therefore, XPS only detected PDMS on the coated cotton surfaces. Further, the calculated C/O/Si atomic ratio

(48.2/26.5/25.2) based on these high resolution spectra were close to the theoretical value of PDMS (C/O/Si = 50/25/25). These XPS results indicate that the cotton fiber surface was completely covered by a layer of polymer and only PDMS block was exposed on the outer surface. Therefore, the PCEA block must have anchored on the cotton fiber surfaces.

2.3.8 Grafted Polymer Amount

To determine the grafting density x or the mass fraction of polymer in the coated cotton, a literature method[4] based on thermogravimetric analysis (TGA) was initially used. Three different kinds of samples, including uncoated cotton, the diblock copolymer itself, and the diblock copolymer-coated cotton were analyzed by TGA (Figure 2.12). The x was determined based on the weight residue values (%) of these samples. If the polymer weight fraction in the coated cotton was x, then the following equation applied:

$$(1 - x)R_C + xR_P = R_{PC} \qquad (2.2)$$

where R_C, R_P, and R_{PC} are the weight residues of uncoated cotton, the polymer, and the polymer-coated cotton. The polymer-coated cotton samples that were characterized in this TGA study were prepared under standard conditions (C = 20.0 mg/mL, IT = 1.0 h on each side and f_{HX} = 80%) and extracted with CH_2Cl_2. Based on the R_C, R_P and R_{PC} of (5.991 ± 0.039)%, (2.615 ± 0.041)% and (5.869 ± 0.054)% from TGA analysis for each sample run in triplet, x was calculated as (3.6 ± 2.8) % from equation (2.2). The uncertainty in x was large because of error propagation, although the uncertainty of each residue value (R_C, R_P and R_{PC}) was small. We double checked the x value using a simple gravimetric analysis method that relied on measuring the weight difference between the coated and uncoated cotton fabrics, using a microbalance.[17] This analysis indicated that the coated quadruple samples analyzed had an average x value of (4.6 ± 0.2)%, which was the same, within experimental error, as (3.6 ± 2.8%), the value determined from TGA. Thus, the grafted copolymer amount under the standard coating conditions was relatively low.

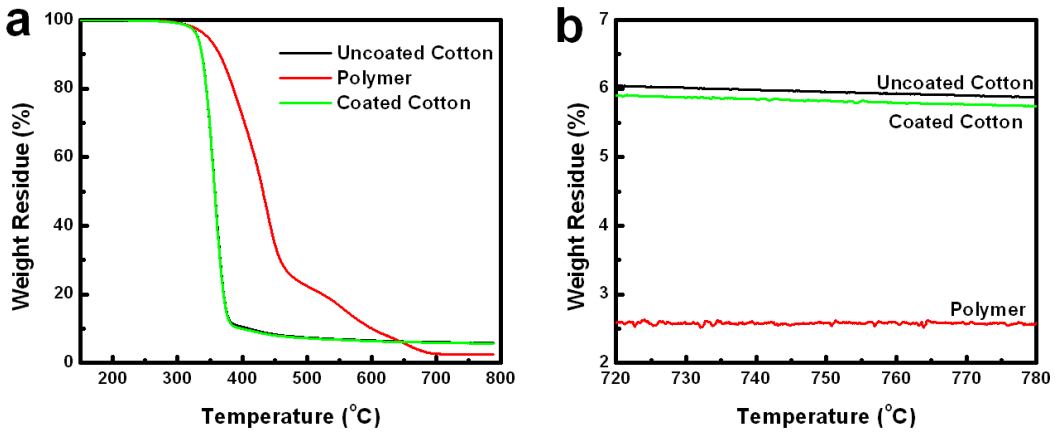

Figure 2.12 TGA traces of uncoated cotton, the diblock copolymer itself, and coated cotton in the range of 150-800 °C (a). Detail of image (a) in the range of 720-780 °C (b).

2.3.9 Coating Thickness Estimation

To further estimate the thickness of the grafted polymer layer, a calculation was performed based on the surface area of the cotton fabrics (A) and density of the diblock copolymer (ρ). The specific surface area of the same type of cotton was estimated in our previous work, and was found to be 1.3 ± 1.0 m^2/g.[4] The density of the diblock copolymer was estimated to be 1.09 g/mL using:

$$1/\rho = f_1/\rho_1 + f_2/\rho_2 \qquad (2.3)$$

where f_1 and ρ_1 were the respective mass fraction (52.2 %) and density (0.97 g/mL)[26] of the PDMS block, while f_2 and ρ_2 were the respective mass fraction (47.8 %) and density (1.25 g/mL)[62] of the PCEA block. If we used the grafting density x that were determined via gravimetric analysis (x = 4.6 ± 0.2%), the thickness (d) of the grafted polymer layer that would be anticipated after the samples had been subjected to irradiation/extraction treatment was found to be 32 ± 26 nm. However, some issues should be noted for the thickness calculation. First, the final estimated value would reflect an average thickness of the grafted polymer layer since the more deeply buried regions of the cotton swatch may have lost more polymer during the extraction, rather than the regions that were close to the surfaces of cotton swatch and had greater exposure to the UV

irradiation. Therefore, the actual grafted thickness in these relatively deeply buried regions of the fabric may have been lower than those that were close to the surface. Another issue that should be noted was the estimation of the surface area (A = 1.3 ± 1.0 m^2/g) of the cotton fabrics, which was based on an assumption of cylindrical cotton fibers with smooth surfaces. However, the actual A may be somewhat larger due to the rough surfaces of the cotton fibers. Therefore, the actual thickness of the grafted polymer layer should be lower than the calculated value. The thickness, of the grafted polymer layer, which was on the scale of tens of nanometers, was sufficiently thin to allow the cotton fabrics to retain their desirable intrinsic properties, such as softness and breathability.

2.3.10 AFM Study of Coatings on Silicon Wafers

To provide insight into the behavior of PDMS-*b*-PCEA micelles during the cotton coating process, we employed the procedures that were used to coat cotton to coat flat silicon wafers. The structures of the coatings at different stages were imaged by atomic force microscopy (AFM). The AFM height images are shown in Figure 2.13. Due to the totally different adsorption properties of silicon wafer and cotton, we do not know if the polymer would behave identically on the two surfaces. Despite this caution, we note that the behavior observed on cotton surfaces was mostly mirrored on silicon wafer surfaces. Before annealing, micellar aggregates were observed on the silicon plates. Thermal annealing smoothed out the background. Patches were, however, left in different regions of the annealed film. These patches were probably aggregates formed from excess polymer that was not needed for brush formation. After extraction by CH_2Cl_2, the coating appeared smooth. However, the water contact angle on it was low at 74 ± 1°. This value, smaller than the reported value of 107°,[63] suggested that the extracted layer was either not dense or not intact. The last property differed from that of the coating on cotton fibers probably due to the shape difference between the coated substrates. The formation of a perfect brush layer on a silicon wafer which has a much larger surface area than a single cotton fiber is probably much more challenging.

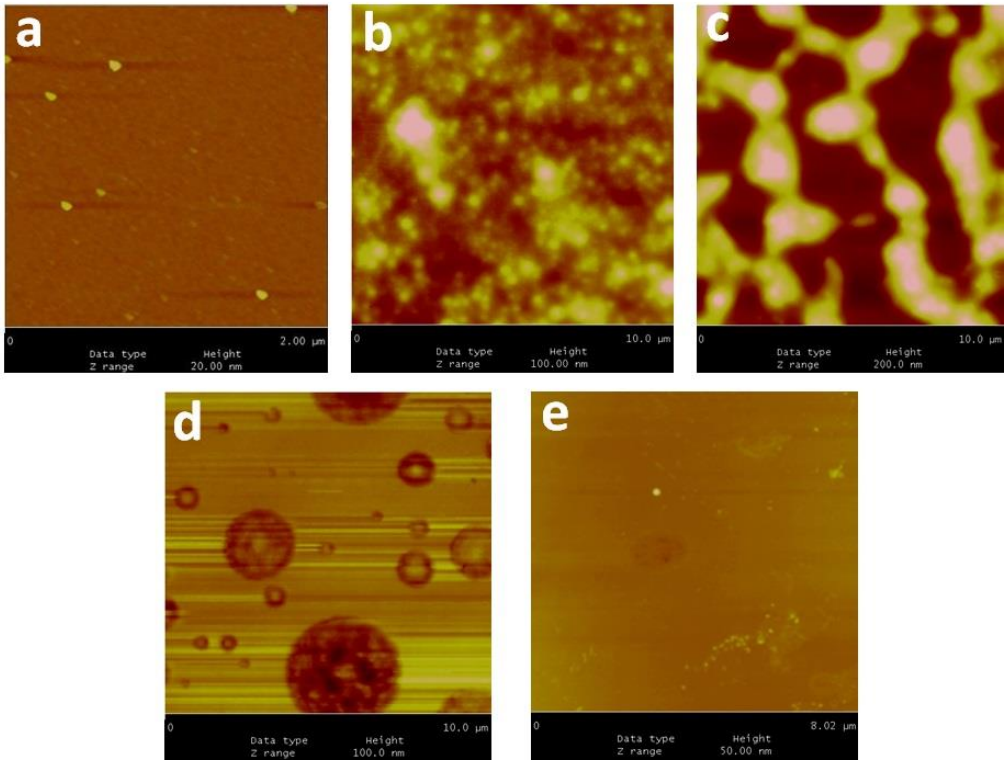

Figure 2.13 AFM topography images of silicon wafers bearing PDMS-*b*-PCEA coatings that were treated differently. (a) Bare silicon wafer, (b) coating that was air-dried for 5 min and then photolyzed, (c) coating that was air-dried for 2 h and then photolyzed, (d) coating that was air-dried for 2 h, annealed at 120 °C for 15 min, and then irradiated, as well as (e) coating that was annealed at 120 °C for 15 min, photolyzed, and then extracted with CH_2Cl_2.

2.3.11 Hydrophilically-Patterned Cotton Fabric and Assembly of Cotton Stamp

The approach to prepare hydrophilically-patterned superhydrophobic cotton fabrics and to use these fabrics as the cotton-based stamps is illustrated in Figure 2.14. First, a cotton swatch was coated using the standard protocol involving cotton soaking, solvent evaporation and coating annealing (Figure 2.14a). Then, one side of the coated cotton fabric was irradiated for 1 h by UV light under a photo-mask made of sculpted aluminum foil glued to a quartz plate (Figure 2.14b). The photolysis caused the anchoring PCEA block of the copolymer in the exposed region to crosslink around the cotton fibers. This was followed by extracting the cotton swatch with CH_2Cl_2

to remove polymer that was initially masked, yielding in an otherwise superhydrophobic cotton swatch a hydrophilic pattern that resembled the original aluminum mask (Figure 2.14c). Finally, the swatch was glued to the support base of a sinter glass filter funnel (Figure 2.14d) and the funnel was filled with ink to yield a stamp.

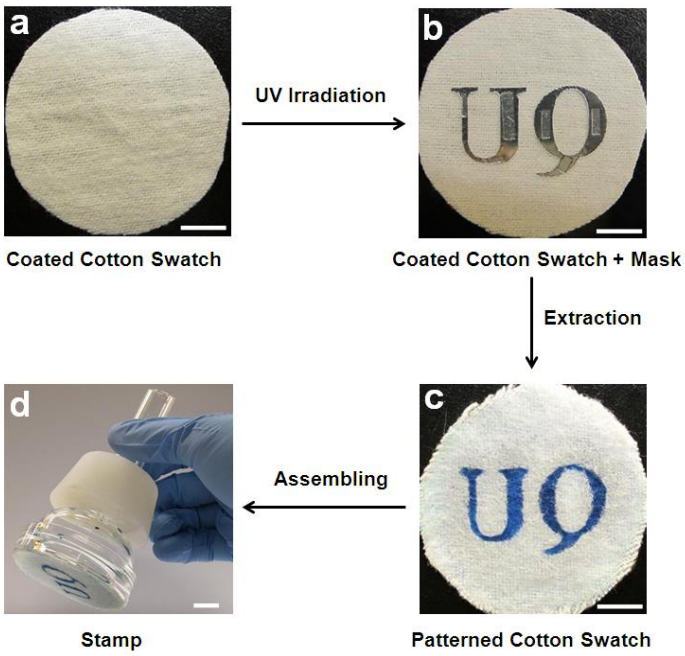

Figure 2.14 Process for preparing the cotton-based stamp. Immersing a cotton swatch is in a polymer micellar solution, taking it out to evaporate solvent, and then annealing the cotton yielded a polymer-coated cotton swatch (a). The coated cotton swatch is subsequently covered with an aluminum mask and irradiated (b). After extracting with CH_2Cl_2, a hydrophilically patterned cotton swatch is obtained (c, the patterned region was dyed by blue ink). This hydrophilically-patterned cotton fabric is subsequently attached to a sinter glass funnel to make a stamp for ink-printing (d). The scale bars represent 1.0 cm.

2.3.12 Pattern Printing on Different Substrates Using Cotton Stamp

As depicted in Figure 2.14, we prepared a cotton-based stamp bearing hydrophilic pattern "QU" and then printed the letters "QU" on various substrates including cotton fabric, semi-synthetic fabric (65% polyester/35% cotton), wood, cardboard, printing paper and aluminum foil. We also tested the effect of changing the viscosity of the aqueous ink by adding water or

poly(ethylene oxide) (PEO, *Mw* = 100,000 g/mol) into a commercially available ink. For the mixtures consisting of water/ink at v/v = 20/1 and ink containing PEO at 10.0 mg/mL, their relative viscosities with respect to that of water were 1.04 and 2.47, respectively. The relative viscosity of the untreated ink was 1.28. It was noted that the quality of the printed pattern was affected by both the surface property of substrate and the viscosity of ink solution.

When diluted ink was applied for printing, the resulted patterns shown in Figure 2.15 indicated that the substrates significantly affected the printing quality. On natural cotton fabric, the replicated pattern was larger and the lines were thicker rather than that on the stamp head (Figure 2.15a). This is because the diluted ink solution wicked quickly on such porous hydrophilic substrate. The hydrophilicity and water wicking ability of natural cotton fabric was extremely high. When a water droplet (5.0 μL) was dropped onto the natural cotton fabric surface, the droplet was absorbed by the cotton immediately. When synthetic fabric and wood were used as the substrates instead of natural cotton fabric, the printed patterns on these surfaces were relatively neat (Figure 2.15b and 2.15c). The hydrophilicity and water wicking ability of synthetic fabric and wood were not as high as those of the natural cotton fabric. When water droplets (5.0 μL) were applied on their surfaces, water could not be completely absorbed within 10 seconds, which was much different to the situation on the natural cotton fabric. However, because of the low viscosity of the diluted ink, the boundaries of the patterns were still slightly fuzzy due to the capillary action. The printed patterns on cardboard and printing paper shown in Figure 2.15d and 2.15e exhibited very good impressions. On these substrates, the diluted ink solution did not wick too fast. When water droplets (5.0 μL) were applied on these substrates, they could stay on the substrate surfaces for a relatively long time. The cardboard need about 15 seconds to completely absorb the water droplet and the printing paper even need more than 150 second to do so. So in general, the sharpness of the boundaries of the reproduced patterns improved as the wettability of the substrate decreased. The pattern on aluminum foil exhibited a different phenomenon, the edge was sharp but the colour in the patterned

region was not uniform. This was caused by the non-wetting property of the aluminum foil and the inability of the ink solution to spread uniformly on the foil. Rather, the ink solution beaded up. After the solvent water evaporated, a non-uniform trace was left behind.

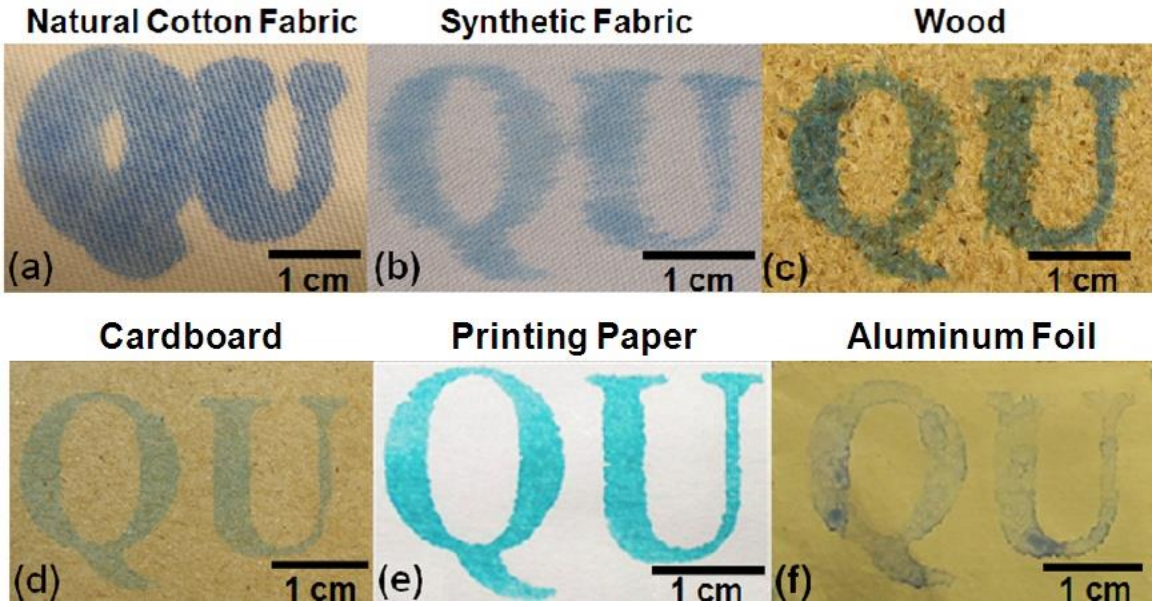

Figure 2.15 Patterns of "QU" that had been printed using the diluted ink onto (a) cotton fabric, (b) semi-synthetic fabric (65% polyester/35% cotton), (c) wood, (d) cardboard, (e) printing paper and (f) aluminum foil. The scale bars represent 1.0 cm.

Because diluted ink solution wicked too fast on some hydrophilic substrates, regular ink with a relatively higher viscosity was applied for printing patterns on different substrates. In this case, the printed patterns on natural cotton fabric (Figure 2.16a) and synthetic fabric (Figure 2.16b) were better than that from the diluted ink solution. Especially on natural cotton fabric, the printed pattern didn't wick as much as the one using diluted ink solution. While the shapes of patterns printed on other substrates were almost as same as those using diluted ink solution. The only difference was that the colour of the regular ink-based patterns was darker than that of diluted ink-based patterns due to the higher concentration of ink.

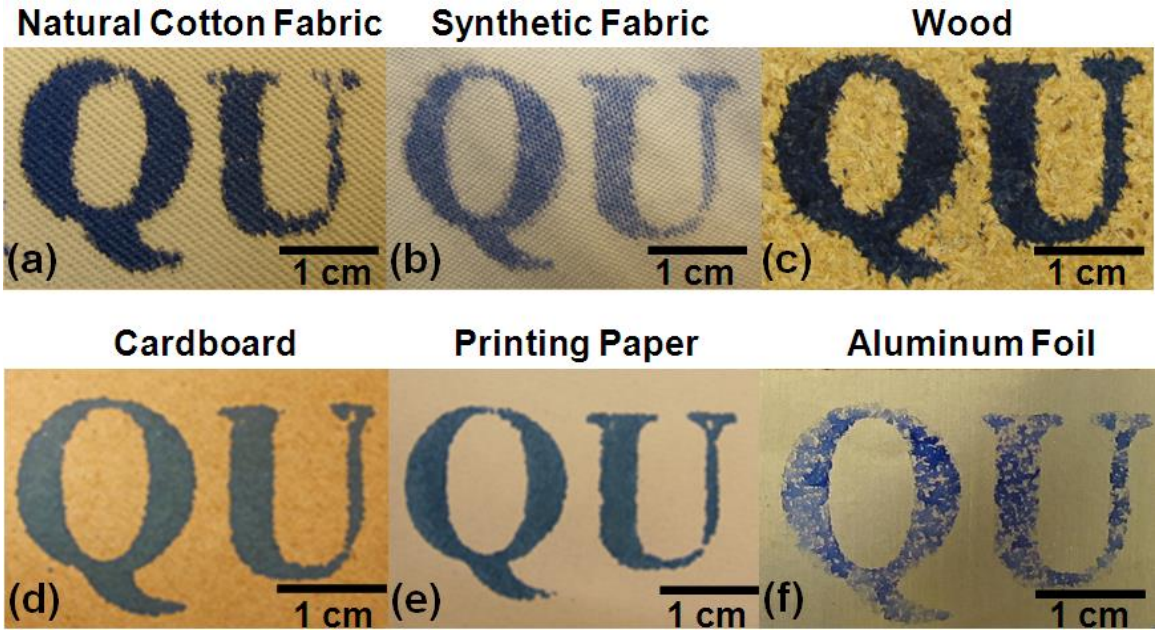

Figure 2.16 Patterns of "QU" that had been printed using regular ink onto (a) cotton fabric, (b) semi-synthetic fabric (65% polyester/35% cotton), (c) wood, (d) cardboard, (e) printing paper and (f) aluminum foil. The scale bars represent 1.0 cm.

To further investigate how viscosity of aqueous solution influences the patterning based on our stamp, patterns were printed onto these six substrates using the PEO-containing ink (Figure 2.17). In this case, patterns on both porous hydrophilic (natural cotton fabric, synthetic fabric and wood) and nonporous hydrophobic (aluminum foil) substrates exhibited best quality comparing to those using regular ink and diluted ink. The addition of PEO in regular ink solution not only increased the viscosity so that prevented the liquid spreading on hydrophilic surface to sharpen the boundaries of patterns, but also decreased the surface tension of water so that weakened the liquid shrinking on hydrophobic surface to make the colour in patterned region more uniform.

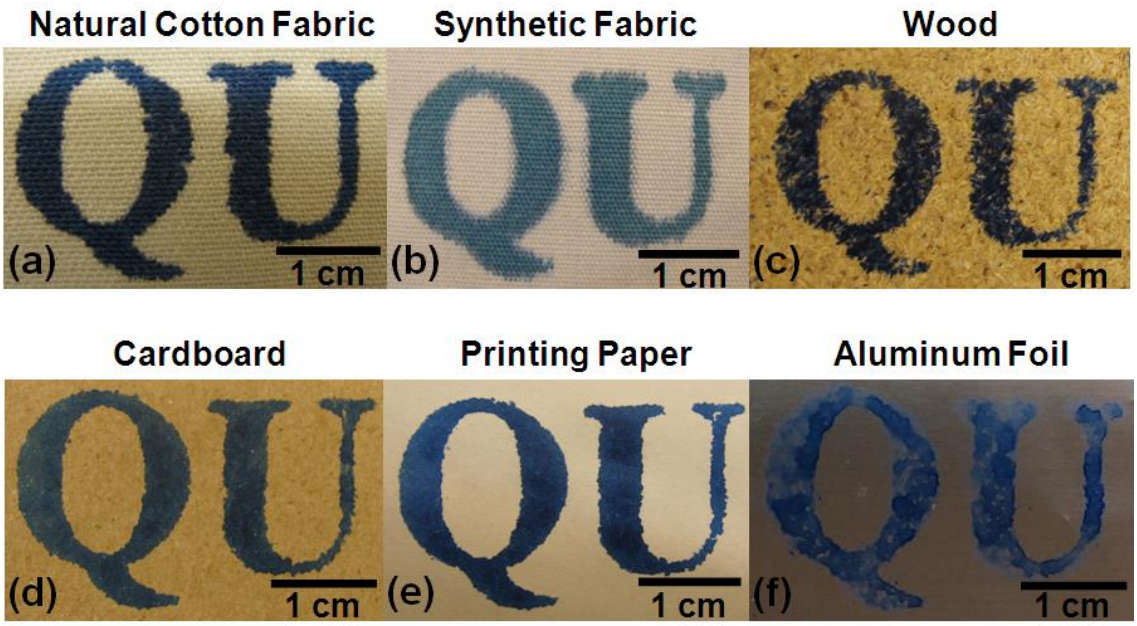

Figure 2.17 Patterns of "QU" that had been printed using PEO-containing ink onto (a) cotton fabric, (b) semi-synthetic fabric (65% polyester/35% cotton), (c) wood, (d) cardboard, (e) printing paper and (f) aluminum foil. The scale bars represent 1.0 cm.

Based on above observations, polymer aqueous solution can be directly used as printing ink. Therefore, we applied fluorescent polymer solution (C = 10.0 mg/mL) as the ink to fabricate fluorescent patterns on substrates using the cotton-based stamp. The polymer used was pyrene-terminated PEO (PEO-Py, *Mw* = 2000 g/mol) which was synthesized in our lab previously.[53] The pattern printed on natural cotton fabric is shown in Figure 2.18. The quality was as same as that of the pattern printed by PEO-containing ink. This indicates that the cotton-based stamp can extend to be used for fabricating fluorescent patterns on fabrics or other substrates.

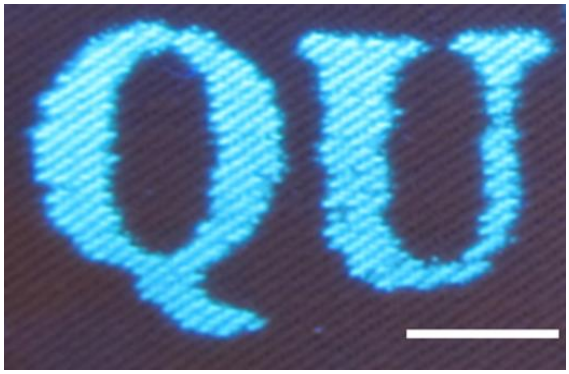

Figure 2.18 Fluorescent pattern of "QU" that had been printed using an aqueous PEO-Py solution as the ink onto cotton fabric. The scale bar represents 1.0 cm.

Besides the surface wettability of the substrates and viscosity of ink solutions, other factors such as stamping pressure, contact time and even cleanliness of the substrates might influence the quality of printed patterns as well although a fully systematic investigation for optimization of the stamping has not been done. However, we noted that even stamping on printing paper using PEO-containing ink, the patterns still had some small defect dots or slightly fuzzy boundaries. This might attribute to the cotton-based stamp itself. The stamp head made of soft cotton fabric might be not flat enough in some areas due to the weave so that there was no fully contact in such areas. On the other hand, the diameter of the cotton fiber is on the scale of 10 μm, the warp and weft thread diameters are 270 ± 10 and 620 ± 10 μm respectively. These limit the resolution of the printed patterns to be millimeter-scale.

The lifetime of the cotton-based stamp was not determined at this stage. However, within the experimental period, no significant failure was observed after hundreds of patterns were printed using one stamp. As shown above, all the "QU" patterns were printed by the same stamp, just a simple rinse with distill water and oven drying were needed before changing ink solutions. The good lifetime reflects the stability of superhydrophobic coating due to the crosslink of the diblock copolymer around the cotton fibers.

2.4 Conclusions

Diblock copolymer PDMS-*b*-PCEA consisting of 58 DMS units and 16 CEA units was synthesized and characterized. The copolymer formed micelles in THF/hexanes containing 80 vol% of hexanes. Soaking cotton swatches in this micellar solution, taking them out to evaporate the solvent, and annealing at 120 °C yielded uniform copolymer coatings on cotton fibers. XPS results and water repellency suggested that these coatings were topped by the PDMS layer. After UV irradiation for 1 h on each side of the coated cotton, the anchoring PCEA crosslinked around the cotton fibers and could not be removed by CH_2Cl_2 extraction. On the other hand, the polymer could be readily extracted from non-irradiated coated cotton. Therefore, a coated cotton sample was irradiated under an aluminum foil mask and then extracted with CH_2Cl_2 to produce hydrophilically-patterned superhydrophobic cotton fabric. The patterned fabric allowed selective permeation of water-based reagents through the hydrophilic regions. This represented the first report on the use of lithography and solvent extraction to produce patterned cotton fabrics. This method should be useful in the future for the preparation of cotton-based portable microfluidic devices as well.

Sealing the base of a sinter glass filtration funnel with the patterned cotton swatch and filling the funnel with an aqueous ink produced a stamp. Pressing the stamp against substrates with different wetting properties produced ink patterns that resembled the original mask. The fidelity of the reproduced pattern was the best on substrates that were wetted by the ink but were not too hydrophilic so as to readily absorb and spread the ink. The pattern fidelity improved on highly hydrophilic substrate such as cotton by increasing the viscosity of the aqueous ink. This printing technique may be useful for rapid printing T-shirts or jerseys in the future.

2.5 Notes and References

The main work described in this chapter has been published as:

Wang, Y., Li, X., Hu, H., Liu, G.,* and Rabnawaz, M. "Hydrophilically patterned superhydrophobic cotton fabrics and their use in ink printing", *J. Mater. Chem. A* 2014, **2**, 8094-8102.

References

1. X. Zhou, Z. Zhang, X. Xu, F. Guo, X. Zhu, X. Men and B. Ge, *ACS Appl. Mater. Inter.*, 2013, **5**, 7208-7214.
2. M. Zhang and C. Wang, *Carbohyd. Polym.*, 2013, **96**, 396-402.
3. B. J. Sparks, E. F. T. Hoff, L. Xiong, J. T. Goetz and D. L. Patton, *ACS Appl. Mater. Inter.*, 2013, **5**, 1811-1817.
4. D. Xiong, G. Liu and E. J. S. Duncan, *Langmuir*, 2012, **28**, 6911-6918.
5. N. A. Ivanova and A. K. Zaretskaya, *Appl. Surf. Sci.*, 2010, **257**, 1800-1803.
6. B. Leng, Z. Shao, G. de With and W. Ming, *Langmuir*, 2009, **25**, 2456-2460.
7. M. Yu, G. Gu, W. Meng and F. Qing, *Appl. Surf. Sci.*, 2007, **253**, 3669-3673.
8. S. N. Guntari, A. C. H. Khin, E. H. H. Wong, T. K. Goh, A. Blencowe, F. Caruso and G. G. Qiao, *Adv. Funct. Mater.*, 2013, **23**, 5159-5166.
9. G. W. Zhang, S. D. Lin, I. Wyman, H. L. Zou, J. W. Hu, G. J. Liu, J. D. Wang, F. Li, F. Liu and M. L. Hu, *ACS Appl. Mater. Inter.*, 2013, **5**, 13466-13477.
10. B. Bhushan and Y. C. Jung, *Progress in Materials Science*, 2011, **56**, 1-108.
11. J. Zimmermann, S. Seeger and F. A. Reifler, *Text. Res. J.*, 2009, **79**, 1565-1570.
12. S. Wang and L. Jiang, *Adv. Mater.*, 2007, **19**, 3423-3424.
13. X. Yao, Y. Song and L. Jiang, *Adv. Mater.*, 2011, **23**, 719-734.
14. Editorial, *Nat. Mater.*, 2005, **4**, 355-355.
15. M. Periolatto, F. Ferrero, A. Montarsolo and R. Mossotti, *Cellulose*, 2013, **20**, 355-364.

16. J. Maity, P. Kothary, E. A. O'Rear and C. Jacobi, *Ind. Eng. Chem. Res.*, 2010, **49**, 6075-6079.

17. B. Deng, R. Cai, Y. Yu, H. Q. Jiang, C. L. Wang, J. A. Li, L. F. Li, M. Yu, J. Y. Li, L. D. Xie, Q. Huang and C. H. Fan, *Adv. Mater.*, 2010, **22**, 5473-5477.

18. H. Wang, J. Fang, T. Cheng, J. Ding, L. Qu, L. Dai, X. Wang and T. Lin, *Chem. Commun.*, 2008, 877-879.

19. S. Ghiassian, H. Ismaili, B. D. W. Lubbock, J. W. Dube, P. J. Ragogna and M. S. Workentin, *Langmuir*, 2012, **28**, 12326-12333.

20. M. K. Sarkar, F. A. He and J. T. Fan, *Thin Solid Films*, 2010, **518**, 5033-5039.

21. A. Vilcnik, I. Jerman, A. S. Vuk, M. Kozelj, B. Orel, B. Tomsic, B. Simonic and J. Kovac, *Langmuir*, 2009, **25**, 5869-5880.

22. H. L. Zou, S. D. Lin, Y. Y. Tu, G. J. Liu, J. W. Hu, F. Li, L. Miao, G. W. Zhang, H. S. Luo, F. Liu, C. M. Hou and M. L. Hu, *J. Mater. Chem. A*, 2013, **1**, 11246-11260.

23. G. Li, H. Zheng, Y. Wang, H. Wang, Q. Dong and R. Bai, *Polymer*, 2010, **51**, 1940-1946.

24. Z. Shi, I. Wyman, G. Liu, H. Hu, H. Zou and J. Hu, *Polymer*, 2013, **54**, 6406-6414.

25. A. Hirao, K. Sugiyama and H. Yokoyama, *Prog. Polym. Sci.*, 2007, **32**, 1393-1438.

26. J. E. Mark, *Polymer Data Handbook. Oxford University Press*, 1999.

27. D. R. Lide, ed,. *CRC Handbook of Chemistry and Physics, Internet Version, CRC Press, Boca Raton, FL*, 2005.

28. A. Solga, Z. Cerman, B. F. Striffler, M. Spaeth and W. Barthlott, *Bioinspir. Biomim.*, 2007, **2**, S126-S134.

29. R. Furstner, W. Barthlott, C. Neinhuis and P. Walzel, *Langmuir*, 2005, **21**, 956-961.

30. R. N. Wenzel, *Ind. Eng. Chem.*, 1936, **28**, 988-994.

31. A. B. D. Cassie and S. Baxter, *Trans. Faraday Soc.*, 1944, **40**, 0546-0550.

32. P. L. Egerton, E. Pitts and A. Reiser, *Macromolecules*, 1981, **14**, 95-100.

33. A. Guo, G. Liu and J. Tao, *Macromolecules*, 1996, **29**, 2487-2493.

34. X. Jiang, S. Luo, S. P. Armes, W. Shi and S. Liu, *Macromolecules*, 2006, **39**, 5987-5994.

35. D. Qin, Y. N. Xia, B. Xu, H. Yang, C. Zhu and G. M. Whitesides, *Adv. Mater.*, 1999, **11**, 1433-1437.

36. R. Maoz, S. R. Cohen and J. Sagiv, *Adv. Mater.*, 1999, **11**, 55-61.

37. D. Hohnholz, H. Okuzaki and A. G. MacDiarmid, *Adv. Funct. Mater.*, 2005, **15**, 51-56.

38. D. Zahner, J. Abagat, F. Svec, J. M. J. Frechet and P. A. Levkin, *Adv. Mater.*, 2011, **23**, 3030-3034.

39. D. A. Bruzewicz, M. Reches and G. M. Whitesides, *Anal. Chem.*, 2008, **80**, 3387-3392.

40. A. K. Yetisen, M. S. Akram and C. R. Lowe, *Lab Chip*, 2013, **13**, 2210-2251.

41. C. M. Cheng, A. D. Mazzeo, J. L. Gong, A. W. Martinez, S. T. Phillips, N. Jain and G. M. Whitesides, *Lab Chip*, 2010, **10**, 3201-3205.

42. S. P. R. Kobaku, A. K. Kota, D. H. Lee, J. M. Mabry and A. Tuteja, *Angew. Chem. Int. Edit.*, 2012, **51**, 10109-10113.

43. P. Bhandari, T. Narahari and D. Dendukuri, *Lab Chip*, 2011, **11**, 2493-2499.

44. B. Zhao, J. S. Moore and D. J. Beebe, *Science*, 2001, **291**, 1023-1026.

45. L. Zhai, M. C. Berg, F. C. Cebeci, Y. Kim, J. M. Milwid, M. F. Rubner and R. E. Cohen, *Nano Lett.*, 2006, **6**, 1213-1217.

46. H. Gau, S. Herminghaus, P. Lenz and R. Lipowsky, *Science*, 1999, **283**, 46-49.

47. X. M. Chen, J. Wu, R. Y. Ma, M. Hua, N. Koratkar, S. H. Yao and Z. K. Wang, *Adv. Funct. Mater.*, 2011, **21**, 4617-4623.

48. A. R. Parker and C. R. Lawrence, *Nature*, 2001, **414**, 33-34.

49. I. B. Burgess, L. Mishchenko, B. D. Hatton, M. Kolle, M. Loncar and J. Aizenberg, *J. Am. Chem. Soc.*, 2011, **133**, 12430-12432.

50. A. Nilghaz, D. H. B. Wicaksono, D. Gustiono, F. A. A. Majid, E. Supriyanto and M. R. A. Kadir, *Lab Chip*, 2012, **12**, 209-218.

51. S. Y. Xing, J. Jiang and T. R. Pan, *Lab Chip*, 2013, **13**, 1937-1947.

52. A. Muhlebach, S. G. Gaynor and K. Matyjaszewski, *Macromolecules*, 1998, **31**, 6046-6052.

53. H. Hu and G. J. Liu, *Macromolecules*, 2014, **47**, 5096-5103.

54. E. Duquesne, J. Habimana, P. Degee and P. Dubois, *Macromol. Chem. Phys.*, 2006, **207**, 1116-1125.

55. K. Huan, L. Bes, D. M. Haddleton and E. Khoshdel, *J. Polym. Sci. A-Polym. Chem.*, 2001, **39**, 1833-1842.

56. S. Bas and M. D. Soucek, *Polym. J.*, 2012, **44**, 1087-1097.

57. R. H. Zheng, G. J. Liu and T. C. Jao, *Polymer*, 2007, **48**, 7049-7057.

58. K. Matyjaszewski and J. H. Xia, *Chem. Rev.*, 2001, **101**, 2921-2990.

59. S. T. Milner, *Science*, 1991, **251**, 905-914.

60. A. Halperin, M. Tirrell and T. P. Lodge, *Adv. Polym. Sci.*, 1992, **100**, 31-71.

61. N. Wang, Master Thesis, Queen's University, 2008.

62. G. J. Liu, J. F. Ding, T. Hashimoto, K. Kimishima, F. M. Winnik and S. Nigam, *Chem. Mater.*, 1999, **11**, 2233-2240.

63. Z. K. He, M. Ma, X. R. Lan, F. Chen, K. Wang, H. Deng, Q. Zhang and Q. Fu, *Soft Matter*, 2011, **7**, 6435-6443.

Chapter 3

Superhydrophobic Cotton Fabrics Coated with Polymeric Nanoparticles and Poly(dimethylsiloxane)-based Diblock Copolymer Bearing Glycidyl for Oil-Water Separation

3.1 Introduction

Cotton fabrics with (super)hydrophobic coatings are very useful in daily life. These water resistant cotton fabrics can be used to make contamination-free T-shirts, coats, table cloth and so on. However, another important application, oil-water separation, based on (super)hydrophobic cotton fabrics has become more attractive in the past decade.[1-11] Since cleaning spilled oil or separating oil from waste water costs large amounts of energy, developing materials which can separate oil-water mixture by either absorption or filtration has become significant. The large specific surface area and strong capillary action of cotton fabrics make them suitable to absorb liquids. Meanwhile, the membrane-like fabrics with pores can be used as filters for liquids as well. Therefore, if such inexpensive materials are coated by a little amount of hydrophobic species to selectively absorb or filter oil phase, they can become a good candidate for oil-water separation.

The (super)hydrophobicity of cotton fabrics normally rely on two factors. One is the low surface energy of coatings and the other is surface roughness of fabrics.[12-14] To achieve the low surface energy, fluorinated compounds and low surface energy polymer such as poly(dimethyl siloxane) (PDMS) have been used for surface coatings.[15-18] However, besides the environmental issue, many fluorinated compounds exhibit very low surface energy (6 - 10 mN/m) that the coated surfaces repel both water and oil.[19-23] So non-fluorinated polymer such as PDMS which has a surface energy about 18 - 20 mN/m is more suitable for cotton coatings for oil-water separation.[11,

[15, 16, 24] PDMS's surface energy is low enough to repel water which has a high surface tension of 72.5 mN/m,[25] but not low enough to repel most common organic liquids which have surface tensions in the range of 20-30 mN/m.[9] The other factor surface roughness can be enhanced by introducing nanoparticles, SiO_2 or metal oxide nanoparticles for example, on cotton fiber surfaces.[7, 8, 15, 26, 27] Although cotton fabrics themselves exhibit microscale roughness, according to Wenzel's theory,[28] further increasing roughness by coating nanoparticles can enhance the water repellency because water will increase its apparent contact angle to minimize the contact area between itself and the PDMS-coated cotton surface. Such nano/micro hierarchical structure can also trap more air between liquid and solid phases so that the water on fabric surface can even stay in Cassie state.[29] In addition, because common low surface tension organic liquids only exhibit contact angles less than 90° on a PDMS surface, according to Wenzel's theory again, they should wet or be absorbed by PDMS-modified cotton fabrics easier if the fabrics' surface roughness increases. Or stating it in another way, increased roughness can make the fabrics more oleophilic.

Based on above arguments, various strategies and materials have been applied to fabricate (super)hydrophobic cotton fabrics for oil-water separation. As mentioned previously, PDMS-based polymer can be used directly to provide the hydrophobicity. For example, terminal functionalized PDMS could be cured by heating to form a crosslinked layer on cotton fiber surfaces.[15, 16, 30] Diblock copolymer poly(dimethylsiloxane)-*block*-poly[2-(cinnamoyloxy) ethyl acrylate] (PDMS-*b*-PCEA) could also form a crosslinked layer around cotton fibers by UV irradiation.[31] In addition, poly(dimethylsiloxane)-*block*-poly[3-(triisopropyloxysilyl) propyl methacrylate] (PDMS-*b*-PIPSMA) was used for cotton coating based on sol-gel chemistry that the polymer could not only form a network around cotton fiber via self-crosslinking reaction, but also form covalent bonds with surface hydroxyl groups of cotton.[32] However, both hydrolysis and condensation reactions during this sol-gel chemistry are reversible.[33] Therefore, developing more kinds of PDMS-based polymer with other anchor block which can form more stable chemical bonds such as ester or ether

linkages should be important. On the other hand, the increase of surface roughness by introducing nanoparticles can further increase water repellency and oil wettability. Therefore, SiO_2, TiO_2 and other metal oxide nanoparticles have been synthesized and coated onto cotton surface since their facile preparation procedures.[5, 7, 8, 15] While, the introduction of polymeric nanoparticles onto cotton fabrics for oil-water separation has not been reported. Cotton coated with full polymeric materials may yield lighter and softer oil absorbent. In addition, crosslinked polymeric materials can swell after absorbing liquid.[34] Therefore, crosslinked polymeric particles may also benefit the oil absorption comparing to those inorganic particles.

As the above proposed reasons, in this chapter, a diblock copolymer poly(dimethylsiloxane)-*block*-poly(glycidyl methacrylate) (PDMS-*b*-PGMA) was synthesized via atom transfer radical polymerization (ATRP)[35, 36] and polymeric nanoparticles bearing styrene (S) and GMA (P(S-GMA)) were synthesized via surfactant-free emulsion copolymerization using divinylbenzene (DVB) as a crosslinker.[37] Neither of them has been used for cotton coatings. PGMA was chosen as anchor block of the diblock copolymer since epoxy can react with hydroxyl groups on cotton surface to form stable ether bonds.[38] Some block copolymers containing fluorinated block and PGMA have been used for cotton coating.[39, 40] These studies revealed that the coating based on PGMA was very stable due to the formation of covalent bonds between coated polymer and cotton substrate. However, block copolymer bearing both PDMS and PGMA has not been used for cotton coating and then oil-water separation, although it has been synthesized for self-assembly study.[41] On the other hand, nanoparticles bearing GMA can also chemically grafted onto cotton through the same reaction mentioned above. Styrene was chosen because it is cheaper and much easier for surfactant-free emulsion polymerization based on our previous study.[37] DVB was used as crosslinker during the polymerization that the final polymeric nanoparticles would be solvent resistant and even benefit the oil absorption due to swollen. Finally, two types of coated cotton were fabricated in this chapter. One was PDMS-*b*-PGMA polymer coated cotton (P-cotton). In

the other one, cotton was coated by a layer of P(S-GMA) nanoparticles and then coated by PDMS-*b*-PGMA (PP-cotton). Their water repellency, oil absorption capacity and oil-water separation ability were investigated and compared. Such comprehensive comparative study between only diblock copolymer coated cotton and both nanoparticles and diblock copolymer coated cotton in oil-water separation also has not been reported. The results described in this chapter revealed that the PP-cotton performed better rather than P-cotton although both of them exhibited hydrophobicity/oleophilicity and oil-water separation ability. These new coatings and their comparison can provide some insight to future study in this area.

3.2 Experimental

3.2.1 Materials

Plain-weave cotton fabric used was purchased from a local store. Before use, the fabric was washed in 5.0 wt% Fisher Sparkleen detergent aqueous solution at room temperature for 30 min before it was rinsed by distilled water three times. The clean fabric was dried at 120 °C for 20 min and was subsequently cut into small pieces to be used for various experiments. The bromide terminated polydimethylsiloxane (PDMS-Br) as macroinitiator was synthesized and characterized in our lab previously.[31] It has 58 units of DMS and its polydispersity index (PDI) is 1.10. Tetrahydrofuran (THF, Fisher) was distilled over sodium and a trace amount of benzophenone. Styrene (S, Sigma-Aldrich, 99.9%), glycidyl methacrylate (GMA, Sigma-Aldrich, 97%) and divinylbenzene (DVB, Sigma-Aldrich, 80%) were purified by distillation under reduced pressure. CuCl (Aldrich, 98%) was purified by stirring in glacial acetic acid and washed with pure ethanol. Chloroform (Fisher, 99.9%) was passed through a membrane filter (Durapore, 0.45μm) before it was used as a SEC eluent. 2,2'-Azobis(2-methylpropionamidine) dihydrochloride (V50, Sigma-Aldrich, 97%), 2,2'-dipyridyl (Acros, 99%), *N*,*N*-dimethylformamide (DMF, 99.8%), hexadecane

(Sigma-Aldrich, 99%), hexanes (Caledon, 98.5%) and toluene (Sigma-Aldrich, 99.5%) were used as received.

3.2.2 Synthesis of Diblock Copolymer PDMS-*b*-PGMA

The diblock copolymer PDMS-*b*-PGMA was prepared via atom transfer radical polymerization, in which PDMS-Br (2.55 g, 0.60 mmol), GMA (2.15 g, 15.0 mmol), THF (15.0 mL) and 2,2'-dipyridyl (203 mg, 1.30 mmol) were initially mixed together in a two-necked round-bottom flask. The flask was then purged with N_2 for 15 min before CuCl (55 mg, 0.60 mmol) was added and the contents of the flask were degassed by three freeze-pump-thaw cycles. The final N_2-filled flask was immersed in a preheated oil bath that was kept at 70 °C. The reaction was stopped after 9 hours by quenching with liquid nitrogen and subsequently introducing air. The crude mixture was cooled to room temperature, diluted with 25 mL THF and filtered through a neutral alumina column using THF as the eluent. Then the polymer solution was concentrated to 4.0 mL and poured into 40 mL of methanol. The precipitated polymer was collected after it had been centrifuged and was subsequently re-dissolved into 4.0 mL THF. This dissolution-precipitation-centrifugation purification treatment was repeated twice before the product PDMS-*b*-PGMA was dried under vacuum for 12 hours at room temperature (yield ≈ 91 %).

3.2.3 Synthesis of P(S-GMA) Nanoparticles

The P(S-GMA) nanoparticles were prepared from surfactant-free emulsion copolymerization of styrene (S), glycidyl methacrylate (GMA) and divinylbenzene (DVB). In a typical preparation, 0.30 g of GMA and 25.0 mL of deionized water were placed in a 125 mL two-neck round-bottom flask and deoxygenated under stirring by bubbling the solution with nitrogen gas for 15 min before 1.00 g of S and 50 mg of DVB were added into the flask. The mixture was then heated to 90 °C, and 40 mg of the initiator V50 (which had been pre-dissolved in 5.0 mL of deionized water) was added to the reaction flask. The solution was left to react for 3 hours under nitrogen protection before the emulsion was filtered through absorbent cotton (cotton ball manufactured by P.C.R.C.

Inc., Canada) to remove any aggregates. The filtrate was centrifuged at 13000 rpm for 10 min to settle the particles and the supernatant was decanted. The particles were re-dispersed into DMF and centrifuged to settle them again before the supernatant was discarded. The rinsing procedure was repeated once more. Finally, the settled particles were dispersed in THF with a concentration of 40 mg/mL before further use.

3.2.4 Cotton Coatings with PDMS-*b*-PGMA or Nanoparticles/PDMS-*b*-PGMA

Two types of coated cotton were studied in this report. The first type denoted as P-cotton was the cotton coated with PDMS-*b*-PGMA polymer. The second type denoted as PP-cotton was the cotton coated by P(S-GMA) nanoparticles followed by polymer coating. Typically, P-cotton was prepared by immersing uncoated cotton samples in a glass vial which contained THF, PDMS-*b*-PGMA (30 mg/mL), triethylamine (10.9 mg/mL) and benzyltrimethylammonium chloride (2.8 mg/mL). The mixture was stirred at 60 °C for one hour. Subsequently, the cotton samples were withdrawn from the coating solution and heated in oven at 100 °C for two hours. Then the coated samples were extracted by hot THF (60 °C) three times (15 min for each time) to remove unstable polymer on the surface. Finally, the samples were dried in oven at 100 °C for 30 min before any use. PP-cotton was prepared similarly. The uncoated cotton samples were immersed in a glass vial which contained THF, P(S-GMA) nanoparticles (40 mg/mL), triethylamine (10.9 mg/mL) and benzyltrimethylammonium chloride (2.8 mg/mL). The later heating, extraction and drying procedures were identical to those in the preparation of P-cotton. Subsequently, these particle coated cotton samples were further coated with PDMS-*b*-PGMA polymer using same procedures which were also described in the preparation of P-cotton.

3.2.5 Water Contact, Sliding and Shedding Angles Measurements

A DataPhysics OCA 15 Pro Optical instrument was used to measure the water static contact angles and sliding angles. The droplet size for contact angle and sliding angle measurements were 5.0 and 10.0 μL respectively. To determine the sliding angle, a water droplet was first dispensed

on a cotton sample on the stage that was levelled. The tilting angle of the stage was then increased gradually. The sliding angle was defined as the minimal stage tilting angle for a water droplet to slide. Water shedding angles were measured using a literature method.[42] First, a cotton sample was attached to a glass plate with double-sided adhesive tape. This glass plate was then placed on a custom-built tilting stage, and a syringe containing water was mounted 1.0 cm above the testing spot. To determine the shedding angle, measurement was started at a tilting angle of 35°. Water droplets (10 μL) were dispensed onto three different spots on each cotton sample. If all of the water droplets bounced or rolled off the sample, the tilting angle was reduced by ~1° via reducing the height of the adjustable end of the tilting stage. This procedure was repeated until one or more of the water droplets would not completely roll off the surface. The lowest tilting angle at which all of the drops completely bounced or rolled off the sample surface was noted as the shedding angles. All the contact angles, sliding angles and shedding angles measurements were performed at room temperature (22 ± 1 °C) and each value was the average measured on at least three specimens for corresponding sample.

3.2.6 Oil Absorption, Pressure-Dependent Water Absorption and Breakthrough Pressure Measurements

For oil absorption capacity measurements, the weight of each dry cotton sample W was recorded by balance first. Subsequently, the cotton sample was immersed in 10 mL oil in a 20 mL glass vial for 1.0 min. Then the weight of cotton sample after oil absorption W' was recorded. The oil absorption capacity C_o was determined as $C_o = (W' - W)/W$. For pressure-dependent water absorption measurements, the weight of each dry coated cotton sample W was recorded by balance first. Subsequently, the sample was placed on water surface, as zero pressure, for 1.0 min. Then the weight of cotton sample W' was recorded. For non-zero pressures, a tweezer was used to force the sample to stay under water at a particular depth (5.0, 10.0, 15.0, 20.0, 25.0 and 30.0 cm respectively) for 1.0 min. The final weight of cotton sample W' under each pressure was recorded

and the water absorption A_w of coated cotton was defined as $A_w = (W' - W)/W$. Breakthrough pressure of each coated cotton sample was measured using a glass tube. The length and inner diameter of this tube were 64.5 cm and 1.20 cm. The tube was clamped vertically and its bottom end was sealed by a piece of coated cotton sample. Then water was added slowly into the tube. When the water started to pass through the hydrophobic cotton fabric, the height of water column was recorded. Then this height was converted to static pressure which was defined as breakthrough pressure P_b. Each value of C_o, A_w and P_b was the average of three measurements.

3.2.7 Oil-Water Separation

To demonstrate oil water separation using absorption method, 125 μL hexadecane (dyed with Oil Red O) and 20 mL water were added into a glass petri dish. Then one piece of each type of cotton sample (~ 1.5 cm * 1.5 cm) was placed to the center of "oil-spilled" area. Photographs were recorded after 30s. To demonstrate oil water separation using filtration method, one piece of each type of cotton sample (~ 3.0 * 3.0 cm) was sandwiched by the two parts of a sinter glass filter funnel. Water-chloroform mixture (v/v = 15.0 mL/15.0 mL) was added into the funnel. All the liquid passed through the cotton filter was collected by a flask while the volume of water left on the top was recorded. To further investigate the reusability of the sample as a filter, same amount of water-chloroform mixture was added to the funnel after the funnel was emptied. The volume of water left on the top was recorded again. This procedure was kept repeating until no water could stay on the top.

3.2.8 Other Characterizations

Size exclusion chromatography (SEC) was performed at 25 °C using a Wyatt Optilab rEX refractive index detector. The three columns were packed by MZ-Analysentechnik with 5 μ AM 500, 10,000 and 100,000 Å gels. The system was calibrated with monodisperse polystyrene (PS) standards. Chloroform was used as the eluent with a flow rate of 1.0 mL/min. The solution samples were filtered by syringe filters (Dikma, PTFE, 0.22 μm) before they were injected into the SEC

system. ^{1}H NMR characterization was performed using a Bruker Avance-300 instrument at 25 °C using chloroform-*d* ($CDCl_3$) as the solvent. Scanning electron microscope (SEM) images of the cotton samples were recorded using a FEI-MLA Quanta 650 FEG-ESEM instrument that was operated at 10-15 kV. Atomic-force microscope (AFM) images were recorded by a Veeco Multimode instrument that was equipped with a Nanoscope IIIa controller and operated in the Tapping Mode. Dynamic light scattering (DLS) measurements were carried out at 20 °C using a Brookhaven BI-200 SM instrument that was equipped with a BI-9000AT digital correlator and a He-Ne laser (632.8 nm). All of the measurements were performed at an angle of 90°. FT-IR spectra were obtained using a Bruker ALPHA FT-IR Spectrometer with ATR sampling module.

3.3 Results and Discussion

3.3.1 Synthesis and Characterizations of Diblock Copolymer PDMS-*b*-PGMA

As shown in Figure 3.1, the diblock copolymer PDMS-*b*-PGMA was synthesized via atom transfer radical polymerization (ATRP) of GMA monomer using PDMS-Br as macroinitiator. The macroinitiator was pre-made by reacting commercially-available hydroxyl-terminated PDMS with 2-bromopropionyl bromide. The details of synthesis and characterization of the macroinitiator used here was described previously in section 2.3.1 – 2.3.2. The repeat units of DMS was calculated as 58 by comparing peaks of terminal group and polymer backbone in ^{1}H NMR spectrum. The polydispersity index of the macroinitiator was determined as 1.10 based on size exclusion chromatography (SEC) result. After ATRP of GMA monomer using this macroinitiator, the final product PDMS-*b*-PGMA was analyzed by SEC in $CHCl_3$ and ^{1}H NMR in $CDCl_3$ to confirm its structure. Figure 3.2 shows the comparison of SEC traces between PDMS-Br macroinitiator and final PDMS-*b*-PGMA diblock copolymer. The later trace obviously shifted to the shorter retention time side indicating the increase of molecular weight after polymerization. The PDI of the diblock copolymer was 1.12 which was calculated based on narrow distributed polystyrene (PS) standard

samples. The repeat units of the second block PGMA was further confirmed by ^{1}H NMR analysis, as shown in Figure 3.3. The integration ratio between the signal corresponding to the PDMS block (peak a) and the signals corresponding to the PGMA block (peaks b, c, d, e and f) suggested that the repeat unit of PGMA was 24 based on a PDMS repeat unit number of 58.

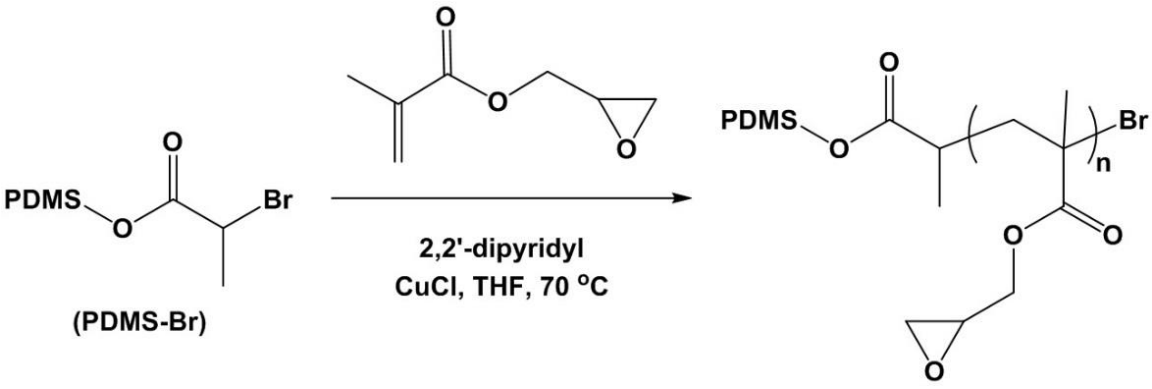

Figure 3.1 Synthesis of PDMS-*b*-PGMA via ATRP.

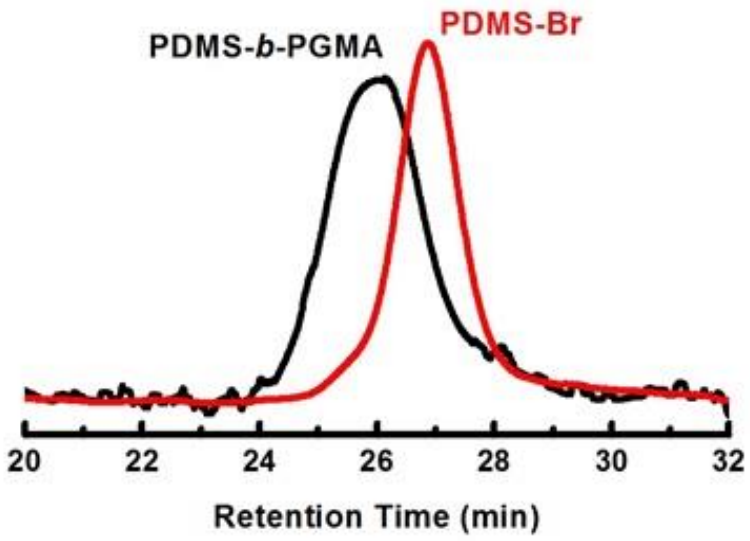

Figure 3.2 SEC traces of macroinitiator PDMS-Br and diblock copolymer PDMS-*b*-PGMA.

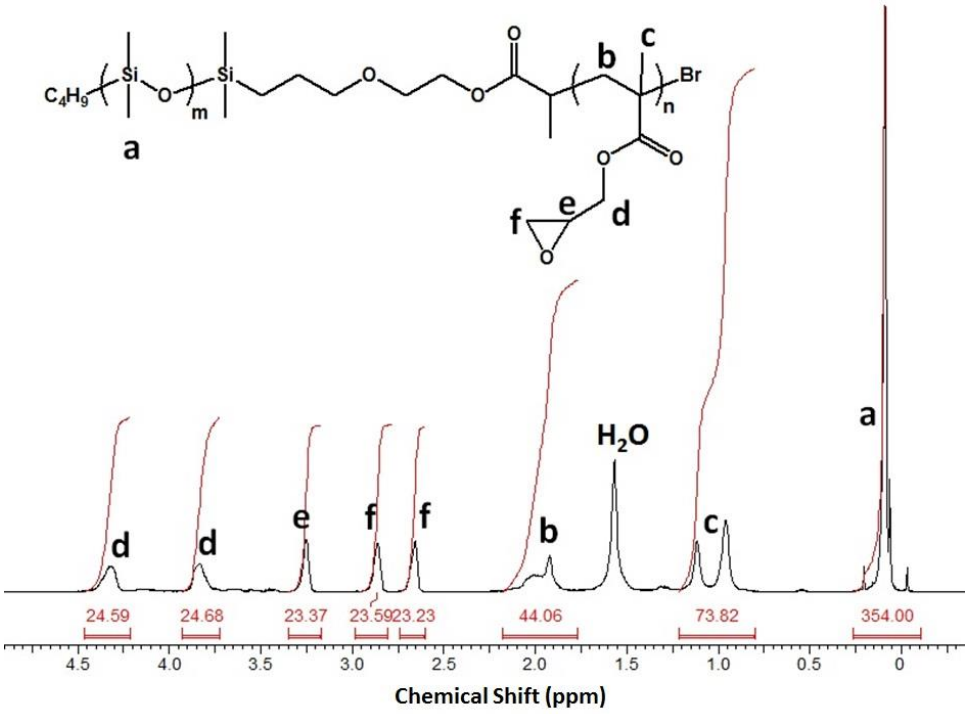

Figure 3.3 ^{1}H NMR spectrum of PDMS-*b*-PGMA.

3.3.2 Synthesis and Characterizations of P(S-GMA) Nanoparticles

The P(S-GMA) nanoparticles were prepared by surfactant-free emulsion copolymerization of styrene (S) and glycidyl methacrylate (GMA) using 2,2′-azobis(2-methylpropionamidine) dihydrochloride (V50) as the initiator and divinylbenzene (DVB) as the crosslinker. GMA was used to introduce epoxide groups to the particles. Meanwhile, DVB served to ensure the structural integrity of the synthesized spheres in solvents. Under optimized condition, the synthesis of nanoparticles was facile and straightforward. After 3 hours of heating at 90 °C, whitish nanoparticle solution or emulsion was obtained. The produced emulsion was very stable that no obvious settling down was observed after one week. Even after one year, the settled particles could be re-dispersed in water to form whitish emulsion by shaking for a few seconds. The size and morphology of the nanoparticles were first analyzed by atomic force microscopy (AFM) after the particles were aero-sprayed onto silicon wafer. The AFM analysis revealed that the nanoparticles

from emulsion polymerization were spherical and smooth (Figure 3.4). In addition, the size distribution of these particles was narrow and the average diameter of them was 278 ± 15 nm based on AFM analysis. The size and size distribution were also confirmed by dynamic light scattering (DLS) using dilute particles aqueous solution. DLS measurement yield a hydrodynamic diameter (d_h) of 307 nm and a polydispersity index (PDI) of 0.06. These results also indicated that the size distribution was narrow, although the average diameter from this measurement was slightly larger than that from AFM analysis. However, this size increase in DLS measurement should attribute to the expansion of particles in solvent. Additionally, the scattering-intensity-average diameter, also known as the z-average diameter, should be higher than the number-average diameter determined via AFM. A small portion of sample was dried under vacuum and used for FT-IR analysis to further confirm the chemical structure of the nanoparticles. As shown in Figure 3.5, the absorption peaks at 1600 cm^{-1} (C=C stretching, aromatic), 760 cm^{-1} and 700 cm^{-1} (C-H bending, aromatic) corresponded to the phenyl of styrene and DVB.[37, 43] The absorption peaks at 1730 cm^{-1} (C=O stretching), 910 cm^{-1} (epoxy ring deformation, asymmetric) and 848 cm^{-1} (epoxy ring deformation, symmetric) corresponded to the GMA.[37, 43] In addition, the presence of epoxy ring peak (910 and 848 cm^{-1}) and the absence of hydroxyl peak (3200-3400 cm^{-1})[43] indicated that the epoxy did not undergo ring opening reaction during the emulsion polymerization. This was important for further cotton coating.

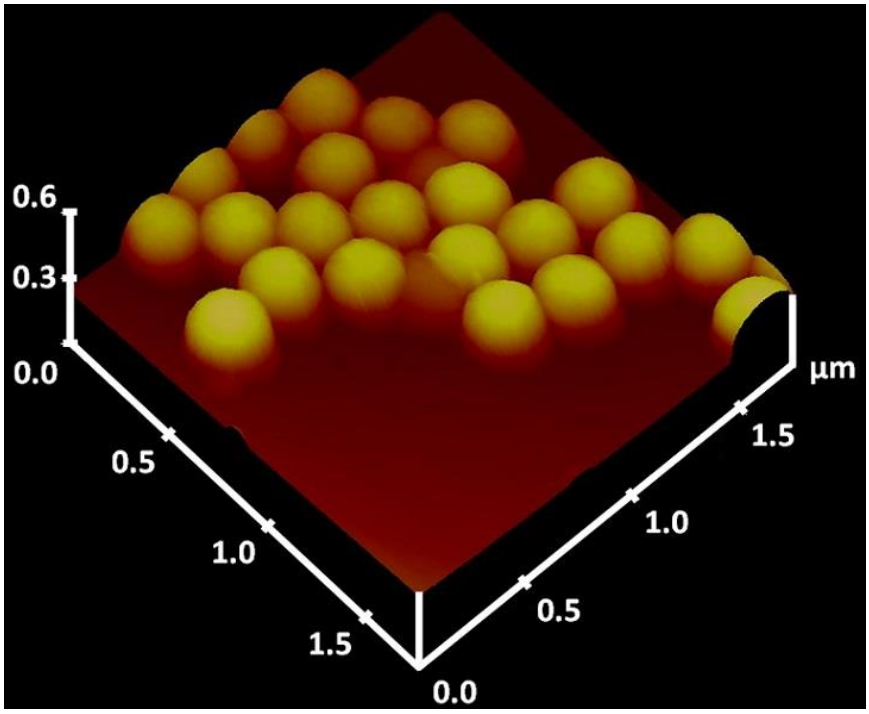

Figure 3.4 AFM 3D image of P(S-GMA) nanoparticles.

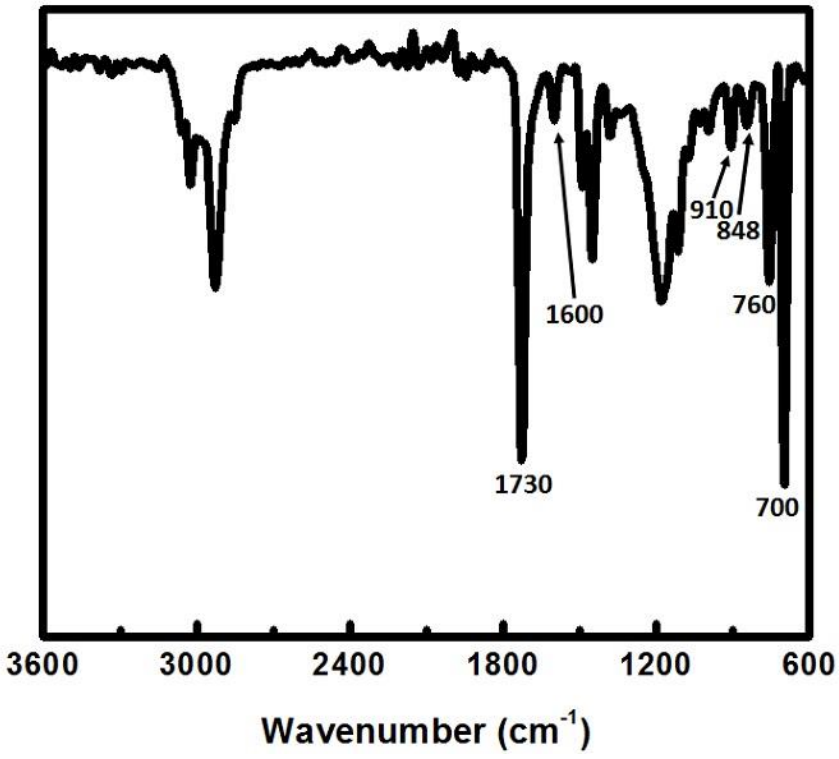

Figure 3.5 FT-IR spectrum of P(S-GMA) nanoparticles.

3.3.3 Cotton Coatings with PDMS-*b*-PGMA or Nanoparticles/PDMS-*b*-PGMA

Two types of coated cotton were produced using essentially same protocol. The first type denoted as P-cotton was the cotton coated with only PDMS-*b*-PGMA polymer based on the easy thermal reaction between hydroxyl groups of cotton and epoxy of the polymer catalyzed by triethylamine and benzyltrimethylammonium chloride.[39] The second type denoted as PP-cotton was the cotton coated with P(S-GMA) nanoparticles first and then coated with PDMS-*b*-PGMA polymer. Similarly, the first step of the second type coating was based on the reaction between hydroxyl groups of cotton and epoxy of nanoparticles. In the second step, the produced hydroxyl groups on the particles after ring-opening reaction and the rest hydroxyl groups on the uncovered region of cotton could further react with PDMS-*b*-PGMA polymer. In addition, one advantage of this stepwise cotton coating using epoxy-based particles and polymer was that the completion of ring-opening in the first step was not required. Since even the residual epoxy on the particles could participate the second step polymer coating via epoxy self-reaction according to a recent study.[39] Finally, both types of coated cotton were extracted by hot THF to remove any unstable polymer or particles. An optimized polymer concentration (30 mg/mL), higher than which the water repellency did not change, was used in both types of coatings.

Scanning electron microscope (SEM) was used to characterize the two types of coated cotton. It was obvious that the P-cotton fibers (Figure 3.6b) had almost identical surface which was smooth comparing to the uncoated cotton (Figure 3.6a). This result was very similar to some results reported previously.[17, 31, 40] In those cases, there was no surface change for cotton fibers coated by thin layer of block copolymer[17, 31] or the change was quite amphibolous.[40] However, the surface of PP-cotton fibers changed significantly (Figure 3.6c). The fiber surface roughness increased obviously since the introduction of nanoparticles. The high magnification image further showed that the fiber surface was uniformly but not completely covered by the nanoparticles. In addition, small clusters of nanoparticles were observed on the fiber surface. This might attribute to the epoxy self-reaction which was reported in literature.[39] Both small interspaces and particle clusters

contributed the increase of surface roughness. Finally, both small interspaces and particles could be covered by PDMS-*b*-PGMA polymer in the second step to obtain low surface energy.

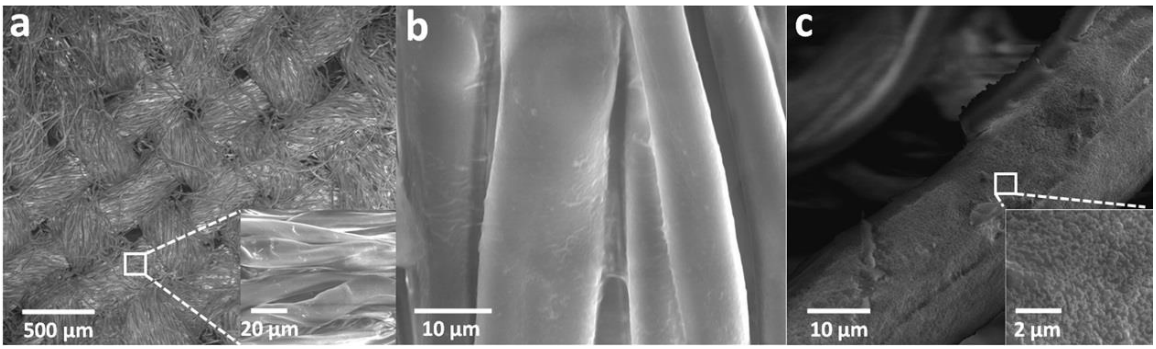

Figure 3.6 SEM images of (a) Uncoated cotton fibers, (b) PDMS-*b*-PGMA polymer coated cotton (P-cotton) fibers and (c) P(S-GMA) nanoparticle + PDMS-*b*-PGMA polymer coated cotton (PP-cotton) fibers.

FT-IR was further used to confirm the successful coatings of both P-cotton and PP-cotton since SEM could only directly confirm the coating of nanoparticles. Comparing to uncoated cotton, as shown in Figure 3.7b, a new peak at 1727 cm^{-1} corresponding to C=O stretching was observed on the spectrum of P-cotton.[43] This was from the PGMA block of the diblock copolymer. Meanwhile, two sharp peaks at 1260 cm^{-1} ($Si-CH_3$, symmetric bending) and 800 cm^{-1} ($CH_3-Si-CH_3$, methyl rocking mode), one broad peak at 1100 cm^{-1} (Si-O-Si, asymmetric stretching) were also observed on P-cotton.[44] These peaks were from the PDMS block of the coated copolymer. These absorption peaks proved that the PDMS-*b*-PGMA diblock copolymer was successfully coated on the cotton fibers after solvent extraction, although there was no difference between the uncoated cotton and P-cotton from SEM. Besides all the polymer peaks discussed above, the spectrum of PP-cotton showed one more peak at 700 cm^{-1} which attributed to the styrene component (C-H bending, aromatic) in the nanoparticles. These results strongly indicated that both nanoparticles and diblock copolymer were stably coated on cotton in the second type of coating, although the SEM image of PP-cotton could not directly show the diblock copolymer on the surface.

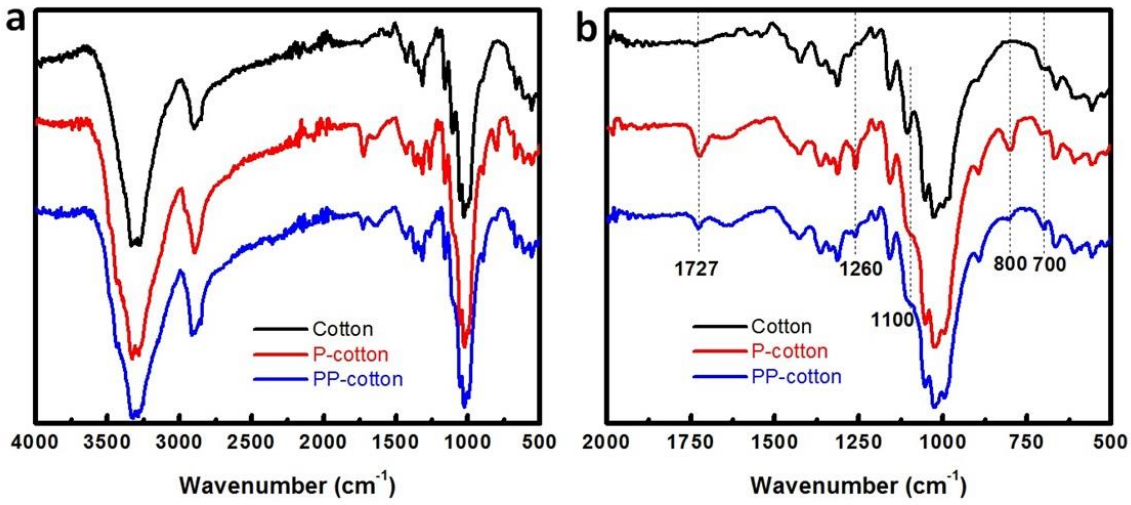

Figure 3.7 FT-IR spectra of uncoated cotton, P-cotton and PP-cotton in the full range from 4000 to 500 cm^{-1} (a) and the magnified range from 2000 to 500 cm^{-1} (b).

3.3.4 Water Repellency of Coated Cotton Fabrics

Water repellency of these two types of coated cotton was firstly studied by measuring the water static contact angles, sliding angles and shedding angles. The shedding angle measurement, specially designed for textiles, uses initial kinetic energy of the dropping water from a height of 1.0 cm to overcome the pinning energy due to the compositional and structural heterogeneity of a surface and a strong interaction between the droplet and the substrate.[42] All the results are summarized in Table 3.1. An obvious trend was observed from the results in Table 3.1. While uncoated cotton absorbed water immediately and exhibited a zero apparent water contact angle, P-cotton showed a contact angle of (151 ± 2)° and shedding angle of (29 ± 3)° due to the low surface energy of PDMS and rough surface of cotton. Meanwhile, PP-cotton showed a higher contact angle of (158 ± 1)° and a lower shedding angle of (11 ± 4)°. In addition, PP-cotton showed a sliding angle of (44 ± 2)° besides the shedding angle, while P-cotton did not show any sliding angle since water droplet could not roll off after it sat on the P-cotton surface. This better water resistant property of PP-cotton must attribute to the further introduction of nanoscale roughness onto

microscale cotton fibers by coating the nanoparticles. Therefore, water on PP-cotton surface should be closer to Cassie state than that on P-cotton surface since more air could be trapped between liquid phase and solid phase.[29]

However, the metastable Cassie state can be transferred to Wenzel state by additional energy such as that from static pressure.[12, 45] Therefore, breakthrough pressures (P_b) of these two types of coated cotton were measured using literature reported method and setup to further evaluate their water repellency.[11, 46] A long glass tube was clamped vertically and its bottom mouth was sealed by coated cotton fabric sample. Water was added into the tube slowly until the cumulated water column generated enough pressure to fully wet and pass through the fabric. The maximal water static pressure at that critical point was defined as P_b. The results showed that PP-cotton exhibited a higher P_b of 3.2 kPa comparing to P-cotton which had a P_b of 1.1 kPa. Since an optimized polymer concentration was already used for both types of coating to reach their best performance, the higher P_b of PP-cotton must due to the introduction of nanoparticles. Interestingly, some theoretical study predicted that the hierarchically structured surface would not increase P_b much comparing to its corresponding microstructure.[45] However, some reported experimental studies revealed that although the P_b could be roughly estimated with some proposed models, there were still numerous details of coating process could significantly influence its value. Therefore, more investigation is required and more factors may be taken into account in future work.[47]

Table 3.1 Water static contact angles, shedding angles, sliding angles and breakthrough pressures of uncoated cotton, P-cotton and PP-cotton.

	Contact angle (°)*	Shedding angle (°)#	Sliding angle (°)#	P_b (kPa)
Cotton	0	N/A	N/A	0
P-cotton	151 ± 2	29 ± 3	N/A	1.1 ± 0.1
PP-cotton	158 ± 1	11 ± 4	44 ± 2	3.2 ± 0.1

*: Volume of water droplet was 5.0 µL. #: Volume of water droplet was 10.0 µL.

3.3.5 Oil-Water Separation Using Coated Cotton Fabrics as Oil Absorption Materials

Both experimental and theoretical work has revealed that a PDMS coated rough surface can repel water but absorb oil or organic solvent easily.[11, 12, 16] This is because the surface tension of PDMS, which is ~20 mN/m, is not low enough to repel low surface tension liquid (typical lower than 35 mN/m). Not surprisingly, our coated cotton samples were easily wetted by low surface tension liquids such as chloroform, methanol, toluene, hexane and hexadecane. Therefore, these coated cotton fabrics can be used for oil water separation. Typically, there are two protocols to use hydrophobic/oleophilic materials for oil-water separation. One is using them as absorption materials, surface modified sponge for instance, to absorb oil liquid on the water surface.[8, 48] The other is using them as filters, porous polymeric membranes for example, to separate oil water mixture by letting oil pass through but blocking water.[11, 46] Since cotton fabrics are suitable for both methods due to their high specific surface area and membrane-like shape, both methods were used to perform the oil-water separation using these two types of coated cotton samples.

Oil absorption was studied first. As shown in Figure 3.8, 125 μL of hexadecane (dyed with Oil Red O) was dispensed on water surface in each petri dish to simulate an oil spill (a, b and c). One piece (~1.5 cm * 1.5 cm) of uncoated cotton (d), P-cotton (e) and PP-cotton (f) were applied to the center of the spilled area to absorb the oil respectively. P-cotton and PP-cotton absorbed the oil efficiently with a few seconds, while uncoated cotton only absorbed quite limited amount of oil. In addition, the uncoated cotton quickly sank into the petri dish bottom while P-cotton and PP-cotton were floating on water surface after oil absorption. These results indicated that, without any coating, the cotton absorbed large amount of water although it absorbed some oil as well. However, the coated cotton only selectively absorbed oil.

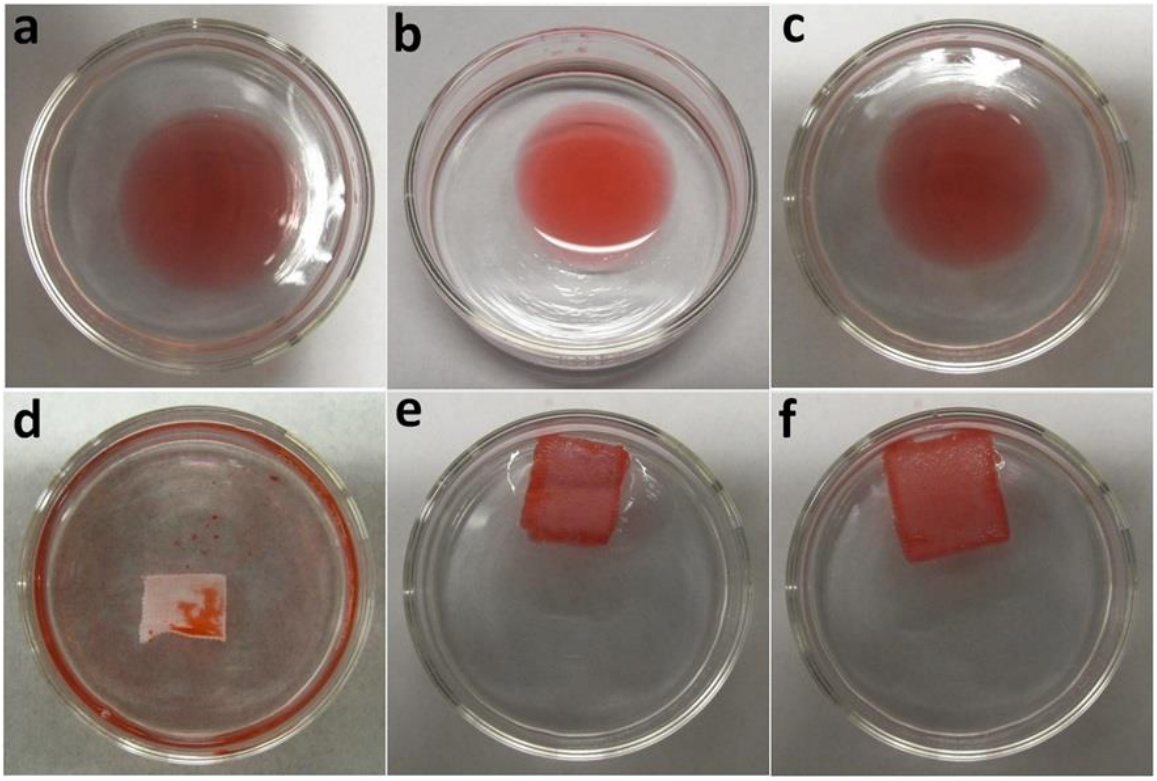

Figure 3.8 (a-c) photographs of 125 μL hexadecane (dyed with Oil Red O) "spilled" on surface of 20 mL water in each petri dish and those after absorption by (d) uncoated cotton, (e) P-cotton and (f) PP-cotton, respectively.

A series of quantitative studies was conducted to further confirm the above conclusion. First, the oil absorption capacities of uncoated cotton, P-cotton and PP-cotton were compared using several common organic solvents as oil models. The oil absorption capacity C_o was defined as $C_o = (W' - W)/W$, where W is the initial weight of dry cotton fabric and W' is the weight of cotton fabric after soaking in oil for 1.0 min. The results showed that the hydrophobic coatings did not sacrifice the oil absorption ability of cotton fabrics, but increased it somewhat (Figure 3.9). It was observed that P-cotton absorbed a slightly larger amount of oil than uncoated cotton. Besides the experimental errors, one reason might be the higher oleophilicity of the coated polymer than that of cellulose itself. More importantly, unlike small molecules, the anchor block PGMA could react with multiple hydroxyl groups on cotton surface and with other PGMA chains to form a crosslinked network. Therefore, the coated polymer could be swollen after solvent absorption and keep more

liquid. Figure 3.9 also showed that PP-cotton exhibited even higher oil absorption capacity. This also could be explained by the swollen polymer and particles. The P(S-GMA) nanoparticles were crosslinked by 3.8% DVB and they could keep more solvent than the diblock copolymer. In addition, the inter-particle space could also contribute the oil absorption capacity compared to the smooth coated P-cotton.

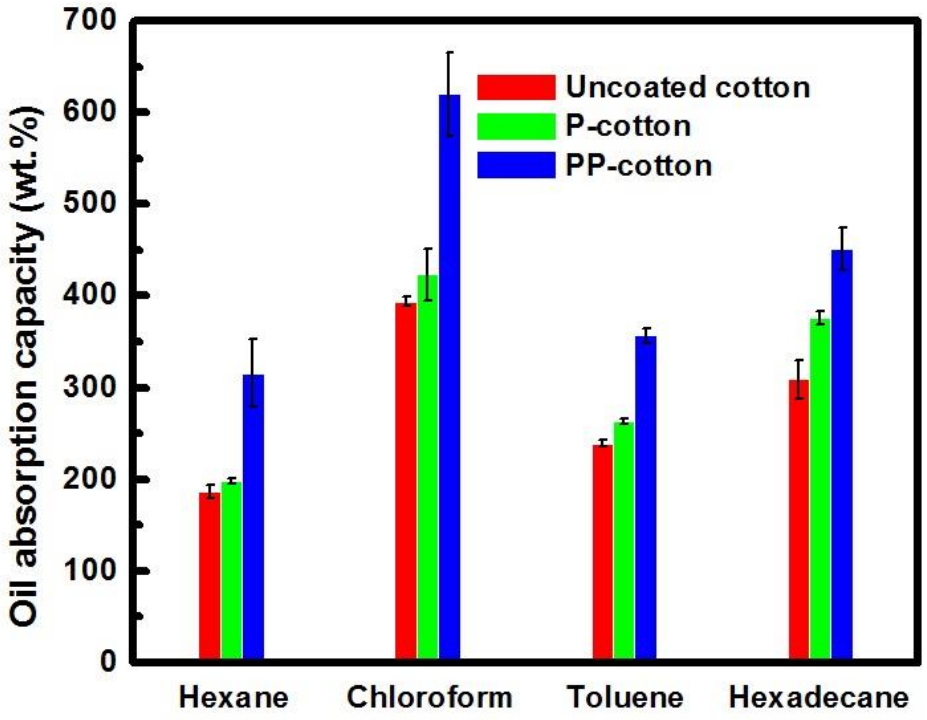

Figure 3.9 Oil absorption capacity of uncoated cotton, P-cotton and PP-cotton.

Although the oil absorption capacity increased somewhat after coating, the oil-water separation should also rely on the water repellency. Uncoated cotton could absorb large amount of water, while coated cotton could repel water when they were used to absorb "spilled oil". That is

why uncoated cotton performed much worse on "spilled oil" absorption even its oil absorption capacity was only slightly lower than that of P-cotton. However, in practical application, for example on the oil-spilled lake, the motion of water and/or cotton will generate some pressure which may cause the transition from metastable Cassie state to Wenzel state. As a result, even coated cotton will be wet by water and its oil absorption capacity will decrease. Therefore, water absorption at different pressures was studied to further investigate the water repellency of these two types of coated cotton. The water absorption A_w of coated cotton was defined as $A_w = (W' - W)/W$, where W is the initial weight of dry cotton fabric and W' is the weight of cotton fabric after it was forced to stay under water at a particular depth (convert to static pressure later) for 1.0 min. The zero depth (or pressure) mean leaving coated cotton float on water surface naturally and the static pressure from its own weight was negligible compared to those from water at different depths. Meanwhile, the water absorption A_w of uncoated cotton was not depth-dependent. So A_w of uncoated cotton was determined by using same equation but the corresponding W' is the weight of fabric after simply soaking in water for 1.0 min. The results in Figure 3.10 showed that the coated cotton barely absorbed water while they were floating on the water surface, while uncoated cotton naturally sank into water and absorbed ~380 wt% of water. This comparison result strongly supported a previous explanation about the different oil-water separation abilities of uncoated and coated cotton shown in Figure 3.8. More interestingly, when the coated cotton samples were forced to stay under water at a particular depth, they started to absorb water. The trend showed that P-cotton absorbed water easier than PP-cotton when the pressure increased. P-cotton absorbed ~ 1 wt% water when it was floating on water's surface and ~ 40 wt% water when it was under water at only 5.0 cm (~ 500 Pa). It kept absorbing more water fast when the depth or pressure increased. However, at the largest depth (30.0 cm) or pressure (~ 3000 Pa) we have applied in our experiments, water absorption of P-cotton (~ 180 wt%) was still much lower than that of uncoated cotton. On the other hand, PP-cotton exhibited better water repellency under pressure. The plot revealed that

it did not absorb any water until it was placed under water deeper than 15.0 cm (~ 1500 Pa). Even under water at 30.0 cm (~ 3000 Pa), PP-cotton only absorbed ~ 20 wt% water.

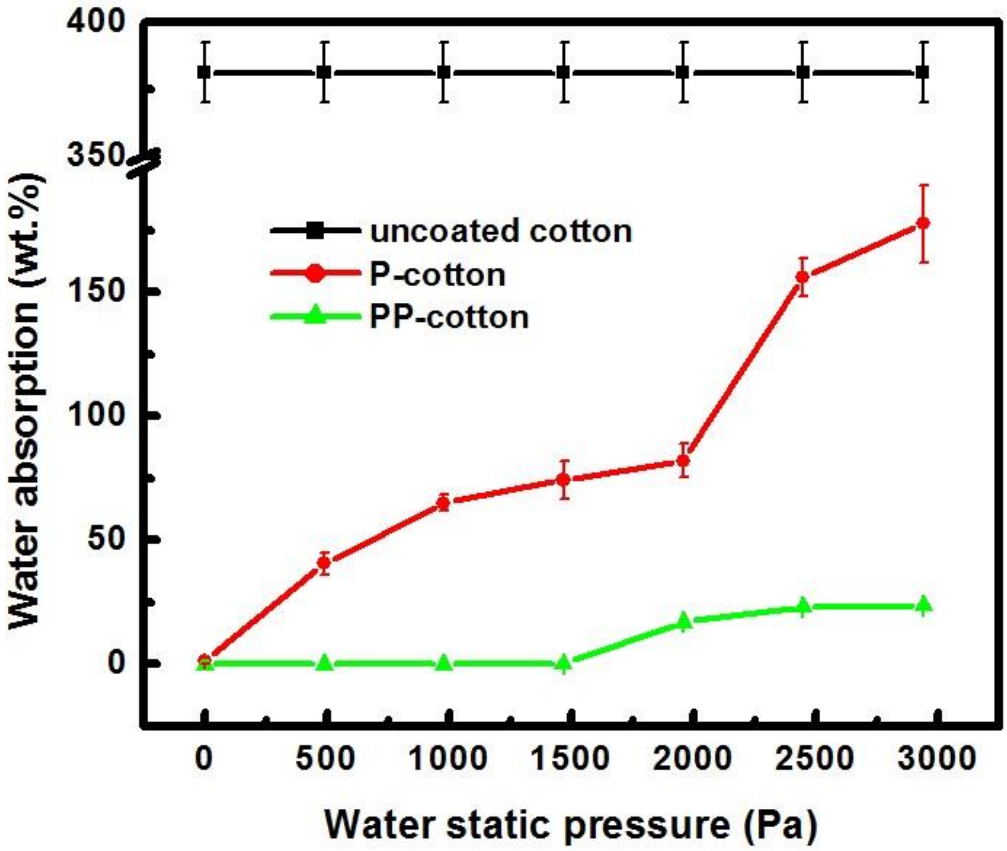

Figure 3.10 Water absorption of uncoated cotton, P-cotton and PP-cotton at different static pressures.

This trend was consistent with the trend of breakthrough pressures. However, two issues were noted based on the comparison of depth- or pressure-dependent water absorption and breakthrough pressure measurements. First, the coated cotton under water could be wet before the static pressure reached P_b. This means water could wet the surface of cotton fibers or some spots of the fabric but not penetrate the whole fabric when the pressure was not large enough. Second, the whole fabric was still not fully wet even when the static pressure reached P_b. This is because the pore size of the cotton fabric was not uniform, the P_b value really depended on those largest pores in the fabric.

Therefore, the depth- or pressure-dependent water absorption properties should be more suitable rather than breakthrough pressures to evaluate the water repellency and so the oil-water separation ability when the cotton fabrics were used as oil absorption materials.

3.3.6 Oil-Water Separation Using Coated Cotton Fabrics as Filter Membranes

As mentioned previously, coated cotton fabrics also could be used as a filter membrane to separate oil and water mixture. So each type of our coated cotton fabrics was used as a membrane to demonstrate the separation of oil-water mixture. As shown in Figure 3.11a, a piece of PP-cotton fabric was sandwiched between the two parts of a sinter glass filter funnel. When chloroform-water mixture (15.0 mL-15.0 mL) was poured into the funnel, chloroform (dyed with Oil Red O) passed through the cotton quickly leaving clear water stay on the top. Considering the different water repellency of the two types of coated cotton discussed in previous sections, one set of quantitative study was conducted to evaluate their efficiency and durability. Using the identical setup and chloroform-water mixture shown in Figure 3.11a, the volume of water remained on the top was measured after first cycle of separation. Then the funnel was emptied and the same amount of mixture was separated again using the same piece of cotton fabric without any treatment. Subsequently, the volume of remained water on the top was measured after the second cycle of separation. More cycles were applied in this way until the water residue on the top was zero. Figure 3.11b plots the results of multi-cycles separation based on P-cotton and PP-cotton. It showed that both types of coated cotton performed well in their first cycle of separation. However, during 2^{nd} - 4^{th} cycles of P-cotton, the water residue volume decreased ~ 3% - 7%. This indicated that water started to wet and even partially penetrate the fabric. Since the 5^{th} cycle, no water could stay on the fabric surface and it all passed through the cotton with oil. Meanwhile, the water residue volume decreased ~ 3% - 23% during the 3^{rd} - 16^{th} cycles of PP-cotton and no water could stay on its surface since the 17^{th} cycle. When these wet cotton fabrics were dried in oven at 120 °C for 30 min, their separation ability came back as good as their first cycle respectively. Therefore, the

failure of water repellency after several cycles was not due to the loss of coating. It might be attributed to some surface reconstruction as well as the removal of some pocketed air by oil. The introduced nanoparticles on PP-cotton might help to trap air better in the inter-particle space and decrease the air removal, so that PP-cotton could repel water for more cycles of separation.

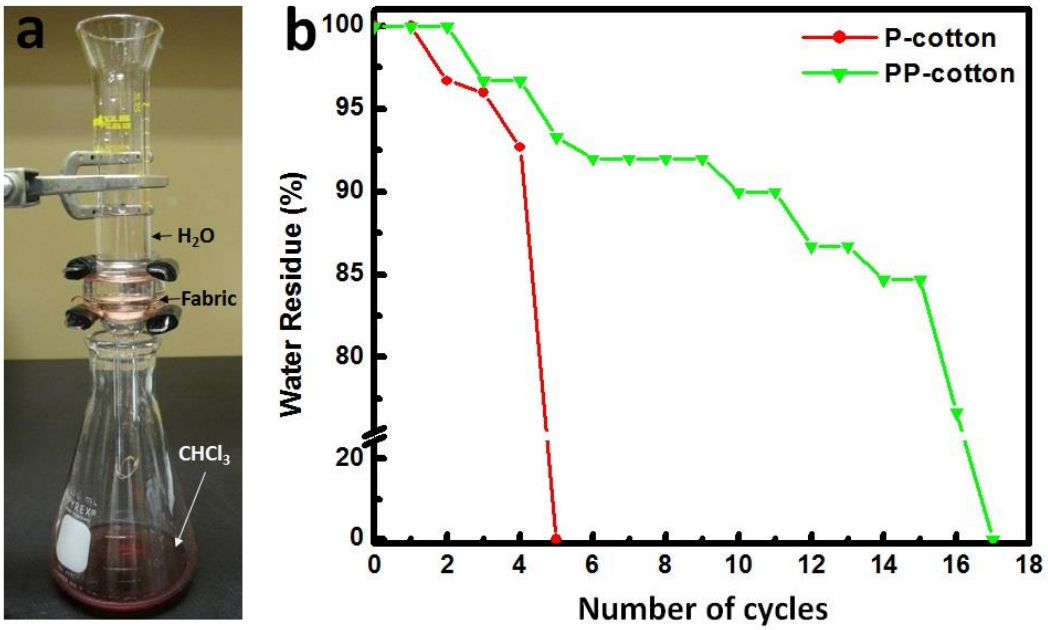

Figure 3.11 (a) Photograph to demonstrate the success of oil-water separation using PP-cotton as a filter membrane. Chloroform (red dyed) passed through the membrane and water stayed on it. (b) Water residue volume relative to initial water volume (15.0 mL) in oil-water mixture as a function of the number of separation cycles.

3.4 Conclusions

Diblock copolymer and polymeric nanoparticles bearing glycidyl groups were synthesized respectively. The copolymer PDMS-*b*-PGMA was synthesized via ATRP using PDMS-Br as macroinitiator and P(S-GMA) nanoparticles were synthesized via surfactant-free emulsion copolymerization of styrene and GMA monomer using DVB as the crosslinker. Cotton fabrics coated with both nanoparticles and diblock copolymer (PP-cotton) or with only diblock copolymer (P-cotton) were confirmed by the combination of SEM, FT-IR and water repellency analyses. The

produced hydrophobic/oleophilic fabrics were further successfully used for oil-water mixture separation as both oil absorption materials and filter membranes. PP-cotton exhibited not only better water repellency, but also higher oil absorption capacity comparing to P-cotton. Both better water repellency and oil absorption should be attributed to the coating of nanoparticles. The nanoscale roughness could increase water repellency and solvent swelling of these crosslinked polymeric particles could contribute to oil absorption. Both the glycidyl-based diblock copolymer and polymeric nanoparticles offered more choices for covalent superhydrophobic cotton coatings and further for oil-water separation. The comparison of these two types of coatings also provided more insight in this research area.

3.5 Notes and References

The main work described in this chapter has been prepared for publication.

References

1. B. Cortese, D. Caschera, F. Federici, G. M. Ingo and G. Gigli, *J. Mater. Chem. A*, 2014, **2**, 6781-6789.
2. Z.-Y. Deng, W. Wang, L.-H. Mao, C.-F. Wang and S. Chen, *J. Mater. Chem. A*, 2014, **2**, 4178-4184.
3. G. Deschamps, H. Caruel, M. E. Borredon, C. Albasi, J. P. Riba, C. Bonnin and C. Vignoles, *Environ. Sci. Technol.*, 2003, **37**, 5034-5039.
4. J. Gu, P. Xiao, J. Chen, F. Liu, Y. Huang, G. Li, J. Zhang and T. Chen, *J. Mater. Chem. A*, 2014, **2**, 15268-15272.
5. J. Y. Huang, S. H. Li, M. Z. Ge, L. N. Wang, T. L. Xing, G. Q. Chen, X. F. Liu, S. S. Al-Deyab, K. Q. Zhang, T. Chen and Y. K. Lai, *J. Mater. Chem. A*, 2015, **3**, 2825-2832.

6. J. Li, L. Yan, Y. Zhao, F. Zha, Q. Wang and Z. Lei, *Phys. Chem. Chem. Phys.*, 2015, **17**, 6451-6457.

7. S. Li, J. Huang, M. Ge, C. Cao, S. Deng, S. Zhang, G. Chen, K. Zhang, S. S. Al-Deyab and Y. Lai, *Adv. Mater. Inter.*, 2015, **2**.

8. B. Wang, J. Li, G. Wang, W. Liang, Y. Zhang, L. Shi, Z. Guo and W. Liu, *ACS Appl. Mater. Inter.*, 2013, **5**, 1827-1839.

9. Z. Xue, M. Liu and L. Jiang, *J. Polym. Sci. B Pol. Phys.*, 2012, **50**, 1209-1224.

10. X. Zhou, Z. Zhang, X. Xu, F. Guo, X. Zhu, X. Men and B. Ge, *ACS Appl. Mater. Inter.*, 2013, **5**, 7208-7214.

11. Z. Wang, Y. Wang and G. Liu, *Angew. Chem. Int. Edit.*, 2016, **55**, 1291-1294.

12. B. Bhushan and Y. C. Jung, *Prog. Mater. Sci.*, 2011, **56**, 1-108.

13. T. L. Sun, L. Feng, X. F. Gao and L. Jiang, *Acc. Chem. Res.*, 2005, **38**, 644-652.

14. A. Tuteja, W. Choi, G. H. McKinley, R. E. Cohen and M. F. Rubner, *Mrs. Bull.*, 2008, **33**, 752-758.

15. Z. Y. Deng, W. Wang, L. H. Mao, C. F. Wang and S. Chen, *J. Mater. Chem. A*, 2014, **2**, 4178-4184.

16. Y. X. Jin, P. Jiang, Q. P. Ke, F. H. Cheng, Y. S. N. Zhu and Y. X. Zhang, *J. of Hazar. Mater.*, 2015, **300**, 175-181.

17. D. Xiong, G. Liu and E. J. S. Duncan, *Langmuir*, 2012, **28**, 6911-6918.

18. B. Deng, R. Cai, Y. Yu, H. Jiang, C. Wang, J. Li, L. Li, M. Yu, J. Li, L. Xie, Q. Huang and C. Fan, *Adv. Mater.*, 2010, **22**, 5473-5477.

19. A. Hirao, K. Sugiyama and H. Yokoyama, *Prog. Polym. Sci.*, 2007, **32**, 1393-1438.

20. Z. Chu and S. Seeger, *Chem. Soc. Rev.*, 2014, **43**, 2784-2798.

21. D. Xiong, G. Liu, L. Hong and E. J. S. Duncan, *Chem. Mater.*, 2011, **23**, 4357-4366.

22. Y.-C. Sheen, Y.-C. Huang, C.-S. Liao, H.-Y. Chou and F.-C. Chang, *J. Polym. Sci. B Pol. Phys.*, 2008, **46**, 1984-1990.

23. A. Tuteja, W. Choi, M. Ma, J. M. Mabry, S. A. Mazzella, G. C. Rutledge, G. H. McKinley and R. E. Cohen, *Science*, 2007, **318**, 1618-1622.

24. J. E. Mark, *Polymer Data Handbook. Oxford University Press*, 1999.

25. D. R. Lide, ed,. *CRC Handbook of Chemistry and Physics, Internet Version, CRC Press, Boca Raton, FL*, 2005.

26. H. F. Hoefnagels, D. Wu, G. de With and W. Ming, *Langmuir*, 2007, **23**, 13158-13163.

27. B. Leng, Z. Shao, G. de With and W. Ming, *Langmuir*, 2009, **25**, 2456-2460.

28. R. N. Wenzel, *Ind. Eng. Chem.*, 1936, **28**, 988-994.

29. A. B. D. Cassie and S. Baxter, *Trans. Faraday Soc.*, 1944, **40**, 0546-0550.

30. X. J. Liu, Y. Xu, K. Y. Ben, Z. Chen, Y. Wang and Z. S. Guan, *Appl. Surf. Sci.*, 2015, **339**, 94-101.

31. Y. Wang, X. Y. Li, H. Hu, G. J. Liu and M. Rabnawaz, *J. Mater. Chem. A*, 2014, **2**, 8094-8102.

32. M. Rabnawaz, Z. J. Wang, Y. Wang, I. Wyman, H. Hu and G. J. Liu, *RSC Adv.*, 2015, **5**, 39505-39511.

33. F. D. Osterholtz and E. R. Pohl, *J. Adhes. Sci. Technol.*, 1992, **6**, 127-149.

34. O. Okay, *Prog. Polym. Sci.*, 2000, **25**, 711-779.

35. K. Matyjaszewski and J. H. Xia, *Chem. Rev.*, 2001, **101**, 2921-2990.

36. J. S. Wang and K. Matyjaszewski, *Macromolecules*, 1995, **28**, 7901-7910.

37. W. J. Jiang, C. M. Grozea, Z. Q. Shi and G. J. Liu, *ACS Appl. Mater. Inter.*, 2014, **6**, 2629-2638.

38. S. Doszlop, V. Vargha and F. Horkay, *Period. Polytech. Chem. Eng.*, 1978, **22**, 253-275.

39. H. L. Zou, S. D. Lin, Y. Y. Tu, G. J. Liu, J. W. Hu, F. Li, L. Miao, G. W. Zhang, H. S. Luo, F. Liu, C. M. Hou and M. L. Hu, *J. Mater. Chem. A*, 2013, **1**, 11246-11260.

40. Z. Q. Shi, I. Wyman, G. J. Liu, H. Hu, H. L. Zou and J. W. Hu, *Polymer*, 2013, **54**, 6406-6414.

41. N. Hameed, Q. P. Guo, Z. G. Xu, T. L. Hanley and Y. W. Mai, *Soft Matter*, 2010, **6**, 6119-6129.

42. J. Zimmermann, S. Seeger and F. A. Reifler, *Text. Res. J.*, 2009, **79**, 1565-1570.

43. D. Pavia, G. Lampman and G. Kriz, *Introduction of Spectroscopy*, Brooks Cole, 2001.

44. C. A. Hepburn, P. Vale, A. S. Brown, N. J. Simms and E. J. McAdam, *Talanta*, 2015, **141**, 128-136.

45. A. K. Kota, G. Kwon and A. Tuteja, *NPG Asia Mater.*, 2014, **6**.

46. W. Zhang, Z. Shi, F. Zhang, X. Liu, J. Jin and L. Jiang, *Adv. Mater.*, 2013, **25**, 2071-2076.

47. K. R. Lamison and A. J. Guenthner, *Appl. Surf. Sci.*, 2012, **258**, 10205-10208.

48. Q. Zhu, Y. Chu, Z. Wang, N. Chen, L. Lin, F. Liu and Q. Pan, *J. Mater. Chem. A*, 2013, **1**, 5386-5393.

Chapter 4

Stable Water-Dispersible Air Nanobubbles Encapsulated with ABC Triblock Copolymer Bearing Fluorinated Block with Super-Low Surface Energy

4.1 Introduction

Trapping air in the central cavity of solid nanocapsules yields encapsulated air nanobubbles. If these bubbles are stable and reflect and scatter ultrasound effectively (being echogenic), they will expand the applications of micrometer-sized bubbles (microbubbles) that are widely used as contrast agents in diagnostic ultrasonography.[1-4] For example, they may find applications in the diagnosis of tumors or in the imaging of blood perfusion due to nanobubbles' ability to permeate the capillary networks of organs.[5-7] In addition, nanobubbles bearing surface recognition functionalities will be useful in ultrasound-regulated drug delivery because their pathways can be visualized by ultrasonography and their carried drugs can be released at the targeted sites when triggered by more powerful ultrasound pulses.[5, 8] While these prospects are tantalizing, the preparation of stable air nanobubbles or nanobubbles of other gases in water has been difficult.[9] In fact, even the term "nanobubbles" is currently misused to refer to the nanoemulsion droplets of highly volatile fluorinated liquids that gasify under ultrasonication to generate transient bubbles.[5, 6] This chapter describes the stabilization of air bubbles in nanocapsules bearing a highly hydrophobic fluorinated internal lining. These nanobubbles reflected ultrasound effectively. More importantly, the nanobubbles withstood ultrasonication ~100 times longer than a third-generation microbubble sample that is among the most stable commercial bubbles. The third-generation microbubbles are much more stable than the first and second generations of microbubbles

consisting of naked and encapsulated air microbubbles, because they contain the filling gas - perfluorinated propane, which has a much lower solubility in water than air.[1]

Air nanobubbles are generally unstable in water because they possess a large surface area-to-volume ratio and are energetically costly to create. Furthermore, a spherical nanobubble of radius r has an internal Laplace pressure P_L of $2\gamma_w/r$,[10] where γ_w, the surface tension of water, is 72.1 mN/m at room temperature.[11] At r = 50 nm, P_L is 29.4 atm and this value increases as r decreases. Thus, air-filled nanobubbles readily dissipate when they are perturbed by ultrasound, for example.[1] Even in the absence of mechanical disturbance, air bubbles dissipate by air solubilization in water once water becomes unsaturated due to changes in atmospheric pressure.[9, 12, 13] Nanobubbles dissipate faster than microbubbles in unsaturated water because of their higher specific surface area as well as their higher internal Laplace pressure and thus higher air solubility at the bubble and water interface.[14]

Encapsulation has been used to inhibit bubble dissipation because a solid shell reduces the rate of air diffusion from an encapsulated cavity into water.[2, 12, 14, 15] According to Epstein and Plesset,[12] encapsulation could also stabilize bubbles via another mechanism involving the elimination of the interfacial tension between the encapsulated air and its surroundings.[15] Since a solid material with a surface tension of zero has not been discovered,[16, 17] no attempts have been made to encapsulate air bubbles using low surface tension materials. Rather, the materials used in the past have included phospholipids,[15] polyesters,[18] and polycyanoacrylate[2] that have surface tensions above 30 mN/m and could not effectively stabilize air nanobubbles.

This chapter describes, against conventional thinking, a low surface tension approach because of our group's prior experience with highly water- and oil-repellant coatings.[19-21] Fluorinated polymers have surface tensions as low as 6.7 mN/m.[16] Upon the immersion of a cotton fabric coated by a perfluorinated polymer in water, water refuses to enter the spaces between the threads and fibers.[20, 22, 23] Rather, a plastron or air layer is trapped between the fabric and water.[20] This

trapped plastron layer has also been recently used to lower the density of "hedgedog" fluorinated particles and to float them in water.[24] It is noted that these phenomena were analogous to the rejection of water by a submerged hydrophobic capillary tube and the requirement of an external pressure p_B to force water into it with:

$$p_B = -\frac{2\gamma_w cos\theta}{r_c} \qquad (4.1)$$

where θ is the contact angle of water on the internal wall of the capillary and $\boldsymbol{r_c}$ is the radius of the capillary. According to eq. (4.1), p_B = 735 atm at r_c = 1 nm and $\theta \approx 120°$, which is the water contact angle on a perfluorinated polymer film.[16,19] Therefore, we imagined that a tremendous pressure was required to force water into a fluorinated capsule that might bear molecular defects with sizes smaller than 1 nm.[16] Consequently, air nanobubbles in fluorinated capsules should be stable even without a vanishing surface tension for the capsular lining.

To verify the hypothesis proposed above, water-dispersible nanocapsules with a fluorinated internal lining from the triblock terpolymer ACF,[25] where A, C, and F denote poly(acrylic acid), poly(2-cinnamoyloxyethyl methacrylate), and poly(2-perfluorooctylethyl methacrylate), respectively (Figure 4.1), were fabricated. Here the A and C blocks were respectively chosen for their solubility in water and ability to photocrosslink. To gain insight into the stabilization mechanism of air nanobubbles, nanocapsules from the triblock terpolymer GCB,[26] where B denotes the oil-soluble poly(*tert*-butyl acrylate) and G denotes the water-soluble poly(glyceryl monomethacrylate) block (Figure 4.2), were also prepared. In contrast to F that has a surface tension of 7.5 mN/m[17] and a water contact angle of 120°,[17, 19] B has the corresponding values of 30.4 of mN/m[27] and 75°,[28] respectively. The used ACF and GCB samples were well-defined and possessed polydispersity indices less than 1.04 because they were derived from precursors synthesized via anionic polymerization.

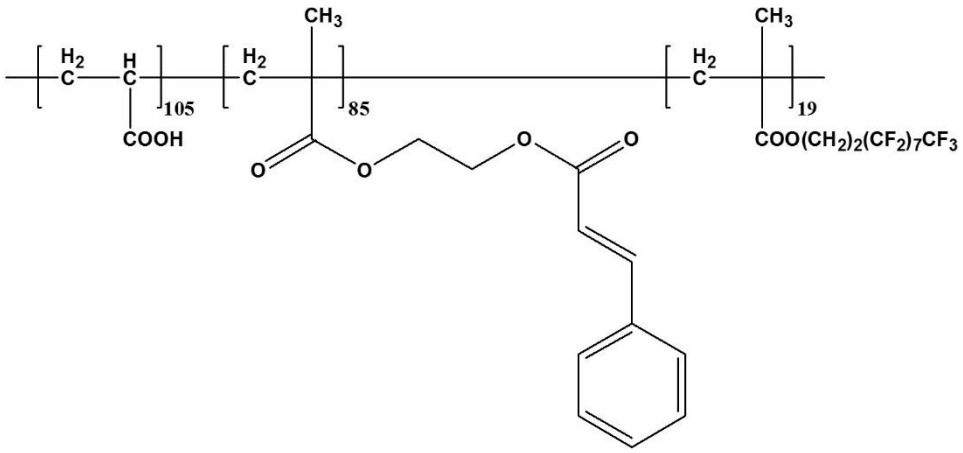

Figure 4.1 Chemical structure of ACF.

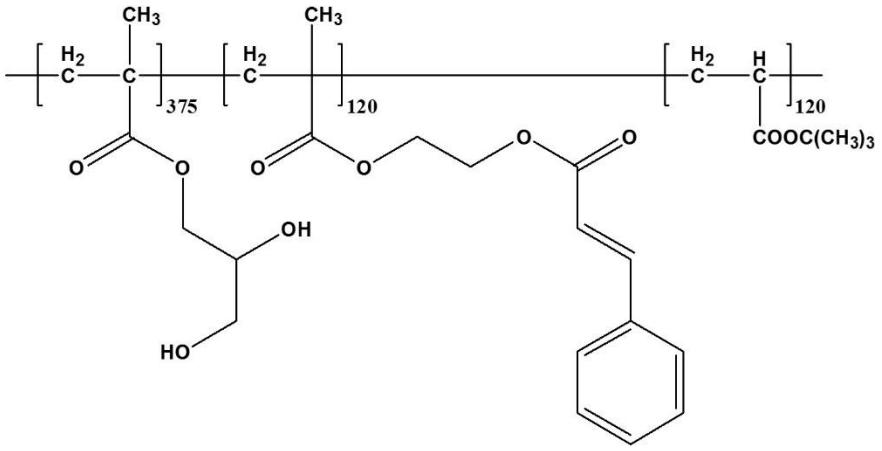

Figure 4.2 Chemical structure of GCB.

4.2 Experimental

4.2.1 Materials

Triblock copolymers ACF and GCB were synthesized according to previously reported procedures.[25, 29, 30] Tetrahydrofuran (THF, 99%, Caledon) was distilled before use. α,α,α-Trifluorotoluene (TFT, 99%, Acros) and sodium hydroxide (NaOH, 97%, Aldrich) were used as received. The commercial phospholipid-encapsulated perfluoropropane microbubble sample was received from the Kingston General Hospital (Canada) having a trade name of Definity®. The

human whole blood was freshly collected from a volunteer and stored in BD Vacutainer® blood collection tubes (BD, Franklin Lakes, NJ, USA) prior to the tests. Each collection tube is 3.0 mL and contains 5.4 mg EDTA as anticoagulant.

4.2.2 Preparation of ACF Nanocapsules

In a typical preparation, 15.0 mg of the ACF triblock copolymer was dissolved in 0.70 mL of THF. TFT (1.50 mL) was subsequently added dropwise into the polymer solution under vigorous stirring to induce the formation of micelles with a dynamic light scattering hydrodynamic diameter of 96 nm. The insoluble poly(acrylic acid) chains formed the micellar cores. This micellar solution was transferred to a 100 mL two-neck round-bottom flask. To one end of the stirring shaft of a mechanical stirrer was mounted a hemispherical Teflon blade, which was 5.0 cm wide and 2.0 cm tall. The blade was inserted into the flask via the central neck of the flask. Under stirring at 1800 rpm and at 20 °C, 8.0 mL of an aqueous NaOH solution (0.0050 M) was added dropwise into the micellar solution over one hour via an automatic syringe pump. The produced emulsion was irradiated for one hour with a focused UV beam to photo-crosslink the C block. The UV beam was generated by a 500 W Hg lamp that was housed in an Oriel 6140 lamp casing and the beam was passed through a 270-nm cut-off filter before it reached the sample. The photo-crosslinked nanocapsules were then purified by dialysis for 3 days against an aqueous solution that was saturated with TFT through a nitrocellulose membrane (450 nm average pore size) prior to characterizations.

4.2.3 Preparation of ACF Nanobubbles

To further prepare ACF nanobubbles, the purified dispersion of ACF nanocapsules or emulsion was immersed into liquid nitrogen for approximately 15 min before it was transferred to a Labconco Freeze Drying System. The final dry powder was withdrawn from the freeze drying system after 24 h and stored in a glass vial with its lid left ajar under ambient conditions for at least

24 h to allow it to reach equilibrium with air. The nanobubbles were then re-dispersed into water via shaking prior to characterizations and evaluations.

4.2.4 Preparation of the GCB Nanocapsules

In a particular preparation, 16.0 mg of the GCB triblock copolymer was dissolved into 0.20 mL of THF prior to the addition of 0.64 mL of TFT. Using same setup described in section 2.2.2, 4.0 mL distilled water was added dropwise into the micellar solution over 1 h under stirring at 1500 rpm and at 20 °C. The produced emulsion was subsequently irradiated by UV light using the above mentioned UV system for 1 h to photo-crosslink the C block. Then the photo-crosslinked nanocapsules were purified by dialysis for 3 days against an aqueous solution that was saturated with TFT through a nitrocellulose membrane (450 nm average pore size) prior to characterizations.

4.2.5 Preparation of the GCB Nanobubbles

To further prepare GCB nanobubbles, the purified dispersion of GCB nanocapsules or emulsion was immersed into liquid nitrogen for approximately 15 min before it was transferred to a Labconco Freeze Drying System. The final dry powder was withdrawn from the freeze drying system after 24 h and stored in a glass vial with its lid left ajar under ambient conditions for at least 24 h to allow it to reach equilibrium with air. The nanobubbles were then re-dispersed into water via shaking prior to characterizations and evaluations.

4.2.6 Transmission Electron Microscopy (TEM)

The dispersions of ACF and GCB nanocapsules or nanobubbles were aero-sprayed onto nitrocellulose-coated copper grids. The TEM samples were subsequently dried under ambient conditions overnight or longer before staining by OsO_4 vapor for 2 h. TEM images were obtained using a Hitachi-7000 instrument operated at 75 kV. The nanocapsule/nanobubble size and size distribution of each sample based on TEM results were measured and calculated from the TEM images using the Nano Measure software.

4.2.7 Atomic Force Microscopy (AFM)

The dispersions of ACF and GCB nanocapsules or nanobubbles were aero-sprayed onto the surfaces of clean Si wafers. After they had been dried under ambient conditions overnight or longer, the samples were analyzed by AFM in the tapping mode, using a Veeco multimode instrument equipped with a Nanoscope IIIa controller. The nanocapsule/nanobubble size and size distribution of each sample based on AFM results were measured and calculated from the 2D AFM height images using the Nano Measure software.

4.2.8 Dynamic Light Scattering (DLS)

The aqueous dispersions of ACF and GCB nanocapsules or nanobubbles were clarified by filtration through 3.1 μm Supor Membrane Filters (Pall) prior to the DLS measurements. All the measurements were carried out at 20 °C using a Brookhaven BI-200 SM instrument that was equipped with a BI-9000AT digital correlator and a He-Ne laser (632.8 nm). All of the measurements were performed at an angle of 90°.

4.2.9 Ultrasonic Image Acquisition

A home-made ultrasound setup which simulated a "human blood vessel" was used for *in-vitro* ultrasonic imaging (Figure 4.3). The simulated "vessel" was a rubber tube that was placed between the probe and specially designed tissue-mimicking material, Sigmacell Cellulose (Sigma Aldrich, St. Louis, MO). The effective length of the "vessel" was fixed to 6.5 cm by two clips, the inner diameter of the "vessel" was 1.00 cm and its wall thickness was 0.10 cm. This "vessel" was filled with water or human whole blood but flow physiology was not imitated. Long-axis views of two-dimensional ultrasound images were obtained using a dedicated vascular ultrasonography device (Vivid E9, GE Healthcare, Wisconsin) equipped with a 9L transducer at 21 °C in the harmonic mode (4 MHz/8 MHz).

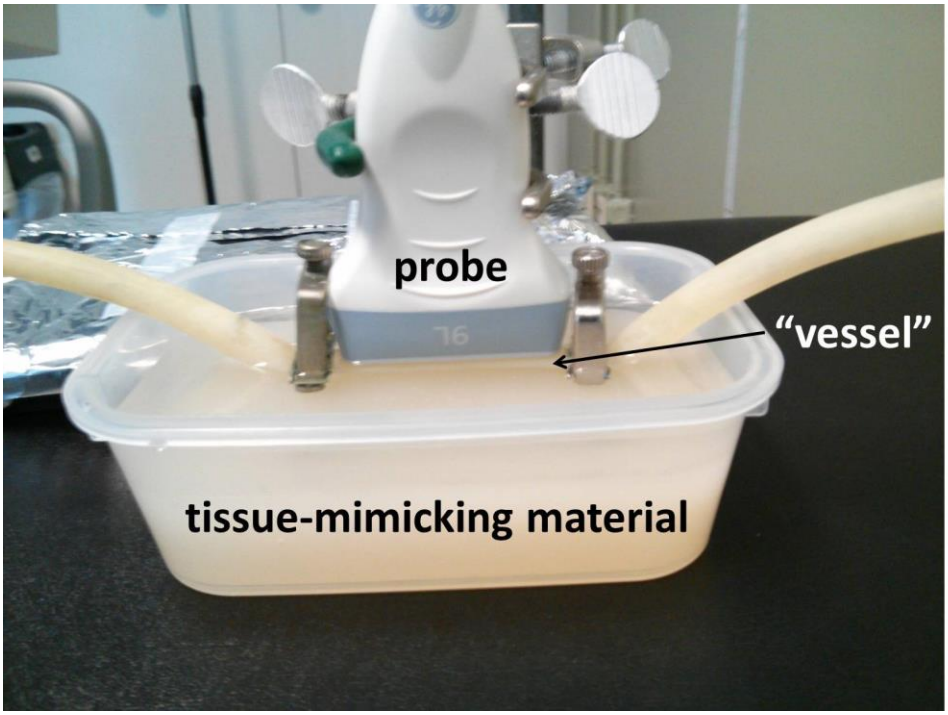

Figure 4.3 Photograph of the experimental setup used for *in-vitro* ultrasound tests.

Each sample, with the same volume of 0.40 mL, was quickly injected into the "vessel" by inserting the needle of a plastic syringe into one end of the "vessel". The "vessel" was washed with distilled water between each injection. The initial polymer concentrations of nanocapsules and nanobubbles solutions involving ACF nanocapsules, ACF nanobubbles and GCB nanobubbles were all 1.6 mg/mL. The aged ACF and GCB nanobubble solutions were prepared by dispersing the corresponding dry particles into water 4 h before their ultrasound tests. The fresh ACF and GCB nanobubbles solutions were prepared by dispersing the corresponding dry particles immediately before their ultrasound tests. The super-aged ACF nanobubble solution was prepared by dispersing ACF dry particles into water 3 weeks before its ultrasound test. The commercially available Definity® microbubbles were prepared by diluting the original liquid product with water (0.10 mL product + 8.90 mL water) immediately before their ultrasound test.

For the echogenicity comparison in water, the 2D ultrasound image of each sample was captured 1 s after its injection (based on ACF nanobubbles signal, the particles could spread and

fill the "vessel" in 1 s) and the "blood" region between walls was analyzed by Image-J software to determine the grayscale intensity. For the stability comparison in water, a series of 2D ultrasound images of each sample were captured at different times 1 s after its injection. The time when the first image was taken was defined as time zero. The "blood" region between the walls of each image was analyzed by Image-J software to obtain the intensity decay data.

For the stability comparison in human whole blood, the procedure was almost identical to that in water except that the tube was shaken for several seconds after 3 minutes of the sample injection.

4.3 Results and Discussion

4.3.1 Syntheses and Characterizations of ACF and GCB Triblock Copolymers

The ACF and GCB triblock copolymers were obtained after hydrolysis of their respective precursors BCF and SCB, where S denotes poly(solketal methacrylate), following previously reported procedures.[25, 29-33] Both precursor triblock copolymers BCF and SCB were synthesized via anionic polymerization. Figure 4.4 and Figure 4.5 show the chemical structures of BCF and SCB, respectively. Because the interaction between SEC column and final ACF/GCB polymers strongly affect the characterization results, these two polymers were characterized first in their precursor forms. Table 4.1 summarizes the characteristics of these two precursors. The ratio of the repeat unit numbers of different blocks (*l*/*m*/*n*) in each copolymer was obtained via ^{1}H NMR analysis by comparing the signal integrations corresponding to the different blocks. The weight- and number-average molecular weight (M_w and M_n) as well as the polydispersity index (M_w/M_n) of each copolymer were obtained via size-exclusion chromatography (SEC) analysis using a series of well-defined polystyrene standards as the calibration standards. The number-average repeat unit numbers *l*, *m*, and *n* were calculated using the corresponding ratio obtained by ^{1}H NMR analysis and the M_n values obtained by SEC analysis.

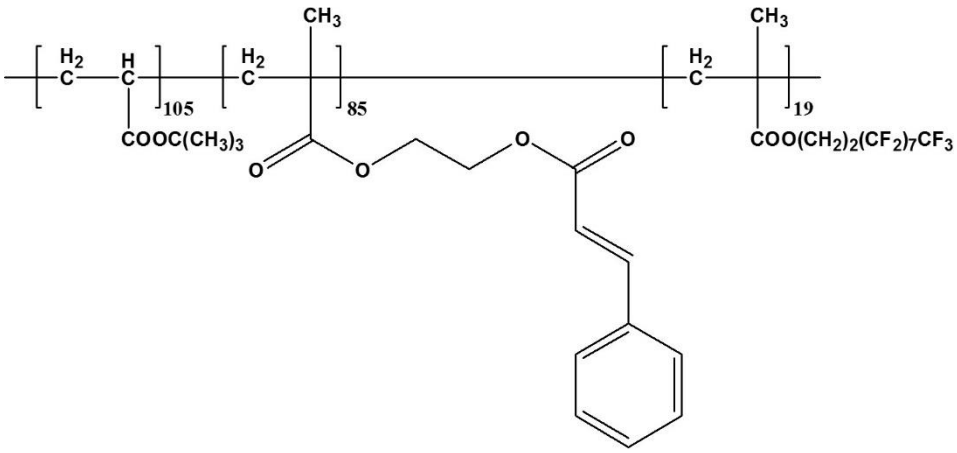

Figure 4.4 Chemical structure of BCF.

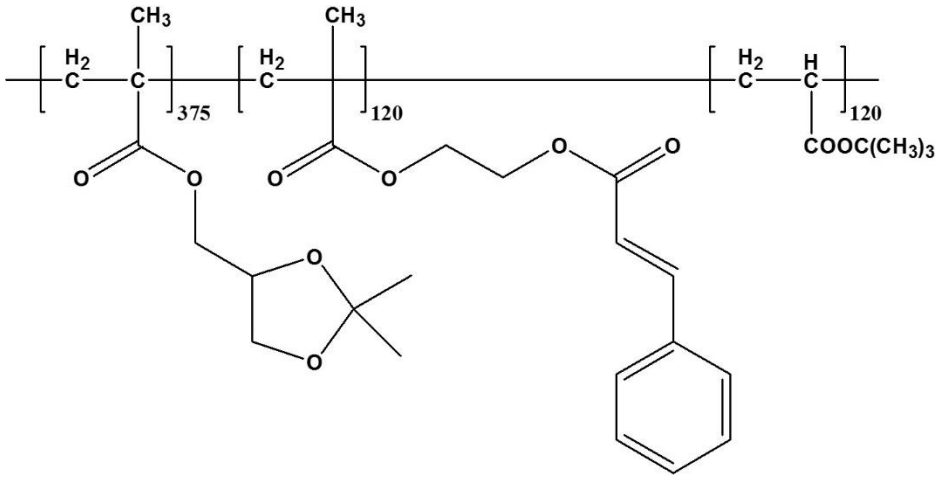

Figure 4.5 Chemical structure of SCB.

Table 4.1 Characterization of the BCF and SCB triblock copolymers.

Copolymer	SEC M_n (g/mol)	SEC M_w/M_n	1H NMR *l*/*m*/*n*	*l*	*m*	*n*
$B_lC_mF_n$	4.6×10^4	1.04	5.5/4.5/1.0	105	85	19
$S_lC_mB_n$	1.2×10^5	1.03	3.1/1.0/1.0	375	120	120

4.3.2 Syntheses of the Nanocapsules and Nanobubbles

To prepare the ACF nanocapsules, 15.0 mg of ACF was dissolved into tetrahydrofuran (THF, 0.70 mL) before trifluorotoluene (TFT, 1.50 mL) was slowly added. Since the mixture solubilized

the C and F blocks but not the A block, the copolymer formed micelles[34-36] with a hydrodynamic diameter of 96 nm as determined dynamic light scattering (DLS). Then 8.0 mL of an aqueous 5.0×10^{-3} M NaOH solution was pumped over a period of 1 h into this mixture, which was thermostated to 20 °C and stirred at 1800 rpm. We speculate that the water addition caused the initial micelles to transition to water-swollen micelles, and then to a water-in-oil emulsion stabilized by ACF, and eventually to an oil-in-water emulsion upon phase inversion.[26, 37, 38] In the final state, the core was probably mainly filled with TFT due to THF's solubility in water. Consequently, the internal and external surfaces of the insoluble C wall should be lined by the F and poly(sodium acrylate) chains, respectively (Structure 2, Figure 4.6). Photolysis of these droplets with UV light crosslinked the C walls to yield "permanent" capsules.[39] We then removed TFT and water from the system via freeze drying to yield hollow capsules (Structure 4, Figure 4.6). After backfilling the capsular cavities with air, we stirred the powdery sample in water to disperse encapsulated air nanobubbles. The GCB "bubbles" were prepared in essentially same method except the NaOH solution was replaced with deionized water during the emulsification step.

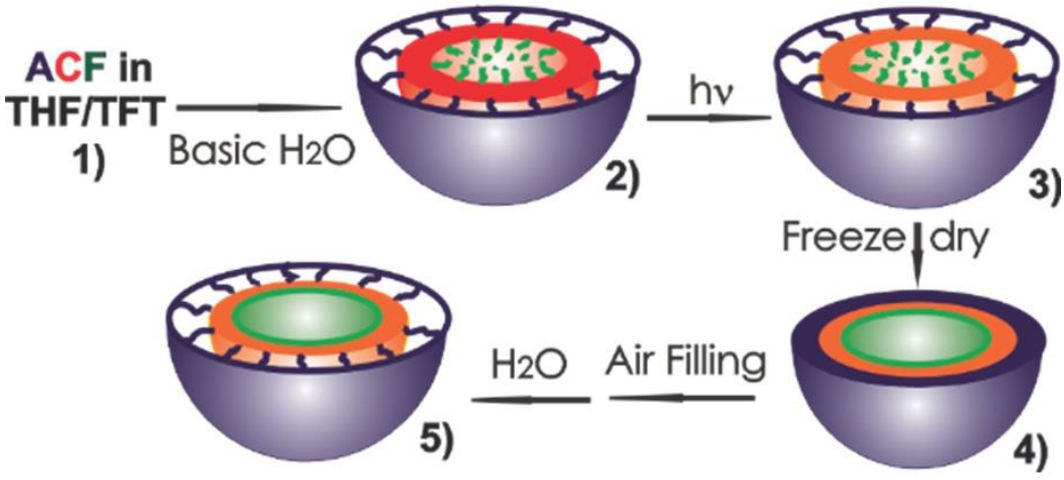

Figure 4.6 Schematic diagram of the ACF nanobubbles preparation process.

4.3.3 Characterizations of the Nanocapsules and Nanobubbles

The nanocapsules and "nanobubbles" thus prepared were characterized by transmission electron microscopy (TEM), atomic force microscopy (AFM) and DLS. Figure 4.7 shows a TEM and an AFM height image of the ACF nanocapsules after they had been sprayed and dried on a cellulose-coated TEM grid and on a silicon wafer, respectively. The observation of the dark rings with a gray center by TEM[40] and of collapsed bowls by AFM[26] as well as the large diameter of the particles relative to the length of the fully stretched ACF chains support the targeted capsular structure.[41] Upon higher magnifications of the TEM image, white dots and stripes were also seen on the capsules. These fine structures should be due to the crystallization or aggregation and thus the uneven distribution of the poly(sodium acrylate) chains on the surfaces of the capsules, a phenomenon similar to that observed on the surfaces of ACF cylindrical micelles that had their A chains stained by uranyl acetate.[25]

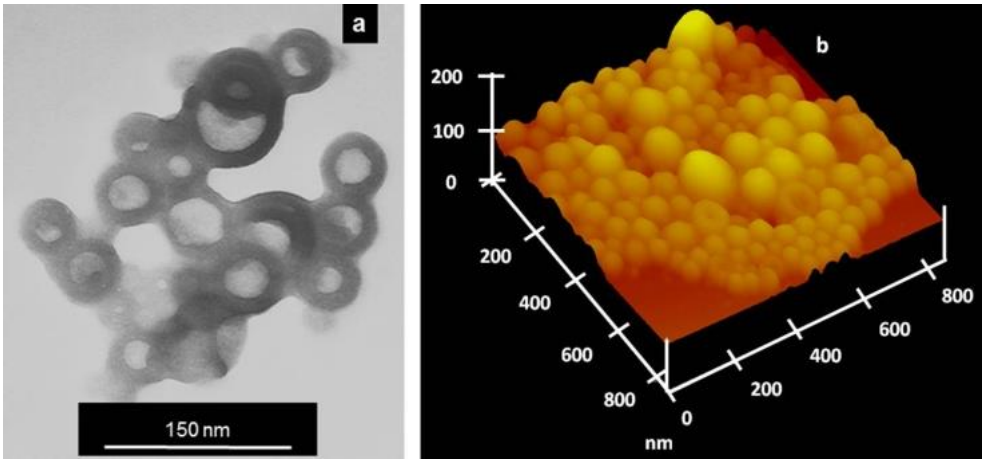

Figure 4.7 (a) TEM and (b) AFM height images of the ACF nanocapsules that had been sprayed onto a cellulose-coated copper grid and a silicon wafer, respectively. The dried TEM specimen was stained with OsO_4.

When the solvents were removed by freeze-dry system, the power-like ACF nanoparticles after equilibrating with air were re-dispersed into water to produce air nanobubbles in water. Small amount of this dispersed solution was aero-sprayed onto a cellulose-coated copper grid for TEM

characterization. As shown in Figure 4.8, the morphology of ACF nanobubbles was identical with that of ACF nanocapsules. This indicated that the encapsulated spherical structure was mechanically stable due to the crosslink of "C" wall. Not surprisingly, the GCB nanobubbles were also obtained since essentially same method was applied for their fabrication. As shown in Figure 4.9, the re-dispersed GCB nanobubbles also contained dark rings with a gray center. Identical to ACF case, the dark rings were from the stain of "C" walls with heavy metal compound. The main difference between GCB and ACF nanobubbles was their sizes. However, this was reasonable due to their different physical properties, such as chain lengths and surface energies, which should affect the emulsification.

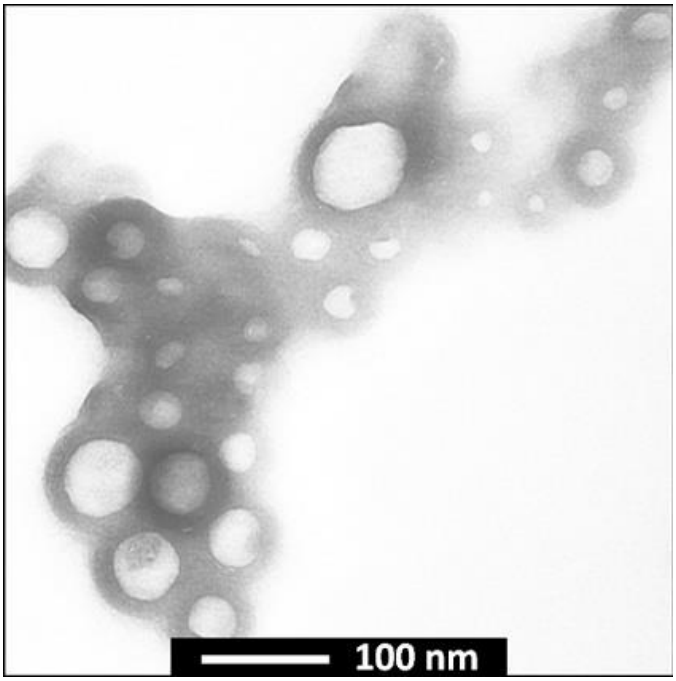

Figure 4.8 TEM image of ACF nanobubbles that had been sprayed onto a cellulose-coated copper grid and then stained with OsO_4.

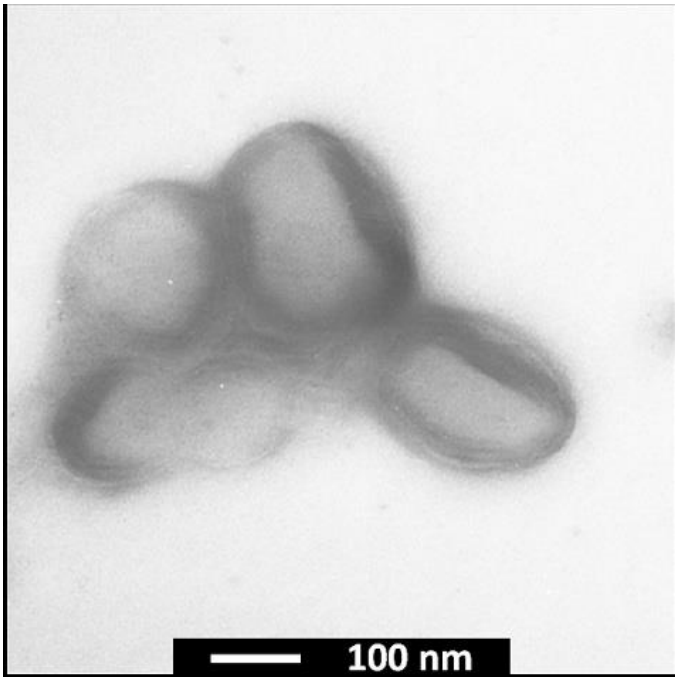

Figure 4.9 TEM image of GCB nanobubbles that had been sprayed onto a cellulose-coated copper grid and then stained with OsO_4.

Successful nanocapsule and nanobubble preparations were also confirmed by the other characterization results as summarized in Table 4.2. Similarly to the P(S-GMA) nanoparticles results discussed in last chapter, the sizes of particles measured in DLS were larger than those measured in microscopies. One reason was that the scattering-intensity-average diameter, also known as the z-average diameter, should be higher than the number-average diameter determined via microscopies.[42] However, the size increase in DLS measurement in this case was higher than the case of P(S-GMA) nanoparticles in last chapter. The main reason should attribute to the expansion of particles in solvent. Different to those P(S-GMA) nanoparticles in last chapter, these ACF and GCB nanoparticles were stabilized by long corona chains which stretched in solvent but collapsed in dry solid state. This relatively large difference between DLS and microscopies measurements were also obtained in literature reports.[43] On the other hand, as same trend shown in TEM results, the AFM and DLS diameters of the ACF nanocapsules and nanobubbles increased, respectively, for the GCB nanocapsules and nanobubbles. Thus, the final GCB bubbles were larger

than the ACF bubbles and would have a lower Laplace pressure. As far as P_L was concerned, the GCB bubbles should be more stable than the ACF nanobubbles.

Table 4.2 Characterization of the ACF and GCB nanoparticles during different stages

Sample	DLS d_h (nm)	DLS Polydispersity	d_{TEM} (nm)	d_{AFM} (nm)
ACF Capsules	196	0.15	73 ± 30	85 ± 24
ACF Bubbles	204	0.16	71 ± 32	115 ± 66
GCB Capsules	423	0.22	202 ± 89	211 ± 64
GCB Bubbles	459	0.25	208 ± 73	225 ± 73

4.3.4 Echogenicity and Thermodynamic Stability of ACF and GCB Nanobubbles in Water

In-vitro ultrasonography was used to detect bubbles and to establish their stability. For such experiments, a vascular ultrasonography device was used in the harmonic mode by sending pulses at 4 MHz and detecting reflected signals at 8 MHz. The artificial vessel consisted of a rubber tube of an inner diameter of 1.0 cm and length of 6.5 cm. This tube was filled with water and placed in artificial tissue composed of a gelled cellulose matrix. We began recording 2-dimensional (2D) cross-sectional images or videos of the tube along the long axis direction 1 s after a sample in 0.40 mL of water was injected into the tube and the recorded images were then analyzed to determine their gray-scale brightness readings.

A total of seven samples were analyzed in water first, which included an ACF nanocapsule sample (Structure 3, Figure 4.6), ACF and GCB nanobubble samples that were freshly dispersed into water, ACF and GCB "nanobubble" samples that were left standing at 21 °C for 4 h, an ACF sample that stood still in water for 3 weeks, and a fresh commercial microbubble sample that consisted of perfluoropropane gas encapsulated in phospholipids. While the former five samples all had a final polymer concentration of 0.125 mg/mL after their injection into the rubber tube, the

concentration of the last sample was unknown but was adjusted so that a reasonable ultrasound signal was obtained.

The analysis yielded the initial image brightness values of 0.013 (ACF nanocapsules), 0.372 (fresh ACF bubbles), 0.366 (ACF bubbles aged for 4 h.), 0.379 (ACF bubbles aged for 3 weeks), 0.260 (fresh GCB bubbles), 0.019 (GCB bubbles aged for 4 h), and 0.435 (commercial bubbles). The lack of a significant signal from the ACF nanocapsules sample confirmed that neither the polymer nor the encapsulated TFT droplets reflected ultrasound effectively. However, fresh ACF or GCB nanobubbles, just like the commercial microbubbles, readily reflected ultrasound and were echogenic. This must have been due to the air trapped in their capsular cavities.

Interestingly, the GCB bubbles aged for 4 h lost their signal and became echolucent. However, as discussed in last section, dispersing nanobubbles into water could not destroy their structures. Therefore, it is suggesting that water seeped through the GCB capsular walls and replaced the air in the cavities. Thus, the B-encapsulated nanobubbles were thermodynamically unstable in water. In contrast, the ACF bubbles 4 h and even 3 weeks after their dispersion in water had the same echogenicity as the fresh ones, suggesting that these F-encapsulated nanobubbles were thermodynamically stable in water.

4.3.5 Energetic Analysis based on a Single Bubble Model

To assess the Gibbs free energy change accompanying air replacement by water in the capsular cavities, a system consisting of one bubble dispersed in a large body of aeriated water was applied since the bubbles in dilute dispersions can be viewed as non-interacting, independent, and equivalent. We assume that the bubble has an inner cavity of radius R and the system consists of the capsule dispersed in a large body of aerated water around the capsule at constant atmospheric pressure and room temperature. As illustrated in Figure 4.10, no water is in the bubble cavity in the initial state. However, the cavity is fully filled with water in the final state since water may diffuse through the polymer wall which contains free volumes. From the initial to the final state,

the original interface between air and the inner wall of the cavity is lost and a new interface between the inner wall and water is created. Therefore, the Gibbs free energy change accompanying this process is

$$\Delta G = 4\pi R^2 \gamma_{wp} - 4\pi R^2 \gamma_p \qquad (4.2)$$

where γ_P is the surface tension of the polymer inner wall and γ_{wp} is the interfacial tension between the polymer wall and water. According to Young's relation, $\gamma_{wp} - \gamma_p = -\gamma_w cos\theta$,[44] where θ is the static contact angle of a water droplet on the polymer wall. Thus, equation 4.2 simplifies to

$$\frac{\Delta G(R)}{4\pi R^2} = -\gamma_w cos\theta \qquad (4.3)$$

When the wall coating material has θ = 75°, the value for B,[28] the free energy change from the initial to the final state is negative. Thus, water spontaneously enters the central cavity of these hollow nanospheres as has been observed experimentally for the GCB nanobubbles. On the other hand, $\Delta G(R)/(4\pi R^2)$ is positive if the inner wall is coated by F, which has θ = 120°.[19] Thus, the F-encapsulated nanobubbles were thermodynamically stable in water.

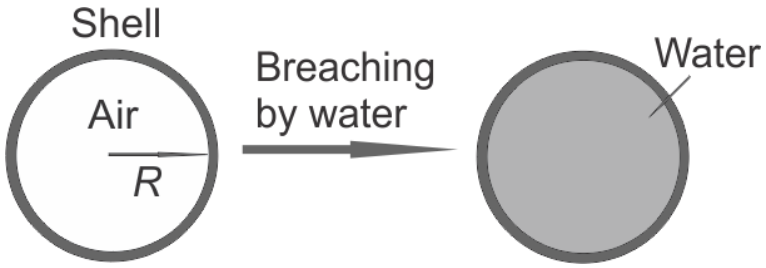

Figure 4.10 Cross-sectional view of a theoretical model of an encapsulated air bubble before and after water breaching.

4.3.6 Stability of Various Bubbles in Water under Ultrasonication

The stability of different bubbles in water under continuous ultrasonication were further investigated and compared using the same *in-vitro* ultrasonographic technique and conditions.

Strikingly, both the fresh and aged ACF bubbles exhibited better stability than the commercial bubbles under continuous ultrasonication. Figure 4.11 compares the 2-D ultrasound images taken at different ultrasonication times after the tube of water was doped with fresh ACF nanobubbles and the commercial microbubbles. The latter sample lost most of its signal after 15 s of ultrasonication. In contrast, the sample containing the fresh ACF nanobubbles became dark only at the top near the ultrasound probe while the bottom section remained bright even after 180 s of ultrasonication. Figures 4.12a and 4.12b plot the variation in the gray scale values of five different samples as a function of the ultrasonication time. The samples that were doped with fresh ACF nanobubbles and ACF nanobubbles that were aged for 4 h behaved analogously and exhibited long-term stability under ultrasonication. The extraordinary stability was also demonstrated for the ACF nanobubbles that were aged for 3 weeks (Figure 4.13). In contrast, the signals of the other samples either quickly faded such as fresh GCB nanobubbles and commercial microbubbles, or was initially negligible such as 4 h aged GCB nanobubbles. Therefore, only the F-encapsulated air nanobubbles were exceptionally stable in water under ultrasound.

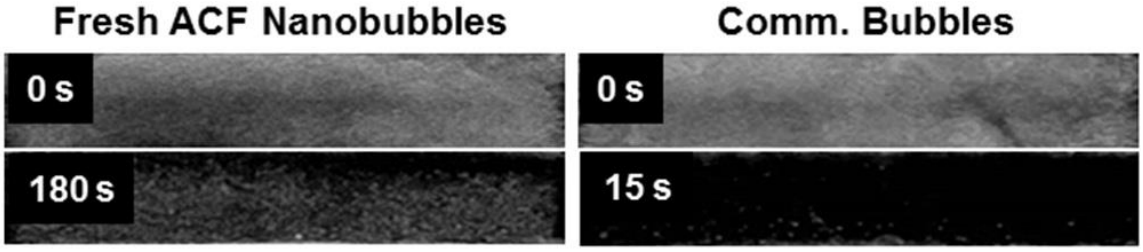

Figure 4.11 2-D ultrasound images of a tube of water at different times after the injection of the fresh ACF nanobubbles and commercial microbubbles.

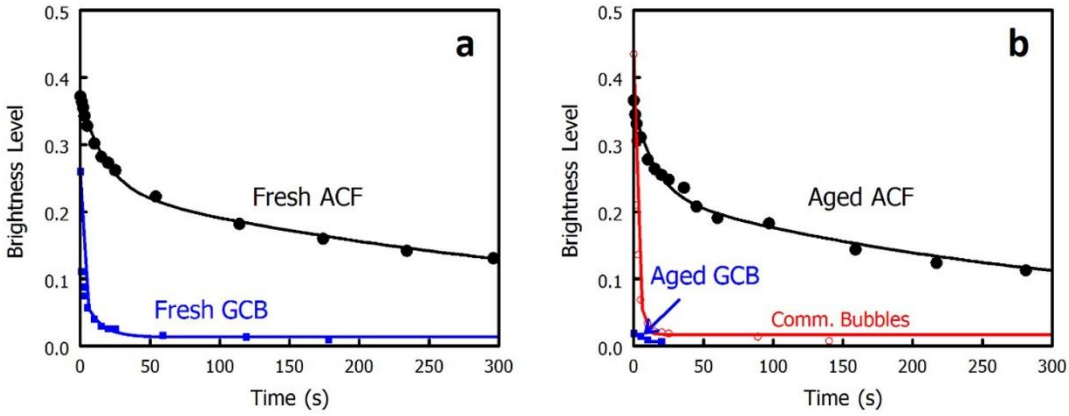

Figure 4.12 Decay in the brightness of ultrasound images of the water-filled tube as a function of the time after the injection of (a) fresh ACF and GCB nanobubbles and (b) 4 h aged ACF nanobubbles, 4 h aged GCB nanobubbles and commercial microbubbles.

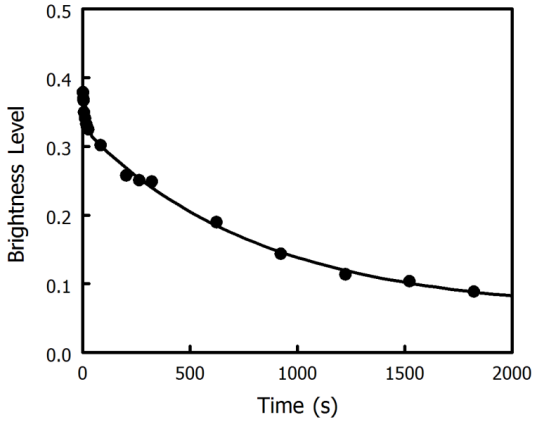

Figure 4.13 Decay in the brightness of ultrasound images of the water-filled tube as a function of the time after the injection of 3 weeks aged ACF nanobubbles.

The ultrasound signal decay data $I(t)$ in Figure 4.12 and Figure 4.13 was fitted using the following phenomenological equation:

$$I(t) = a_0 + a_1 e^{-t/\tau_1} + a_2 e^{-t/\tau_2} \qquad (4.4)$$

where a_1 and a_2 are the weighting factors for the decay terms with lifetimes τ_1 and τ_2, respectively. The parameters thus obtained (Table 4.3) were then used to calculate the average signal lifetimes for the decaying terms using:

$$\langle \tau \rangle = \frac{a_1\tau_1 + a_2\tau_2}{a_1 + a_2} \qquad (4.5)$$

The average lifetimes thus obtained for the fresh GCB nanobubbles, the commercial microbubbles, the fresh ACF nanobubbles, and the 4 h aged ACF nanobubbles were 3.7, 2.5, 226, and 186 s, respectively. While the fresh and 4 h aged ACF nanobubbles had essentially the same longevity, the commercial microbubbles and fresh CGB nanobubbles were equally short-lived. Quantitatively, the lifetime of the ACF bubbles was ~100 times longer than that of the commercial bubbles.

Table 4.3 Fitting parameters and lifetimes obtained from treating the decay data for ultrasound signals.

Sample	a_0	a_1	τ_1 (s)	a_2	τ_2 (s)	$\langle\tau\rangle$ (s)
Fresh GCB	0.014	0.177	0.71	0.072	11.0	3.7
Fresh ACF	0.044	0.132	18.0	0.192	371	227
Aged ACF	0.044	0.126	15.9	0.183	303	186
ACF aged for 3 weeks	0.059	0.053	9.4	0.268	825	690
Comm. Bubbles	0.017	0.142	2.48	0.280	2.49	2.49

One issue was noted that the ACF nanobubbles aged for 3 weeks showed extraordinary stability. However, the surprising discovery was that this bubble sample was even more stable than the fresh ACF nanobubble and the ACF nanobubbles that were aged for only 4 h. The abnormally high stability of the long-aged ACF nanobubbles deserves a detailed study but is beyond the scope of current study. Since this set of data was determined not on the same day as the other sets of data although same conditions were applied, the stability improvement could have a trivial non-interesting origin, i.e. due to the reduced power delivery by the ultrasound probe. More interesting would be the improved packing regularity of the perfluorinated octyl groups of the F block. The F block is known to form a liquid crystalline phase at room temperature. The packing regularity may improve as the sample was left to age at room temperature for long time.

However, the signal from thermodynamically stable ACF nanobubbles eventually decayed under ultrasound although it was much slower than GCB and commercial samples. Therefore, one ACF nanobubble sample (the fresh ACF nanobubbles) was analyzed by TEM after 30-min

ultrasonication in water to explore a possible decaying mechanism. TEM result indicated that the nanobubbles retained their structural integrity after ultrasonication (Figure 4.14). Therefore, displacement of air by water in the cavities should be the main cause for the loss in echogenicity.

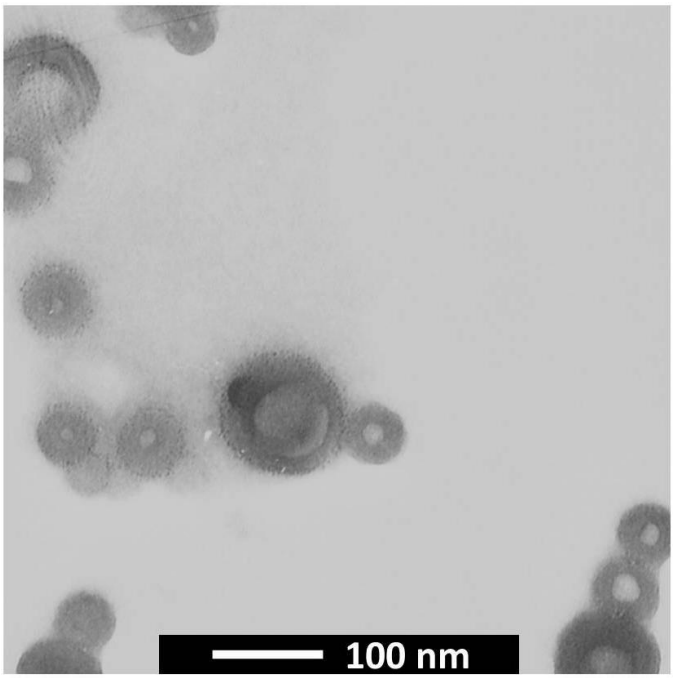

Figure 4.14 TEM image of ACF nanobubbles that had been collected after 30-min of ultrasonication test in water.

4.3.7 Stability of ACF Nanobubbles in Human Whole Blood under Ultrasonication

To demonstrate the potential of the ACF nanobubbles in real applications, the behavior of ACF nanobubbles and the commercial microbubbles in human whole blood under ultrasound was compared. As in water, the ACF nanobubbles exhibited in blood a greatly improved stability under ultrasonication than the commercial microbubbles. Figure 4.15 compares the 2-D ultrasound images taken at different ultrasonication times after the blood-filled tube was doped with fresh ACF nanobubbles and the commercial microbubbles, respectively. The signal at time zero was non-uniform because the blood, unlike water, was viscous and the bubble solutions could not be quickly

mixed with the blood instantaneously. Because of this, the decay data was not quantitatively analyzed. The important message from the ultrasonographs was that the ACF nanobubbles were also stable in human blood and were more stable than the commercial microbubbles.

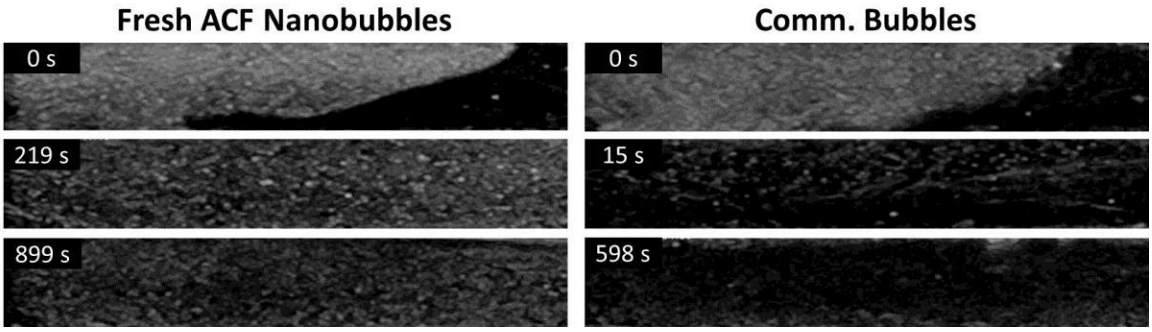

Figure 4.15 2-D ultrasound images of a tube of human whole blood at different times after the injection of the fresh ACF nanobubbles and the commercial microbubbles.

4.4 Conclusions

Inspired by surface coating with low surface energy polymer, this chapter described the work which has for the first time entrapped air securely in fluorinated polymer nanocapsules and prepared stable encapsulated air nanobubbles in water. These bubbles were echogenic and thermodynamically stable in water. More strikingly, these bubbles were much more stable both in water and in human whole blood under ultrasonication than a commercial third-generation ultrasonography contrast agent. Results of this work suggest that changing the encapsulating material is a viable approach for the preparation of stable encapsulated air microbubbles and nanobubbles. Due to the ability for the small nanobubbles to permeate capillary networks of organs and tissues, future versions of these nanobubbles, which may be called fourth-generation bubbles, may find applications in advanced diagnostics and drug delivery.

4.5 Notes and References

The main work described in this chapter has been published as:

Wang, Y., Liu, G.,* Hu, H., Li, T., Johri, A., Li, X., and Wang, J. "Stable encapsulated air nanobubbles in water", *Angew. Chem. Int. Ed*. 2015, **127**, 14499-14502.

References

1. H. Becher and P. Burns, *Handbook of Contrast Echocardiography - Left Ventricular Function and Myocardial Perfusion* Springer, Frankfurt and New York, 2000.
2. E. Stride and M. Edirisinghe, *Soft Matter*, 2008, **4**, 2350-2359.
3. K. Ferrara, R. Pollard and M. Borden, *Annu. Rev. Biomed. Eng.*, 2007, **9**, 415-447.
4. M. Postema and G. Schmitz, *Ultrason. Sonochem.*, 2007, **14**, 438-444.
5. R. Cavalli, A. Bisazza and D. Lembo, *Int. J. Pharm.*, 2013, **456**, 437-445.
6. N. Rapoport, K. H. Nam, R. Gupta, Z. G. Gao, P. Mohan, A. Payne, N. Todd, X. Liu, T. Kim, J. Shea, C. Scaife, D. L. Parker, E. K. Jeong and A. M. Kennedy, *J Control. Release*, 2011, **153**, 4-15.
7. X. Z. Fan, L. F. Wang, Y. L. Guo, H. P. Tong, L. Li, J. Ding and H. Y. Huang, *Nanotechnology*, 2013, **24**, 325102.
8. R. Suzuki, T. Takizawa, Y. Negishi, N. Utoguchi and K. Maruyama, *Int. J. Pharm.*, 2008, **354**, 49-55.
9. J. I. Park, E. Tumarkin and E. Kumacheva, *Macromol. Rapid Commun.*, 2010, **31**, 222-227.
10. P. Atkins, *Physical Chemistry; 6th ed*, Freeman, New York, 1998.
11. D. R. Lide, *CRC Handbook of Chemistry and Physics; 76th ed*, CRC Press, Boca Raton, 1995.
12. P. S. Epstein and M. S. Plesset, *J. Chem. Phys.*, 1950, **18**, 1505-1509.
13. X. H. Zhang, A. Khan and W. A. Ducker, *Phys. Rev. Lett.*, 2007, **98**.

14. S. Ljunggren and J. C. Eriksson, *Colloids Surf. A Physicochem. Eng. Asp.*, 1997, **129**, 151-155.

15. J. J. Kwan and M. A. Borden, *Adv. Colloid Interfac.*, 2012, **183**, 82-99.

16. T. Nishino, M. Meguro, K. Nakamae, M. Matsushita and Y. Ueda, *Langmuir*, 1999, **15**, 4321-4323.

17. A. Hirao, K. Sugiyama and H. Yokoyama, *Prog. Polym. Sci.*, 2007, **32**, 1393-1438.

18. W. J. Cui, J. Z. Bei, S. G. Wang, G. Zhi, Y. Y. Zhao, X. S. Zhou, H. W. Zhang and Y. Xu, *J. Biomed. Mater. Res. B Appl. Biomater.*, 2005, **73B**, 171-178.

19. D. Macoretta, M. Rabnawaz, C. M. Grozea, G. J. Liu, Y. Wang, A. Crumblehulme and M. Wyer, *ACS Appl. Mater. Inter.*, 2014, **6**, 21435-21445.

20. D. Xiong, G. Liu and E. J. S. Duncan, *Langmuir*, 2012, **28**, 6911-6918.

21. Y. Wang, X. Y. Li, H. Hu, G. J. Liu and M. Rabnawaz, *J. Mater. Chem. A*, 2014, **2**, 8094-8102.

22. J. P. Zhang and S. Seeger, *Angew. Chem. Int. Ed.*, 2011, **50**, 6652-6656.

23. A. Solga, Z. Cerman, B. F. Striffler, M. Spaeth and W. Barthlott, *Bioinspir. Biomim.*, 2007, **2**, S126-S134.

24. J. H. Bahng, B. Yeom, Y. C. Wang, S. O. Tung, J. D. Hoff and N. Kotov, *Nature*, 2015, **517**, 596-599.

25. Y. Gao, X. Y. Li, L. Z. Hong and G. J. Liu, *Macromolecules*, 2012, **45**, 1321-1330.

26. R. H. Zheng and G. J. Liu, *Macromolecules*, 2007, **40**, 5116-5121.

27. F. Pan, P. Wang, K. Lee, A. Wu, N. J. Turro and J. T. Koberstein, *Langmuir*, 2005, **21**, 3605-3612.

28. C. Mengel, A. R. Esker, W. H. Meyer and G. Wegner, *Langmuir*, 2002, **18**, 6365-6372.

29. X. Y. Li, Y. Gao, X. J. Xing and G. J. Liu, *Macromolecules*, 2013, **46**, 7436-7442.

30. X. H. Yan, G. J. Liu and Z. Li, *J. Am. Chem. Soc.*, 2004, **126**, 10059-10066.

31. A. Hirao, H. Kato, K. Yamaguchi and S. Nakahama, *Macromolecules*, 1986, **19**, 1294-1299.

32. F. Henselwood and G. J. Liu, *Macromolecules*, 1997, **30**, 488-493.

33. T. Ishizone, K. Sugiyama, Y. Sakano, H. Mori, A. Hirao and S. Nakahama, *Polym. J.*, 1999, **31**, 983-988.

34. H. Cui, Z. Chen, S. Zhong, K. L. Wooley and D. J. Pochan, *Science*, 2007, **317**, 647-650.

35. J. B. Gilroy, T. Gadt, G. R. Whittell, L. Chabanne, J. M. Mitchels, R. M. Richardson, M. A. Winnik and I. Manners, *Nat. Chem.*, 2010, **2**, 566-570.

36. A. H. Groschel, A. Walther, T. I. Lobling, F. H. Schacher, H. Schmalz and A. H. E. Muller, *Nature*, 2013, **503**, 247-251.

37. P. Fernandez, V. Andre, J. Rieger and A. Kuhnle, *Colloid Surf., A*, 2004, **251**, 53-58.

38. N. Anton, J.-P. Benoit and P. Saulnier, *J Control Release*, 2008, **128**, 185-199.

39. A. Guo, G. Liu and J. Tao, *Macromolecules*, 1996, **29**, 2487-2493.

40. L. F. Zhang and A. Eisenberg, *Science*, 1995, **268**, 1728-1731.

41. D. E. Discher and A. Eisenberg, *Science*, 2002, **297**, 967-973.

42. W. J. Jiang, C. M. Grozea, Z. Q. Shi and G. J. Liu, *ACS Appl. Mater. Inter.*, 2014, **6**, 2629-2638.

43. F. Liu, J. W. Hu, G. J. Liu, S. D. Lin, Y. Y. Tu, C. M. Hou, H. L. Zou, Y. Yang, Y. Wu and Y. M. Mo, *Polym. Chem.*, 2014, **5**, 1381-1392.

44. B. Bhushan and Y. C. Jung, *Prog. Mater. Sci.*, 2011, **56**, 1-108.

Chapter 5

Conclusions and Future Work

5.1 Conclusions

In this thesis, several kinds of block copolymers bearing a low-surface-energy block have been synthesized and used for various applications. In summary, an AB diblock copolymer PDMS-*b*-PCEA was synthesized via ATRP and derivatization and has been used to fabricate superhydrophobic cotton fabric and patterned fabric. Another AB diblock copolymer PDMS-*b*-PGMA was synthesized via ATRP has been used for superhydrophobic coatings and for oil-water separations. In addition, an ABC triblock copolymer PAA-*b*-PCEMA-*b*-PFOEMA was synthesized via anionic polymerization and derivatization and used for the preparation of oil-in-water nanoemulsion. The emulsion droplets were then converted to stable water-dispersible air nanobubbles.

Firstly, a diblock copolymer PDMS-*b*-PCEA has been synthesized via ATRP and derivatization and characterized by NMR and SEC. This copolymer formed micelles in mixtures of THF and hexane. Superhydrophobic cotton fabrics could subsequently be fabricated using this copolymer by a simple micellar solution soaking method. The XPS and surface wetting property analyses indicated that the PDMS block formed the exposed surfaces of these polymer coatings after the coated samples were treated by thermal annealing, UV crosslinking and solvent extraction. Furthermore, photolyzing the cotton swatches under a mask only crosslinked the anchoring PCEA layer around the fibers in the unmasked regions. The polymer in the non-irradiated regions was readily extracted by solvent, thus regenerating the pristine cotton fibers. Since PDMS-coated regions were superhydrophobic and the regenerated cotton was hydrophilic, these treatments yielded hydrophilically-patterned superhydrophobic cotton fabrics. While water-based solutions

such as ink readily permeated the hydrophilic regions, they were blocked in the superhydrophobic regions, thus yielding localized sections that were not covered by ink. Thus, inverted ink or dye reservoirs held by these cotton swatches were used as stamps for ink or dye printing, reproducing the original lithographic mask pattern. The pattern has been printed onto various substrates including hydrophilic fabrics, cardboard, paper, wood, and hydrophobic aluminum foil. The quality of the reprinted patterns on different substrates could be readily adjusted by tuning the viscosity of the ink solution.

In the second study, another PDMS-based AB diblock copolymer PDMS-*b*-PGMA has also been synthesized via ATRP and characterized by NMR and SEC. In comparison with PDMS-*b*-PCEA, this new diblock copolymer contains a stronger anchoring block PGMA that can not only self-crosslink around cotton fibers but also form covalent bonds between itself and cotton fibers. Not surprisingly, superhydrophobic cotton fabrics were easily obtained after the cotton substrates had been coated with PDMS-*b*-PGMA via a catalyzed solution soaking method. In addition, polymeric nanoparticles bearing GMA have been covalently attached onto cotton fiber surfaces before PDMS-*b*-PGMA was grafted onto the attached spheres and onto residual cotton fiber surfaces. Cotton substrates, coated with either the block copolymer itself or with a combination of these nanoparticles and the copolymer, were characterized by SEM, FT-IR and water repellency analyses. In this case, another application, oil-water separation, has been studied using these coated cotton fabrics since they are both superhydrophobic and oleophilic. The results of this investigation indicated that cotton fabrics coated by both nanoparticles and PDMS-*b*-PGMA (denoted as PP-cotton) performed better than those only coated by PDMS-*b*-PGMA (denoted by P-cotton) in oil-water separations. PP-cotton exhibited not only better water repellency including a higher water static contact angle, lower water shedding and sliding angles, higher breakthrough pressure and lower depth-dependent water absorption, but also higher oil absorption capacity in comparison with P-cotton. In addition, PP-cotton fabrics also showed better reusability than P-cotton fabrics when

they were used as filters for oil-water separations. The improved water repellency, oil absorption and final oil-water separation performance of PP-cotton can be attributed to the introduction of polymeric nanoparticles. The nanoscale roughness provided by these particles can enhance their water repellency, while solvent swelling of these crosslinked polymeric particles can contribute to their oil absorption capabilities.

The observation that water was unable to enter inter-thread and inter-fiber spaces of cotton fabrics coated by PDMS prompted us to investigate the use of low-surface-tension polymers in stabilizing air nanobubbles in water. In this endeavor, a fluorinated ABC triblock copolymer PAA-*b*-PCEMA-*b*-PFOEMA was synthesized via anionic polymerization and derivatization. Through an innovative approach, this copolymer was used to prepare stable water-dispersible air nanobubbles which had great potential in ultrasound-based diagnostic and therapeutic applications. These nanobubbles with a highly hydrophobic fluorinated internal lining were fabricated by removing the liquid from the cavities of oil-in-water nanocapsules (nanoemulsions) using a freeze-drying method. The precursor nanocapsules were fabricated via a simple emulsion inversion point (EIP) method using TFT as an oil phase, a NaOH solution as the water phase and the triblock copolymer as a surfactant. Both the nanobubbles and their nanocapsule precursors were characterized by TEM, AFM and DLS. Finally, ultrasound imaging experiments indicated that the air nanobubbles encapsulated by this fluorinated block copolymer had greater thermodynamic stability in water than those encapsulated by PGMA-*b*-PCEMA-*b*-PtBA (a control nanobubble sample with a hydrophilic internal lining). More interestingly, the nanobubbles had a lifetime under ultrasonication that was ~100 times longer than that of a commercial microbubble sample. Using this unconventional strategy, this work has not only exploited a novel application for our block copolymer bearing an ultra-low surface energy block, but also significantly enhanced the air nanobubbles' stability, which has been a critical limitation of existing micro/nanobubbles.

5.2 Future Work

5.2.1 Patterned Fabrics/Paper Coatings for Portable Analytical Devices

As mentioned in Chapter 2, hydrophilically patterned superhydrophobic fabrics or paper can be used for the preparation of portable analytical devices.[1, 2] These energy efficient devices are very useful for convenient diagnostics in developing countries or in areas where access to electricity may be limited. In general, a hydrophobic material will be coated on particular regions of a piece of paper or fabric as barriers. Then the aqueous solution of a test sample, such as a blood sample, can flow along the uncoated hydrophilic channels via capillary action (Figure 5.1). Wax is a typical hydrophobic material commonly employed as a barrier. However, the poor controllability of melted wax during the coating process limits the final resolution of these devices. In addition, the produced devices can also become damaged when the temperature is high due to the low melting point of wax.

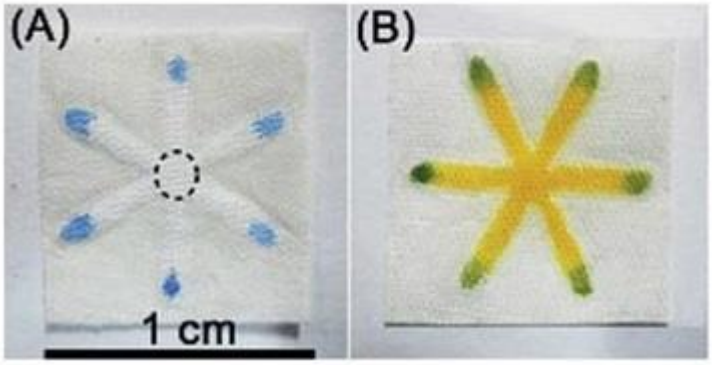

Figure 5.1 Cloth-based analytical devices fabricated by using wax as barriers. Reprinted from Nilghaz, A.; Wicaksono, D.; Gustiono, D.; Majid, F.; Supriyanto, E.; Kadir, M. *Lab Chip*, 2012, **12**, 209.

A PDMS-based photo-crosslinkable block copolymer, such as PDMS-*b*-PCEA described in Chapter 2, could provide a promising candidate for this application since one advantage of photolithography is that it can provide controllable patterns with high resolutions. Furthermore, a

coating based on a crosslinked polymer would be stable against exposure to various solvents or high temperatures. Therefore, PDMS-*b*-PCEA or similar block copolymers may provide suitable hydrophobic barriers for these analytical devices. However, the depth of the coating should be carefully investigated and optimized. In contrast with simple surface coatings, the hydrophobic barrier must penetrate across the entire paper or fabric. In order to decrease the cost or simplify the preparation, other coating methods such as directly printing a polymer solution onto paper or fabric substrates using a designed computational program could also be developed in the future.

5.2.2 Emulsified Oil-Water Separation Using Block Copolymer-Coated Cotton Fabrics

The separation of emulsified oil-water mixtures plays an important role in many production and purification processes. For example, water needs to be separated from water-in-oil emulsions formed during oil production processes to increase the quality of oil; and oil needs to be removed from oil-in-water emulsions during wastewater treatment processes so that the water can be reused. Obviously, the separation of emulsified oil-water mixtures is a much greater challenge than that of simple oil-water physical mixtures. Therefore, developing a wider range of block copolymers and methods for emulsion separation is significant.

We recently developed a novel Janus coated cotton fabric as a membrane for oil-in-water emulsion separations. The Janus cotton was coated by a premade PDMS-*b*-PCEA copolymer on one face, and its other face was then modified with poly(dimethylaminoethyl methacrylate) (PDMAEMA, Figure 5.2) via *in situ* free radical polymerization.[3] PDMAEMA was introduced because it readily underwent protonation and it could thus demulsify surfactant-stabilized oil-water mixtures. Therefore, the demulsified oil-water mixtures could be easily separated by the PDMS-*b*-PCEA-coated side of the membrane.

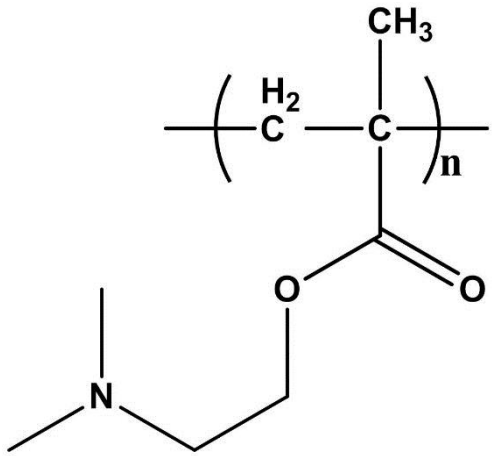

Figure 5.2 Chemical structure of PDMAEMA.

However, this recently published coating method is still too complex for practical applications, although it shows excellent promise. Inspired by this work and the work described in Chapter 3, PDMAEMA-*b*-PGMA can be synthesized via controlled radical polymerization. This diblock copolymer and the previously mentioned diblock copolymer PDMS-*b*-PGMA will be coated onto each side of a cotton fabric by a simple aero-spray method. An optimized Janus cotton fabric should be as efficient as the previously developed Janus cotton fabric in emulsion separation. However, coating these two premade diblock copolymers onto a cotton fabric through this approach would be much more facile and convenient. More importantly, the optimization of the final Janus cotton based on a systematic study may provide a much easier and more accurate means of tuning the membrane's performance by simply adjusting the polymer chain lengths or polymer concentrations.

5.2.3 Stable Nanobubbles Encapsulated by Biocompatible Block Copolymers

Although Chapter 4 points to a new direction for the preparation of stable air nanobubbles, the ABC triblock copolymer itself that was used in that study limits the actual application of these new nanobubbles. Although this ABC triblock copolymer is well-defined, its synthesis via anionic polymerization requires very stringent conditions. This polymerization method is only suitable for

fundamental research during the early stages of a long-term project. Second, although this triblock copolymer has been used to prove our new concept, a biocompatible polymer is necessary for future investigations and ultimately for potential biomedical applications.

According to our theoretical estimation described in Chapter 4, the biocompatible polymer PDMS might also form a stable hydrophobic internal lining for nanobubbles since the water contact angle θ on a smooth PDMS film is higher than 100°. In order to stabilize the nanobubbles in water, long PAA chains can be retained for PAA's biocompatibility. Therefore, a diblock copolymer such as PDMS-*b*-PAA (Figure 5.3) might be suitable for the preparation of stable nanobubbles. These nanobubbles would be prepared in a similar manner as the ACF-based nanobubbles described in Chapter 4, via emulsification, crosslinking and freeze-drying treatments. Rather than relying on the UV irradiation technique that has been employed to crosslink the ACF nanocapsules, the crosslinking of PDMS-*b*-PAA nanocapsules will be performed by using a crosslinker such as a diamine compound. Intra-particle but not inter-particle crosslinking can be achieved by tuning the particle and crosslinker concentrations.[4, 5]

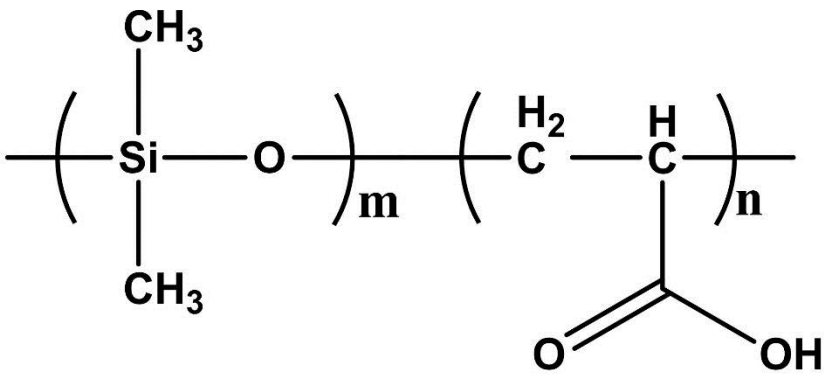

Figure 5.3 Chemical structure of PDMS-*b*-PAA.

References

1. A. Nilghaz, D. H. B. Wicaksono, D. Gustiono, F. A. A. Majid, E. Supriyanto and M. R. A. Kadir, *Lab Chip*, 2012, **12**, 209-218.

2. S. Y. Xing, J. Jiang and T. R. Pan, *Lab Chip*, 2013, **13**, 1937-1947.

3. Z. Wang, Y. Wang and G. Liu, *Angew. Chem. Int. Ed.*, 2016, **55**, 1291-1294.

4. K. B. Thurmond, T. Kowalewski and K. L. Wooley, *J. Am. Chem. Soc.*, 1997, **119**, 6656-6665.

5. K. B. Thurmond, T. Kowalewski and K. L. Wooley, *J. Am. Chem. Soc.*, 1996, **118**, 7239-7240.